_____

MICROWAVE BEAM SHAPING USING THE PRINCIPLE OF IMAGES APPLIED TO CYLINDRICAL REFLECTORS

A THESIS

Presented to

the Faculty of the Graduate Division

by

Paul Trice Hutchison

In Partial Fulfillment

of the Requirements for the Degree

Doctor of Philosophy in the School

of Electrical Engineering

Georgia Institute of Technology

August, 1959

MICROWAVE BEAM SHAPING USING THE PRINCIPLE OF IMAGES APPLIED TO CYLINDRICAL REFLECTORS

Approved:

F. Kenneth Hurd

D. L. Finn

V. D. Crawford

Date Approved by Chairman: 7/6/65

ACKNOWLEDGEMENTS

I wish to thank my thesis advisor, Dr. F. Kenneth Hurd, for his patience and support during this investigation. I also express my appreciation to Dr. D. L. Finn, Dr. V. D. Crawford, and Dr. W. B. Mullen for reading this manuscript, and to Dr. W. F. Atchison of the Rich Computer Center for making IBM 650 time available to me. I also thank my wife and son for their patience and consideration during the time this study was in progress.

TABLE OF CONTENTS

LIST OF TABLES

LIST OF ILLUSTRATIONS

CHAPTER I

INTRODUCTION

Microwave antennas having a so-called "cosecant-squared" radiation pattern[1] in the vertical plane and a uniformly narrow beam in the horizontal plane are in widespread use for airborne mapping and search radar applications. The general shape of this pattern, for an air-search radar, is shown in Figure 1 as a polar plot of the antenna gain function $G(\Theta)$ vs. the elevation angle Θ . This beam, which is mechanically scanned in the horizontal plane, "searches" most of the region above the earth. The distance r_o is proportional to the power gain of the antenna and can be expressed as h csc Θ. To insure that all like targets within the angular coverage region and at a common altitude h appear as equal-strength echoes on the radar screen, the power density illuminating these targets at various elevation angles must be constant. Since the power density from the radar is inversely proportional to r_o^2, the gain function $G(\Theta)$ must vary as $\csc^2\Theta$ within the desired angular coverage region. The general category of patterns having a $\csc^2\Theta$ or similar shape[2] are called shaped beams or vertical-coverage beams, and the antennas that produce them are called shaped-beam antennas.

Existing methods of beam shaping.--The radiation patterns of parabolic cylinders fed by line sources and paraboloids fed by point sources all have symmetrical shapes characteristic of the main-lobe diffraction pattern of an equiphase-aperture antenna.[3] Changing the aperture size

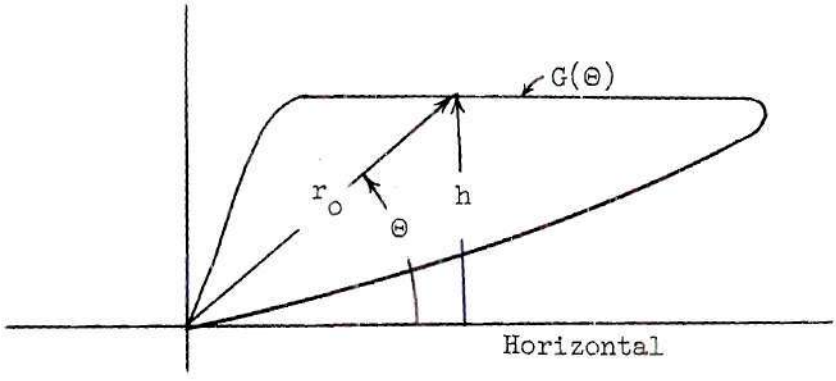

Figure 1. Polar Plot of the Gain of a Shaped-beam Antenna

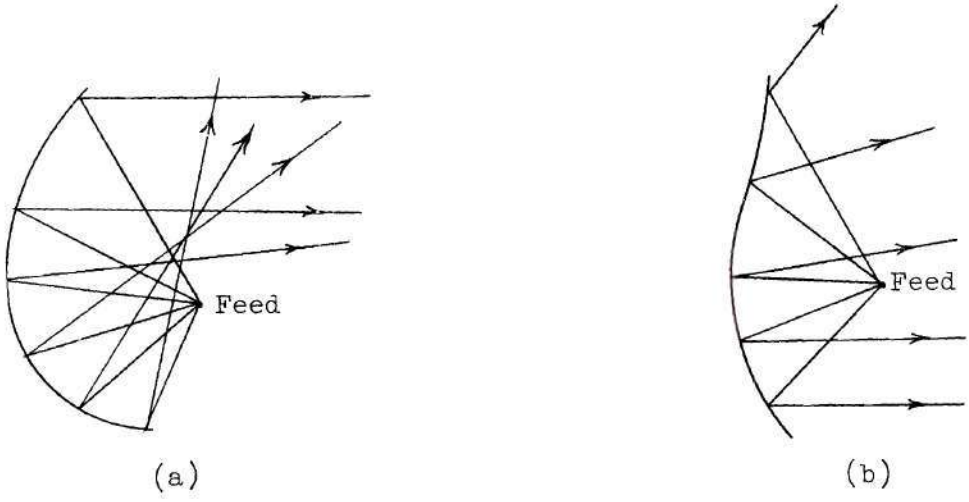

Figure 2. Reflector Shapes to Produce an Asymmetrical Flared Beam

changes only the scale factor for the angular coordinates of the symmetrical pattern. The characteristic shape of the pattern can be altered only by changing the phase of the field intensity over the aperture. The phase variation can be achieved by altering the shape of the reflector or by changing the characteristics of the feed. Both methods have been used to obtain shaped-beam antennas.

Figures 2(a) and 2(b) show the cross-section views of two non-parabolic cylindrical reflectors each fed by a single line source. The rays in these figures indicate how these reflectors produce the shaping of the beams. In both cases the azimuth beamwidths are determined entirely by the line sources. Chu[4] has arrived at a method of calculating the surfaces of these reflectors to give some specified vertical-plane pattern if the radiation pattern of the primary source is known. The radiation pattern of the horn feed, which directs energy into the reflector, is called the primary or feed pattern, and the secondary radiation pattern is that produced by the current on the reflector plus any direct radiation from the feed. Chu's procedure is based entirely on geometrical optics and conservation of energy and, while it is not difficult in principle, it is very tedious in practice because graphical integrations are required. Chu's method has proved very satisfactory for reflectors with a large but varying radius of curvature. However, the method neglects all diffraction effects and thus gives no evidence of the frequency sensitivity of the antenna. As a consequence, with this method it is necessary to design and build a prototype antenna which is then altered experimentally to modify the radiation pattern. In spite of these difficulties, Chu's synthesis method is the best existing method

for obtaining shaped-beam antennas.

This thesis presents a new method for obtaining shaped-beam antennas which has significant advantages over existing methods. This new method can be best understood by considering first the antenna of Figure 3, which shows a conducting paraboloid of revolution fed by three waveguide-type horns.[5] If only horn one is energized, the secondary radiation pattern will have a maximum value on the axis and a half-power beamwidth directly proportional to the wavelength and inversely proportional to L. If only horn two is energized, the resulting secondary pattern maximum is at some angle above the axis proportional to the displacement of the horn below the axis. For this condition the mouth of the reflector is not an equiphase surface. If all three horns are energized, there are three secondary beams with angular displacements determined by the angular separation of the horns. If the horns are spaced and fed properly, the combination of the beams can give a smooth shaped beam over limited angles.

As the single horn feed of a paraboloid is moved off axis, the beam-focusing properties of the reflector are impaired, resulting in a wider beam in both principal planes. An increase in beamwidth in the vertical plane is desirable, but any appreciable widening in the horizontal plane is undersirable because it limits the angular coverage of this antenna. For line sources used with cylindrical parabolas, the problem of horizontal-plane beam widening is eliminated because the beamwidth in this plane is derived entirely from the feed. However, the electrical and mechanical problems for the single line-source feed are so formidable that building a multiple line-source feed is impractical, if not

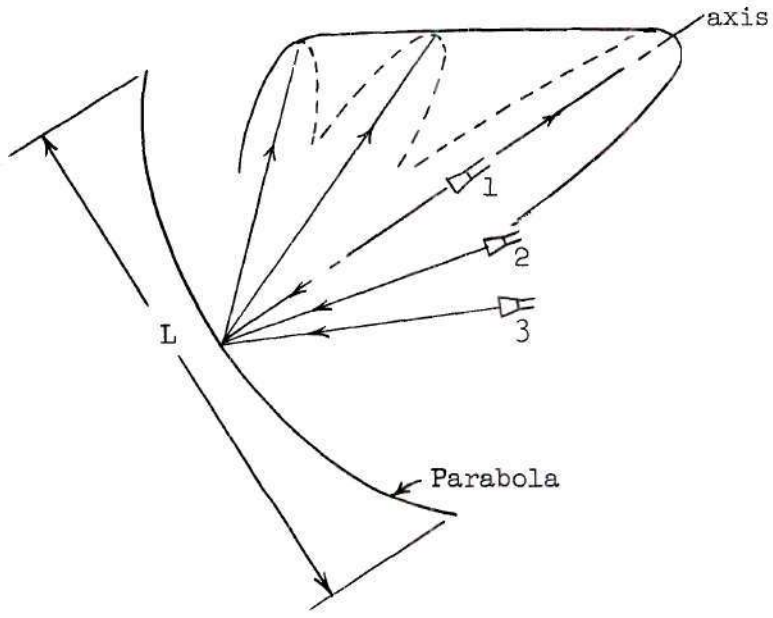

Figure 3. A Multiple-feed Antenna

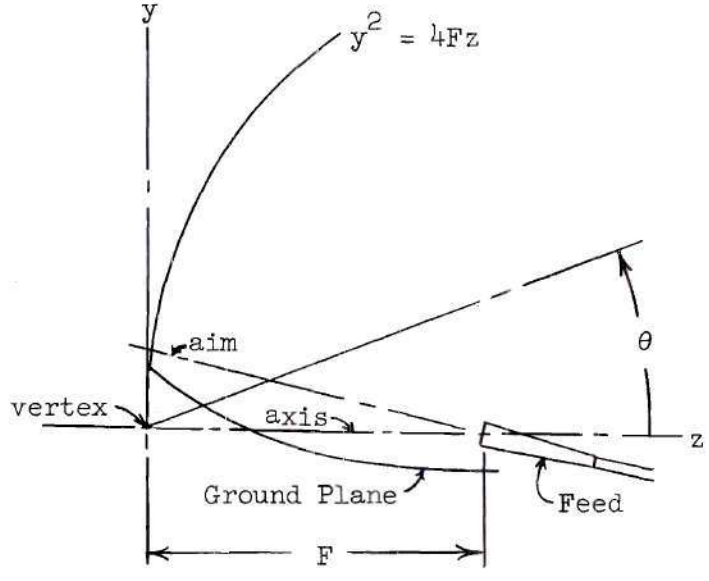

Figure 4. Cross Section of an Image Beam-shaping Antenna

impossible.

The image method of beam shaping.--The new method of shaping the secondary pattern presented here uses the same principles as the multiple-feed system, but the effect of off-axis feeds is created by a conducting surface, which will be called a ground plane, placed beneath the horn as shown in Figure 4. The energy from the feed that is intercepted by the ground plane is reflected into the parabolic section and creates the same general condition as that in the multiple-feed antenna. The energy reflected from the ground plane can be treated as emanating from a single image when the ground plane is flat and from multiple images when the ground plane is curved. It will be seen that the power division between the main and image horns can be controlled by the aim of the horn and the shape of the ground plane.

The far-field radiation pattern of the ground-plane antenna considered in this analysis is the combination of the scattered field from a metal reflector plus some, usually small, direct radiation from the line feed. For most elevation angles, the scattered field is by far the larger of the two components. As an aid in the analysis, the scattered field will be treated as the superposition of three beams: (1) the main beam, (2) the image beam, and (3) the direct ground-plane beam. The main beam is caused by the current distribution on the parabolic section of the reflector when the ground plane of Figure 4 is removed. These currents are a result of direct radiation from the feed into the parabola and they produce an almost symmetrical beam having a maximum along the axis of the parabola. The image beam results from currents on the parabolic reflector due to energy reflected from the

ground plane into the parabola. The image beam is asymmetrical and will be maximum at some angle above the axis of the parabola. The shape of this image beam is determined by the size of the parabolic section, the shape of the ground plane, the frequency, and the radiation characteristics of the feed. For the simplest case, a single flat ground plane, the energy reflected from the ground plane can be considered to emanate from a single image of the real horn. Curved and broken ground planes in general give the effect of a parabola fed with multiple images and usually produce wider image beams than those produced by flat ground planes.

The direct ground-plane beam is the beam caused directly by the ground-plane currents. Since most of the radiation from these currents is intercepted by the parabola, this beam is usually small. However, some ground planes cause a direct beam which is comparable to the main and image beams at the larger values of θ where the main and image beams are small.

Objectives of this study. --This study examines analytically and experimentally the validity and feasibility of the application of image principles to shaped-beam antennas. Although the method of analysis used can be applied to paraboloids and cylindrical parabolas, this study is restricted to cylindrical parabolas with ground planes added to give beam shaping.

In addition to proving experimentally that image principles of beam shaping can be used successfully on cylindrical reflectors, this study has two other objectives: (1) to develop a method of calculating the radiation pattern of image-beam antennas of arbitrary shape, and (2)

to develop a design procedure to provide a specified shaped beam. Since one problem is the inverse of the other, and since problems of the first kind are much easier to solve, the general procedure will be to find the solution to problems of the second kind by successive approximations involving recurrent problems of the first kind. The procedure used to calculate patterns of reflector-type antennas having single reflection surfaces such as those used in image beam-shaping antennas has not been treated analytically or experimentally, except briefly by the author.[6]

The three diffraction zones and a summary of succeeding chapters.--The method of solution of the problem presented in the remainder of this study deals with electric and magnetic fields caused by reflections of waves from conducting surfaces. Before proceeding with the detailed analysis covered in succeeding chapters, it is desirable to present a short discussion on the three diffraction zones surrounding a reflector or an aperture.

When an electromagnetic wave impinges on a conducting surface, electric charges and currents are set up on the surface so the boundary conditions are satisfied. Theoretically, the electric and magnetic fields due to the current and charge distributions can be expressed in terms of current distribution only. The integral expressions which result are very difficult to evaluate exactly even for simple surfaces and simple current distributions. Since the currents on the surface are treated as infinitesimal dipole radiators, the field outside the conductor is a vector-phasor addition of contributions from all the radiators. In order to evaluate the integrals in practical cases, certain approximations must be made. The region outside the conductor is usually

divided into three zones which are determined mathematically by the nature of the approximations used in evaluating the integrals.

The near zone is the region close to the conductor where no simplifying approximations in the integrals can be made. In cases where the integrals have been worked out in detail,[7] it was found that for surfaces with a radius of curvature large compared to a wavelength, the field differs little from that calculated using geometrical optics. The term "near" is determined by the size and shape of the conductor, the wavelength, and the current distribution. Near-field theory will be used in Chapter II to calculate the reflected waves from flat and curved ground planes. These reflected waves plus the direct waves from the horn determine the current distribution on the reflector and thus the far-field radiation pattern. Near-field measuring techniques and a comparison of calculated and measured near fields are presented in Chapter III.

Beyond the near zone is a second diffraction zone called the Fresnel zone. The Fresnel-zone patterns are dependent on the distance from the reflector and are of little importance in radar work. Fresnel-zone fields are very difficult to evaluate and are found graphically with aids such as the Cornu spiral. The Fresnel zone will not be considered in this study.

Finally, when the distance from the conductor is very large compared to the size of the conductor, the zone is called the far-field or Fraunhofer zone. In the far-field zone the simplifying assumptions which make the integrals manageable are valid for most cases of interest. In Chapter IV, the general far-field formulas[8] presented by Silver are

applied to parabolic cylinders and cylindrical ground planes. However, even with the simplifying assumptions, calculation of the far fields in terms of the currents is very time consuming. Chapter V presents "universal" design curves which predict the approximate magnitude and phase of the main and image beams. The use of the design curves reduces the number of calculations required to obtain a prescribed beam shape. Chapter VI compares the measured and calculated far-field patterns for several image beam-shaping antennas and shows sample problems illustrating the use of design curves developed in Chapter V. The final chapter covers the conclusions of this study and recommendations for future work on the image beam-shaping antenna.

CHAPTER II

THE NEAR FIELD

It will be shown in Chapter IV that the scattered far field from a conducting surface can be expressed as an integral equation involving the reflector geometry and the incident magnetic field intensity at the surface of the reflector. The dependence of this equation, Equation (14), on the magnetic field requires an accurate knowledge of the fields at every point on the reflector surface. For a typical image beam-shaping reflector, such as shown in Figure 4, conventional ray theory can be used to find the component of the magnetic field due to direct surface illumination by the feed. However, a reflected wave from the ground plane must be considered when calculating the total magnetic field along the surface of the parabolic section. The purpose of this chapter is to develop equations to give the magnetic field along the parabolic reflector due to direct energy from the horn and due to reflected energy from the ground plane. Before analyzing the problem of finding the magnetic field at the reflector, it is necessary to describe some general characteristics of line feeds.

Characteristics of line feeds.--The directivity of the cylindrical reflector-type microwave antenna in one plane is determined almost entirely by the primary feed because, in this plane, the reflector has zero curvature and thus provides no focusing. To obtain the directivity usually required, a line-type source is placed along the focal line of

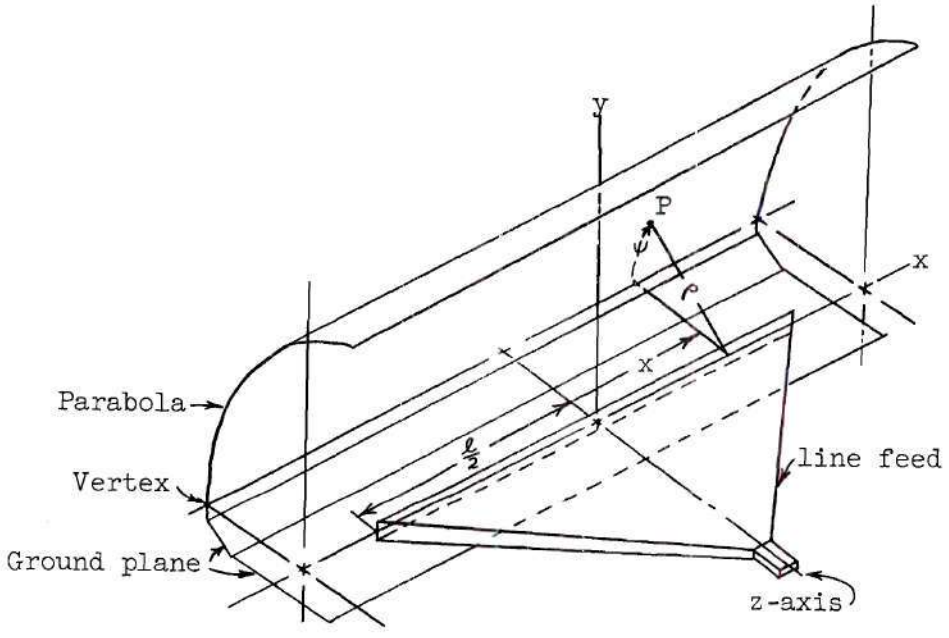

Figure 5. Oblique View of Horn Feed and Reflector

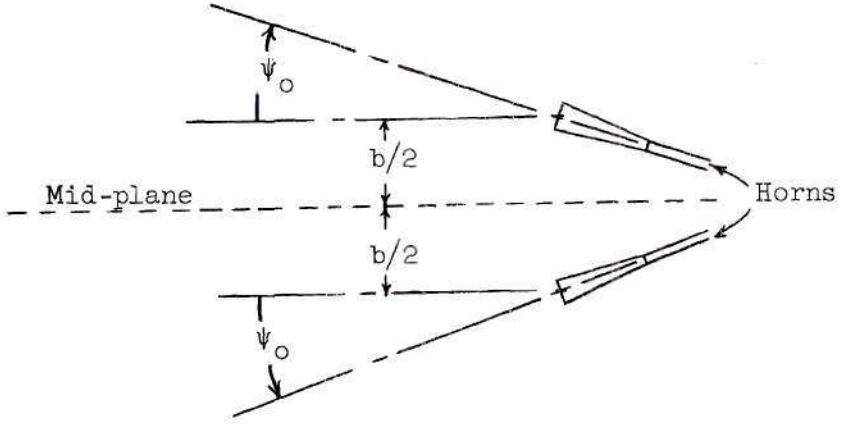

Figure 6. Cross Section of Two Line Sources Aimed ψ_o Degrees from the Mid-plane

the cylindrical parabola as shown in Figure 5. A practical line feed can take the form of a long narrow aperture of length $\ell \gg \lambda$ over which the phase of the field intensity if constant. The field produced by such a radiator is usually for descriptive purposes divided into three fields: (1) the near field, (2) the Fresnel field, and (3) the far field. The near-field, or cylindrical-wave, region can be subdivided into the zone in the immediate vicinity of the source and a quasi-radiation[9] zone where the distance from the source is greater than the narrow source dimension but less than ℓ^2/λ. In the quasi-radiation zone, the $\bar{E}$- and $\bar{H}$-components are essentially tangent to the cylindrical wavefronts and mutually perpendicular to each other.

The magnitude of the quasi-radiation field from the line-type feed in Figure 5 is a function of both x and ψ, but the phase is invariant with x. When the source is horizontally polarized, the electric field intensity is in the x-direction. When the source is vertically polarized, the E-vector is in the y-z plane and perpendicular to $\bar{\rho}$, so that it is vertical only along the z-axis, but this inconsistency has universal acceptance. If the cylindrical wave from an isolated line source is vertically polarized, the quasi-radiation-zone fields are given by Equations (1) and (2).[10] These equations describe the steady-state fields around the feed in Figure 5 when the reflector is removed.

$$\bar{H}_d = \bar{i} K_1 \left[\frac{P_t \, G(\psi) \, G(x)}{\rho} \right]^{\frac{1}{2}} \epsilon^{\, j(\omega t - \beta\rho)} \tag{1}$$

$$\bar{E}_d = K_1 \, \eta \left[\frac{P_t \, G(\psi) \, G(x)}{\rho} \right]^{\frac{1}{2}} \epsilon^{\, j(\omega t - \beta\rho)} (\bar{j} \cos\psi + \bar{k} \sin\psi) \tag{2}$$

K_1 is a constant of proportionality.

P_t is the power transmitted by the line source.

$G(\psi)$ is the relative power gain of the horn in the y-z plane.

$G(x)$ is the relative power gain of the horn in the x-direction.

$\beta = 2\pi/\lambda$, where λ is the free-space wavelength.

$\omega = 2\pi f$, where f is the frequency.

$\bar{i}$, $\bar{j}$, and $\bar{k}$ are the unit vectors of a rectangular coordinate system.

t is the time.

η is the intrinsic impedance of free space.

j is $\sqrt{-1}$.

$\bar{H}_d$ and $\bar{E}_d$ are the magnetic and electric field intensities at point P due only to direct radiation from the source. The bar above the letters shows they are vector quantities.

ψ, x, and ρ are the coordinates shown in Figure 5.

The field above a flat ground plane.--If the parabolic section of the reflector in Figure 5 is removed, the total magnetic field intensity above the ground plane is the sum of a direct ray $\bar{H}_d$ from the horn and a reflected ray $\bar{H}'_d$ from the ground plane. If the perfect-conducting ground plane is flat and infinitely large and the narrow dimension of the line source is infinitely small, the principle of images[11] can be applied to obtain exact expressions for $\bar{E}$ and $\bar{H}$ anywhere above the ground plane. To justify the use of images, consider two identical horns fed with equal power and positioned symmetrically about a plane midway between them as shown in Figure 6. When the horns are properly fed, the total electric field intensity along the mid-plane is normal to the plane and

the total magnetic field is tangential. These are the conditions on $\bar{E}$ and $\bar{H}$ necessary to satisfy the boundary conditions at the surface of the conductor. Proper feed or phasing of the two horns requires the vertical components of the electric field intensities at corresponding points on the horns to be equal and the horizontal components to be equal in magnitude and 180 degrees out of phase. Thus the conditions along the dotted line in Figure 6 are the same as those along the ground plane in Figure 7, and the total field intensity above the ground plane can be obtained by considering the reflected energy from the ground plane as emanating from the image-horn. The image-source radiation corresponds to a geometrical reflection of the cylindrical wave from the main feed. At each point on the ground plane, reflection occurs as though the incident cylindrical wave were an infinite plane wave. If the line source is infinitely thin, the current distribution functions of $\bar{E}$ and $\bar{H}$ over the horn aperture cannot be changed by the proximity of the ground plane, but the magnitudes may be changed by a constant factor. This statement is similar to the statement that the dipole moment of an infinitesimal dipole may be changed by the presence of a ground plane but the current distribution on the dipole cannot change. If the feed is directive in the vertical plane, i.e., the vertical aperture is finite, the amplitude distribution functions of $\bar{E}$ and $\bar{H}$ over the aperture will be significantly changed only when the horn is aimed into the ground plane and energy reflected from the ground plane goes back into the horn. Some interaction between the horn and ground plane always exists, but the effects are small in most applications to beam shaping.

The effect of the ground plane on the power radiated by the horn

was measured by comparing the voltage standing-wave ratio in the waveguide feeding the horn with and without the ground plane. These measurements showed that the presence of the ground plane has virtually no effect on the horn radiation even when the horn is aimed 20 degrees below the z-axis in Figure 7. The vertical dimensions of the horns used in this study were between 0.8 and 1.2 wavelengths.

On the basis of image theory, the reflections from an infinite flat ground plane, as shown in Figure 7, are calculated by using geometrical optics or ray theory. The total magnetic field above the ground plane is the sum of the wave from the image plus the direct wave calculated by using Equation (1) or the equivalent expression for horizontal polarization. In the special case of vertical polarization, the total magnetic field intensity along the parabolic path in Figure 7 is theoretically

$$\bar{H}_i = \bar{H}_d + \bar{H}_d' = \bar{i}K_1 \sqrt{P_t\, G(x)} \left\{ \left[\frac{G(\psi)}{\rho}\right]^{\frac{1}{2}} \epsilon^{-j\beta\rho} + \left[\frac{G(\phi)}{r}\right]^{\frac{1}{2}} \epsilon^{-j\beta r} \right\}, \quad (3)$$

where $\epsilon^{j\omega t}$ is understood, P_t is the power radiated by the horn in free space, and $\bar{H}_d'$ is the magnetic field of the wave reflected from the ground plane. The subscript "i" on the total magnetic field intensity indicates it is the incident field onto the metal parabola, when one is used.

With the source horizontally polarized, the electric field intensities $\bar{E}_d$ and $\bar{E}_d'$ are colinear in the quasi-radiation zone and the total electric field above the ground plane is given by the phasor addition of the two components,

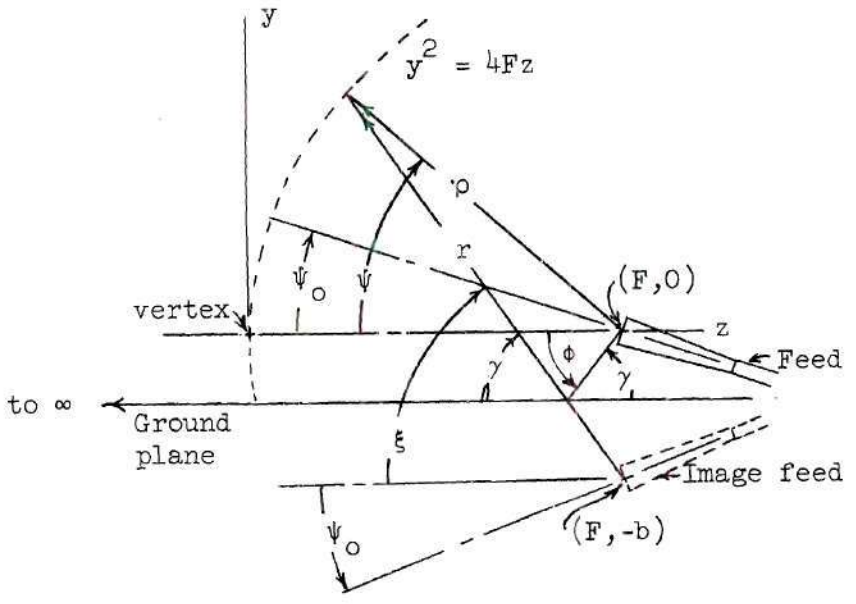

Figure 7. Ground-plane-feed Geometry

$$\bar{E}_i = \bar{E}_d + \bar{E}'_d = iK_1\eta\sqrt{P_t\, G(x)}\left\{\left[\frac{G(\psi)}{\rho}\right]^{\frac{1}{2}} \epsilon^{-j\beta\rho} + \left[\frac{G(\phi)}{r}\right]^{\frac{1}{2}} \epsilon^{-j(\beta r + \pi)}\right\}. \quad (4)$$

For this polarization, the $\bar{H}_d$ and $\bar{H}'_d$ quantities are not colinear but the components can easily be found from the geometry of Figure 7. The $\epsilon^{j\pi}$ term accounts for the 180 degree phase reversal of the reflected wave that the ground-plane surface.

Geometrical optics furnishes a relatively simple way to evaluate the reflected waves from flat surfaces very large compared to a wavelength. Before treating reflections from smaller ground planes, it is desirable to treat reflections from a true line source over an infinite ground plane by considering the reflected wave as the contribution from all currents on the ground plane. It is well known that the surface-current density on a perfect conductor is equal to the tangential

magnetic field intensity at the ground plane, so the ground-plane currents can be calculated using Equation (1) or the equivalent expression for horizontal polarization. Since the true line source is infinitely long, Equation (1) is valid for all values of ρ and ψ. Since the phase of the magnetic field from the line source is independent of x, the currents on a strip of the ground plane dz wide, infinitely long, and parallel to the x-axis all have the same phase and form a line source of current elements. The ground plane can thus be considered as an array of line-source current elements which radiate cylindrical waves. The cylindrical nature of the waves from the ground-plane strips reduces the problem of finding the radiation from the ground-plane elements to a two-dimensional one. If the reflected wave in the plane $x = 0$ in Figure 7 is needed, it can be calculated by summing only the effects of currents along the ground plane in the $x = 0$ plane. If the array of current elements in the $x = 0$ plane is considered as being made up of two arrays separated by the parabola, when one moves from right to left, there is a progressive though non-linear phase lag in the currents on the array to the left of the parabola. Although the array on the left of the parabola is not an end-fire array,[12] it is similar, and it will produce a maximum radiation at some angle less than arcsin b/2F from the negative z-axis. For this continuous current distribution, there is only one major lobe, so the radiation from this array in the first quadrant is small compared to the maximum. The qualitative argument that only current elements on the right side of the parabola make significant contributions to the fields in this region forms the basis for assuming the fields on the right side of the parabola can be found using ray optics, even when the

ground plane extends no further than the parabola. Thus, Equations (3) and (4) were used to calculate the total fields above flat ground planes extending from the parabola to a point back of the bottom lip of the feed. The agreement between the calculated and measured data presented in Chapter III justifies the restricted use of ray optics in calculating reflections from ground planes only six wavelengths wide.

Curved ground planes.--Concave ground planes establish multiple images and give secondary shaped beams having much wider angular coverage than beams caused by the flat ground planes. The further need for and use of curved ground planes are discussed in Chapter V. In this section, the treatment of reflections from flat ground planes is extended to cover concave and convex types.

If the radius of curvature of the ground plane is large compared to a wavelength, it can be considered flat over any small region, and reflection at any point can still be assumed to occur as though the incident cylindrical wave were an infinite plane wave. Geometrical optics is again used to find the phase of the direct and reflected fields. The method of calculating the magnitude of the reflected wave from a flat ground plane is modified to account for the focusing or defocusing properties of the curved plane.

In Figure 8, the steady-state power through a wedge of unit length and angle $d\phi$ is the same as that through a wedge of unit length and angle $d\xi$. Some error is expected here since this analysis is based on geometrical optics, which is exact only at zero wavelength. The time-average power dP_i incident on the area $(d\ell)$ (1) can be expressed in two ways,

$$dP_i = \frac{|E_i|^2}{2\eta} r_1 d\phi = \frac{|E_i|^2}{2\eta} d\ell \sin \gamma, \tag{5}$$

where r_1 is the distance from the feed to the ground plane, γ is the complement of the angle of incidence, and E_i is the peak electric field intensity incident onto the ground plane. The power reflected from this area is

$$dP_r = \frac{|E_r|^2}{2\eta} R_1 d\xi = \frac{|E_r|^2}{2\eta} d\ell \sin \gamma, \tag{6}$$

where E_r is the peak magnitude of the reflected electric field intensity at the ground plane and R_1 is a distance shown in Figure 8. From Equations (5) and (6) it is evident that $|E_i| = |E_r|$. From the same equations, R_1 can be found in terms of r_1, ϕ, and ξ as

$$R_1 = r_1 \frac{d\phi}{d\xi}. \tag{7}$$

Again, conservation of power dictates

$$\frac{|E_d'|^2}{2\eta} (r_2 + R_1) d\xi = \frac{|E_r|^2}{2\eta} R_1 d\xi; \tag{8}$$

therefore

$$E_d' = \left[\left|\frac{R_1}{r_2 + R_1}\right|\right]^{\frac{1}{2}} E_r = \left[\left|\frac{R_1}{r_2 + R_1}\right| \frac{P_t\, G(\phi)\, G(x)}{r_1}\right]^{\frac{1}{2}} K_1 \eta, \tag{9}$$

where E_d' is the peak value of the reflected electric field at point P on the parabolic surface.

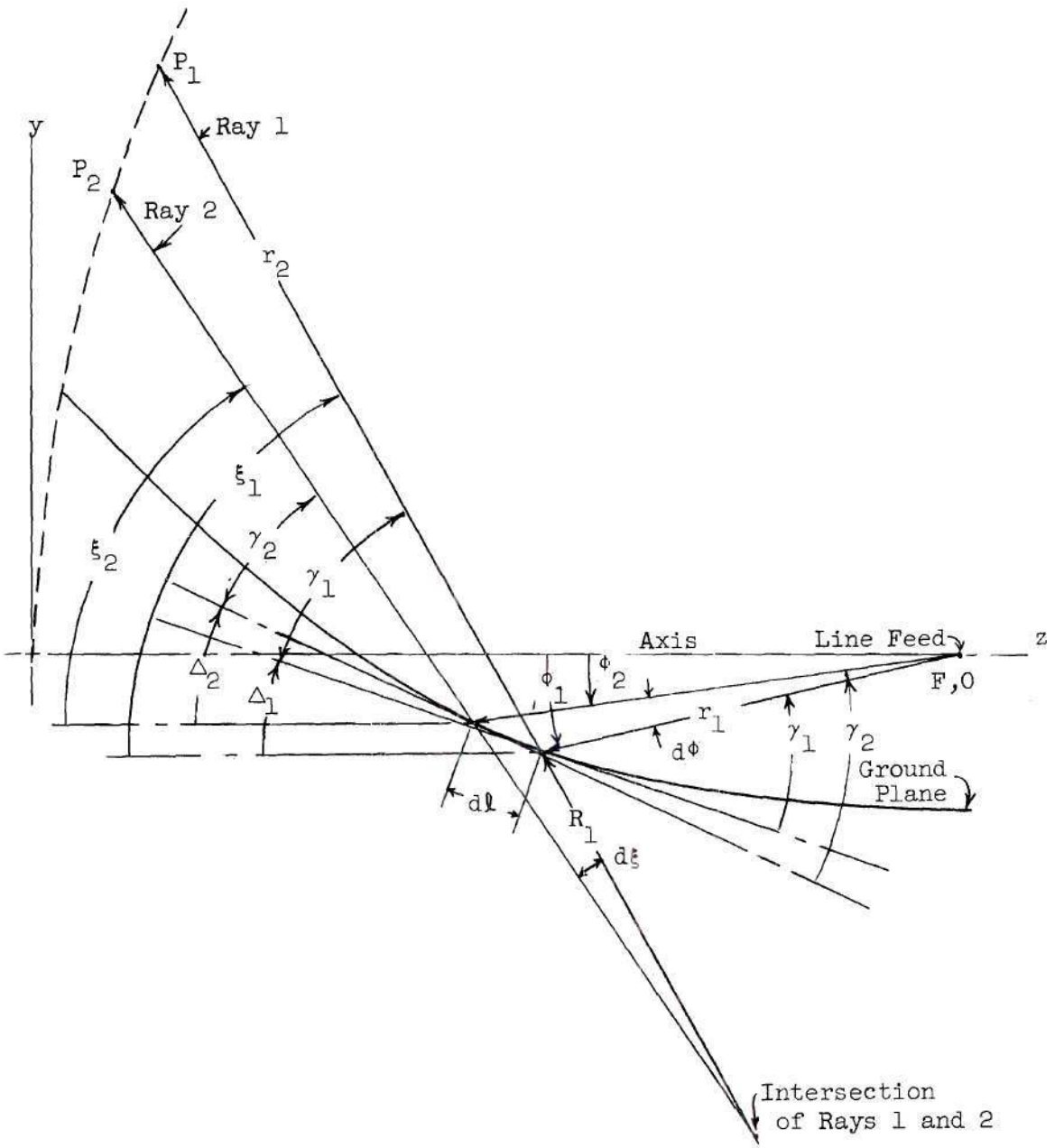

Figure 8. Geometry of Feed Above a Curved Ground Plane

The focusing properties of the ground plane can be analyzed by studying the variation of $d\xi/d\Phi$ in Equation (7). ξ is the angle the reflected ray from the ground plane makes with the horizontal and is positive when measured in the clockwise direction. Φ is the angle of the ray from the horn into the ground plane, and is measured counter-clockwise, as shown in Figure 8. The rate of change of ξ with respect to Φ shows how rapidly the rays diverge after reflection, compared to the divergence of the rays from the feed before reflection. This analysis will be made by considering ground planes of three shapes.

(1). When the flat ground plane is horizontal as shown in Figure 7, $\xi = \gamma = \Phi$, where γ is the complement of the angle of incidence. Since $d\xi/d\Phi = 1$, the distances R_1 and r_1 are equal, which proves the reflected rays all apparently emanate from a single image beneath the ground plane. The divergence of the rays after reflection from the ground plane is the same as the divergence of the rays from the main feed. When the ground plane makes an angle α, measured clockwise with the horizontal, $\xi = \alpha + \Phi$ and $\Phi = \gamma - \alpha$, so $d\xi/d\Phi$ is still unity.

(2). It can be seen from Figure 8 that the angle between the reflected rays 1 and 2 is smaller for a concave ground plane than for a flat ground plane. If, for example, the ground plane were a parabolic cylinder with the feed at the focal line, rays 1 and 2 would be parallel, indicating no divergence of the rays after reflection, i.e., $d\xi/d\Phi = 0$ and $R_1 = \infty$. For a concave ground plane with small curvature, $d\xi/d\Phi$ is usually greater than zero and a function of Φ. For a ground plane having a small radius of curvature, it is possible for $d\xi/d\Phi$ to be negative, in which case the reflected rays converge to some point above the ground

plane. This condition of convergence of rays above the ground plane is described here by a negative value of R_1. It is theoretically possible within the approximations used, for the focusing properties of the ground plane to make the reflected rays converge on the parabola, giving $R_1 = -r_2$ and producing an infinite field intensity over a zero space on the parabola. In practice, however, the field intensity cannot be infinite since the source does not emit a true cylindrical wave and the reflections calculated using geometrical optics are approximate. Therefore, the method of calculating the reflected waves as given by Equation (9) cannot be used when R_1 is negative and approximately equal to r_2 in magnitude. If the rays from any one section of the ground plane converge inside the parabola, the rays from another section will converge on the parabola, making Equation (9) unusable. For this reason, the method of calculating ground-plane reflections presented here is good for negative values of R_1 only if $|R_1| > r_2$ for all parts of the ground plane. This method is valid for positive values of R_1 so long as the radius of curvature of the ground plane is large compared to a wavelength.

(3). The divergence of the rays after reflection from the ground plane is greater than the divergence before reflection only when the ground plane is convex in cross section. The general equations developed in this section can be applied to convex ground planes, provided there is no shadow region and provided the radius of curvature of the ground plane is large.

For all three ground-plane shapes, the phase of the reflected wave is based on the optical path between the feed and point P on the parabola. This path can be calculated by the following step-by-step procedure, if

the shape of the ground plane can be expressed as some function $y = f(z)$.

(1). Assuming some initial value of ϕ, find the intersection (z_1, y_1) of the line r_1 with the ground plane, i.e., satisfy $y_1 = (z_1 - F) \tan \phi$ and $y_1 = f(z_1)$.

(2). Calculate the angle $\gamma = \Delta + \phi$ where

$$\tan \Delta = - \left. \frac{df(z)}{dz} \right|_{z = z_1}.$$

(3). Obtain the equation of the line r_2,

$$y = -z \tan \xi + (y_1 + z_1 \tan \xi),$$

where $\xi = \gamma + \Delta$.

(4). Solve the two simultaneous equations

$$y_p = -z_p \tan \xi + (y_1 + z_1 \tan \xi),$$

and

$$y_p^2 = 4Fz_p,$$

for the intersection of line r_2 and the parabola.

If the wave is polarized parallel to the ground plane, the phase of the reflected wave at P lags the reference field, the line source, by $\beta(r_1 + r_2) + \pi$. For vertically polarized waves there is no phase shift at the ground plane and the phase lag at P is $\beta(r_1 + r_2)$.

The final expression for the total electric field intensity at P for horizontal polarization is

$$\bar{E}_i = \bar{i}K_1 \eta \sqrt{P_t\, G(x)} \left\{ \left[\frac{G(\psi)}{\rho} \right]^{\frac{1}{2}} \epsilon^{-j\beta\rho} + \left[\left| \frac{R_1}{r_2 + R_1} \right| \frac{G(\phi)}{r_1} \right]^{\frac{1}{2}} \epsilon^{-j\,[\beta(r_1 + r_2) + \pi]} \right\}. \tag{10}$$

For vertical polarization, the total magnetic field is

$$\bar{H}_i = \bar{i}K_1 \sqrt{P_t\, G(x)} \left\{ \left[\frac{G(\psi)}{\rho} \right]^{\frac{1}{2}} \epsilon^{-j\beta\rho} + \left[\left| \frac{R_1}{r_2 + R_1} \right| \frac{G(\phi)}{r_1} \right]^{\frac{1}{2}} \epsilon^{-j\beta(r_1 + r_2)} \right\}. \tag{11}$$

Equations (10) and (11) and the geometry of the reflector, such as shown in Figure 8, are used to find the incident magnetic field intensity at the surface of the parabolic cylinder. The far field is then expressed in terms of this magnetic field.

CHAPTER III

NEAR-FIELD MEASUREMENT TECHNIQUES AND COMPARISON OF CALCULATED AND MEASURED FIELDS

The general problem of near-zone measurements is to sample accurately a given field distribution by means of a small probe or coupling loop.[13] The presence of the sampling element always alters the original field distribution to some extent, so the smaller the sampling element the better. However, as the size of the probe or loop is decreased, the power output of the radio-frequency source must be increased to give the same reading on the indicating instrument. The size and orientation of the transmission line between the sampling element and the detector is alsc very important from the standpoint of altering the original field. Parallel-wire lines are unsatisfactory at microwave frequencies, so small coaxial cables should be used. The far-field calculations in Chapter IV require that the magnetic field incident on the reflector surface be known. However, the magnetic field is difficult to measure because the small loops required for such measurements have very poor impedence properties and thus require an excessively high-power RF source to give accurate readings at points of low field intensity. The measurements in these experiments are performed with a small dipole antenna which measures the electric field intensity. If the measured electric field intensities agree with the calculated values, it follows that the calculated magnetic fields are also correct.

Waves polarized normal to the axis of the parabola.--The apparatus used to measure the relative electric field intensity around a line source polarized parallel to the narrow dimension of the feed is shown in Figure 9. This condition corresponds to vertical polarization when the horn is in its normal position in the completed antenna. A type 723A/B reflex Klystron oscillator furnished energy to the horn through a variable attenuator, not shown. The waveguide horn had a small dielectric lens in the mouth to create an equiphase surface over the horn aperture. The height of the pick-up antenna above the plexiglass template was the same height as the center of the horn. The pickup antenna could be moved circumferentially and radially. The axis of rotation of the support arm did not necessarily go through the exact end of the horn, because the center of feed[14] is inside the mouth of the horn. A small, 0.083 inch OD, rigid, vertical coaxial cable supported the dipole and touched the parabolic template. This plexiglass template caused very little reflection and served only as a guide to facilitate movement of the dipole along the parabolic path. The RF source (frequency = 9300 mcps) was amplitude modulated by a 1,000 cps square wave. The output of the bolometer detector, which was connected to the output of the rigid coaxial cable, was applied to a narrow-band amplifier, Hewlett-Packard model 415B. Since the diameter of the small coaxial cable, normal to the E-field, was only 0.065 wavelengths, the perturbation error introduced was small. As a verification of this, the coaxial line was covered with an absorbing cloth and no differences in readings were discernable. The sampling half-wave dipole, perpendicular to the radius arm ρ, was 0.63 inch long and had an associated quarter-wave balun to prevent RF currents

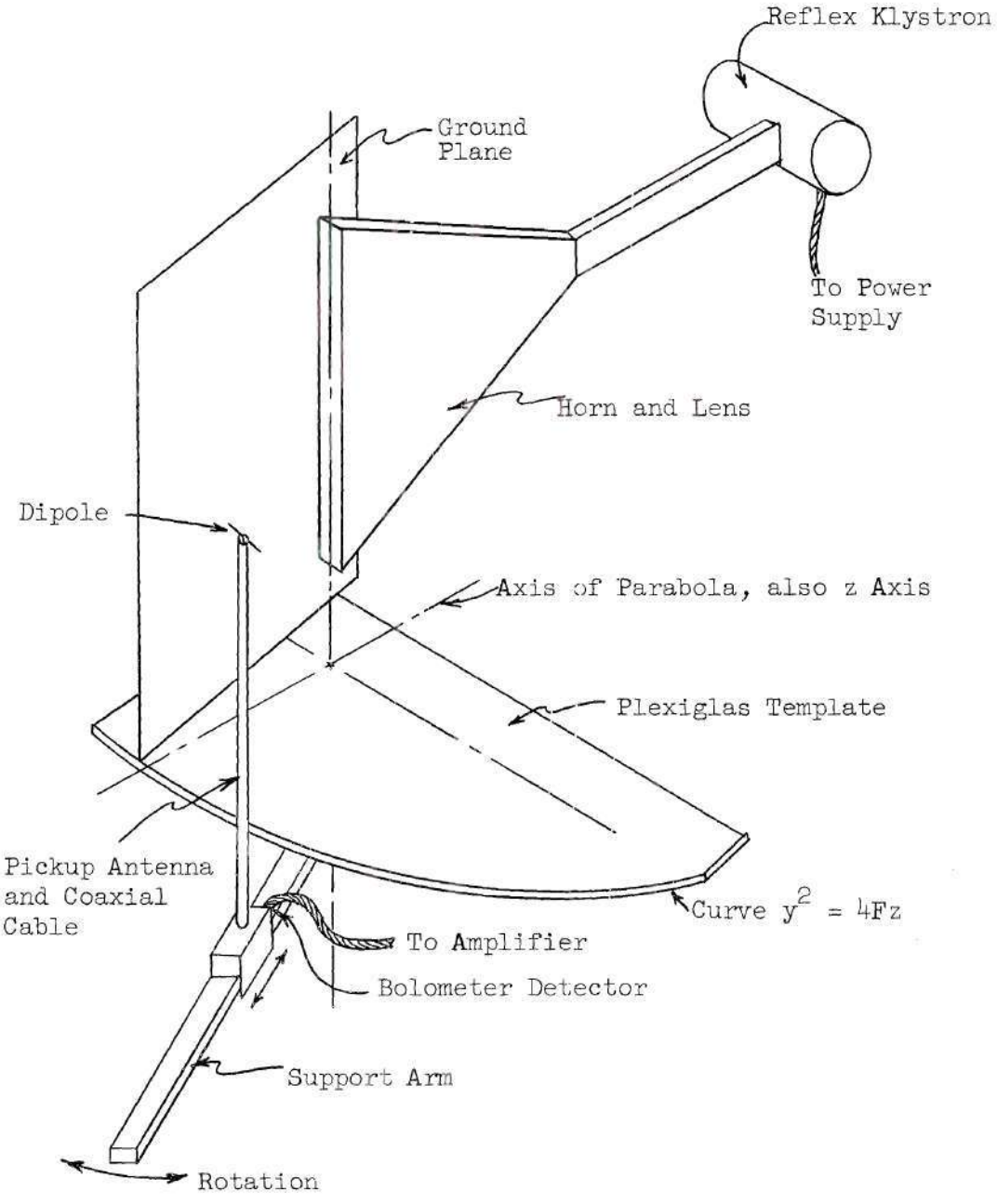

Figure 9. Apparatus for Measuring Near Fields above a Ground Plane

from moving down the outside of the coaxial line.

When the apparatus in Figure 9 is functioning properly, the meter reading on the 415B amplifier should be proportional to the square of the peak value of the electric field intensity parallel to the pickup dipole. The squared relation is due to the square-law bolometer detector used to demodulate the RF waves. Of course, the actual meter reading depends on the power transmitted, the impedance match of the RF receiving system, and the gain setting of the amplifier. The procedure used in taking the measured data in Figures 11, 12, 13, 14(b), and 16 was to adjust the gain setting of the amplifier and power output of the transmitter so that a fixed reference field intensity was obtained with the ground plane removed and the dipole at $y = 0$. The ground plane was then put into position and readings were taken at various values of y without making any change in the gain setting of the amplifier. After the readings were taken, the ground plane was removed and the field at $y = 0$ was measured again to see if there had been any change in the power output of the generator.

It can be seen from Figure 10, which shows the top view of the apparatus shown in Figure 9, that the total theoretical electric field intensity at the dipole will not be parallel to the dipole. The E-vector resulting from direct radiation from the horn is perpendicular to ρ and hence parallel to the dipole, but the E-vector reflected from the ground plane is perpendicular to r and thus makes an angle $(\xi - \psi)$ with the dipole. Thus the total component of the electric field parallel to the dipole is the phasor sum of $\dot{E}_d$ and $\dot{E}'_d \cos(\xi - \psi)$. The dot over the E shows it is a phasor quantity. $\dot{E}_d$ and $\dot{E}'_d$ are the direct and reflected

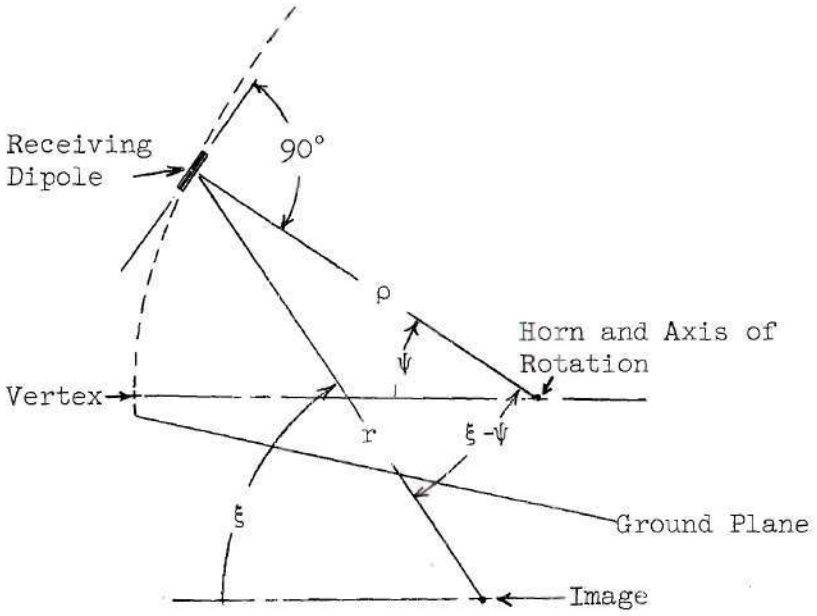

Figure 10. Orientation of the Feed, Ground Plane, and Receiving Dipole

electric fields which are related to the $\dot{H}_d$ and $\dot{H}'_d$ quantities in Equation (3) by the intrinsic impedance of free space. Since the dipole moves in the x = 0 plane, the theoretical E-field component parallel to the dipole, $\dot{E}_{par}$, is

$$\dot{E}_{par} = \eta K_1 \sqrt{P_t\, G(0)} \left\{ \left[\frac{G(\psi)}{\rho} \right]^{\frac{1}{2}} \epsilon^{-j\beta\rho} + \left[\frac{G(\phi)}{r} \right]^{\frac{1}{2}} \epsilon^{-j\beta r} \cos(\xi - \psi) \right\}. \quad (12)$$

Since the dipole is moved along the parabolic path and since ψ, ϕ, ρ, and r can all be expressed in terms of y, the field as given by Equation (12) can be found in terms of y. Of course, ϕ and r are also functions of the position of the ground plane; but, for any one ground-plane position, ϕ and r can be expressed in terms of y and parameters.

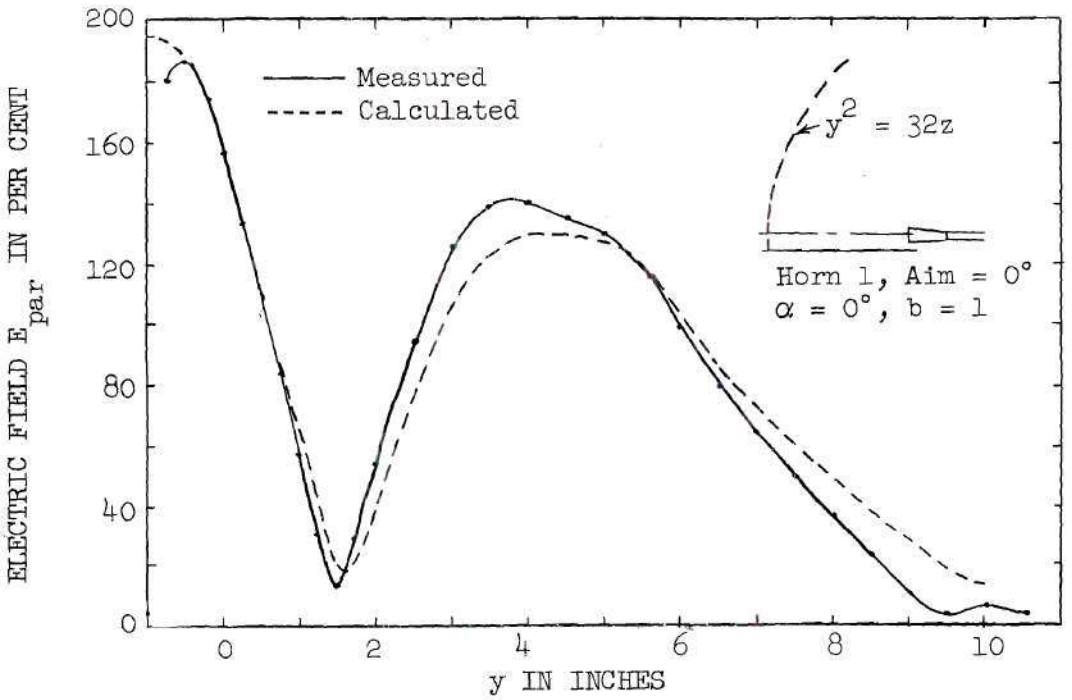

Figure 11 (a)

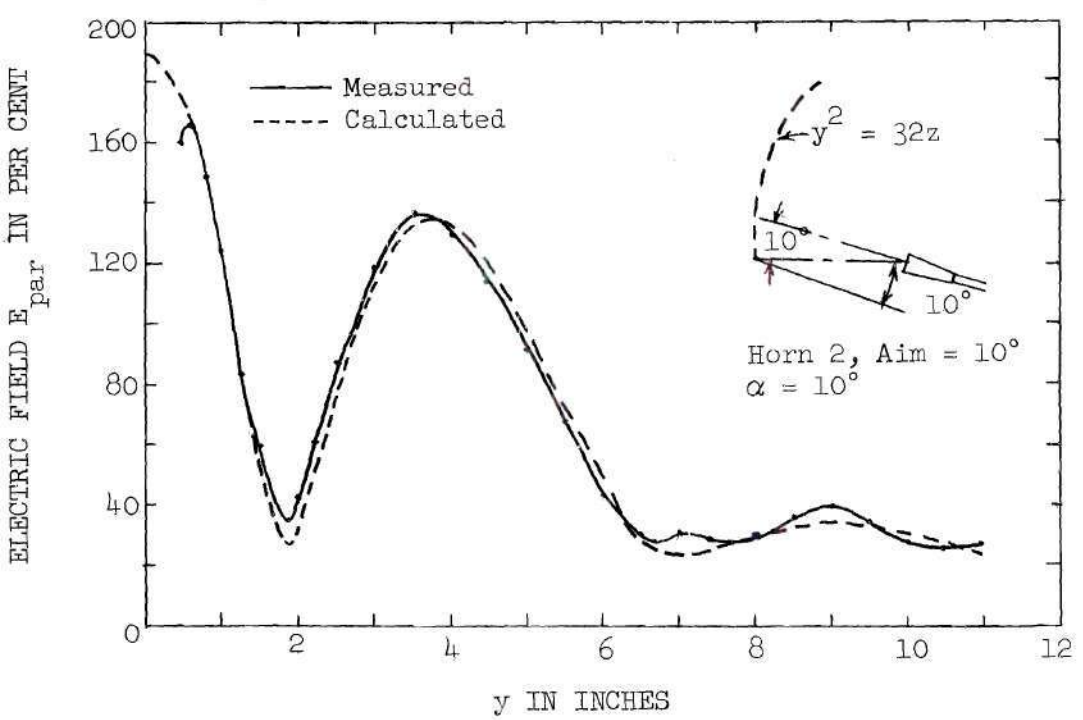

Figure 11 (b). Near Field Above a Ground Plane (Vertical Polarization)

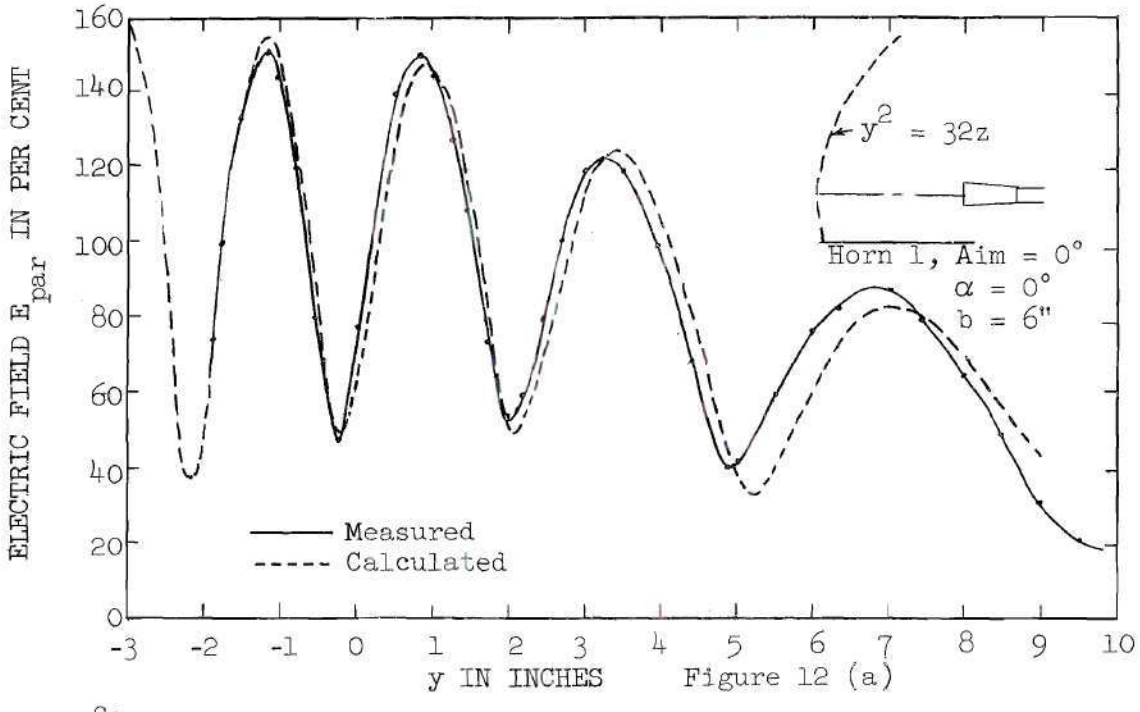

Figure 12 (a)

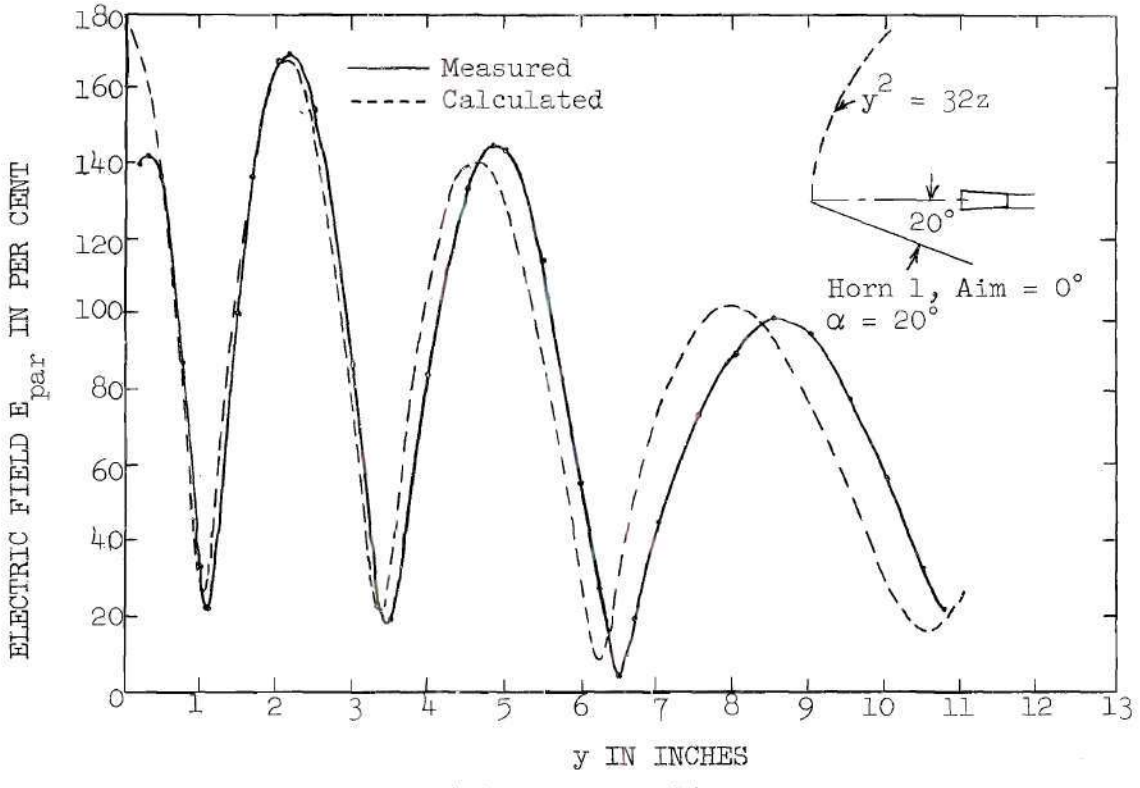

Figure 12 (b). Near Field Above a Ground Plane (Vertical Polarization)

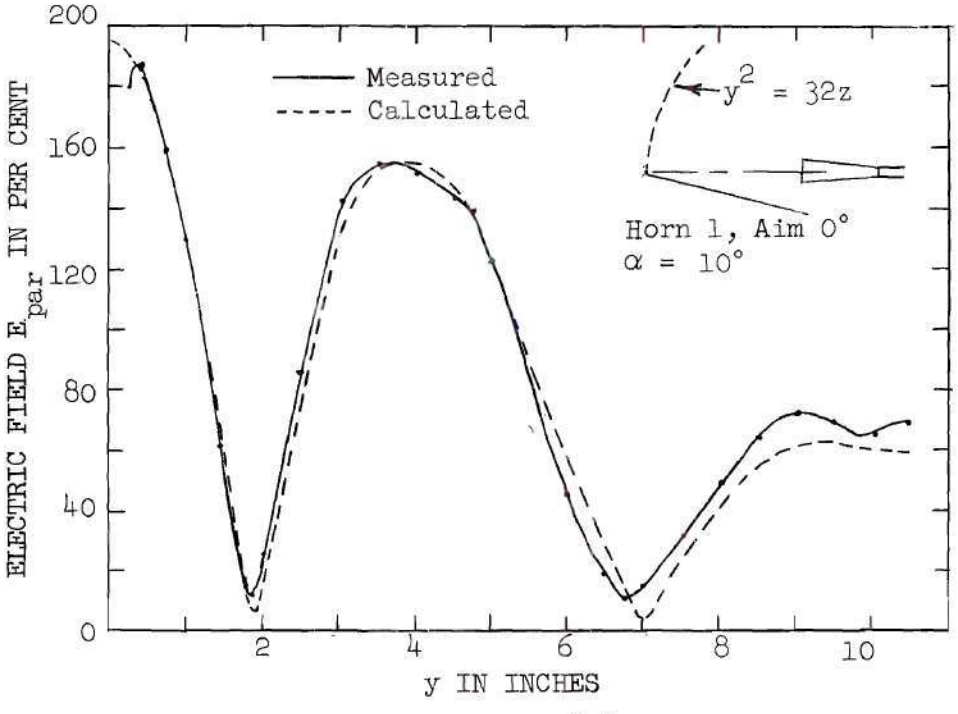

Figure 13 (a)

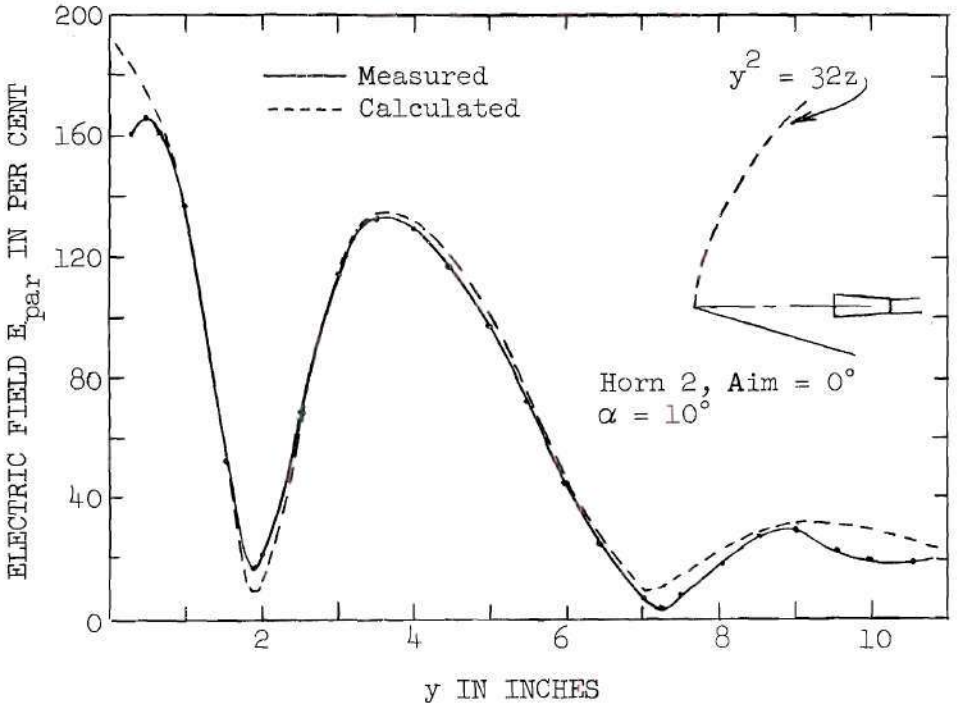

Figure 13 (b). Near Field Above a Ground Plane (Vertical Polarization)

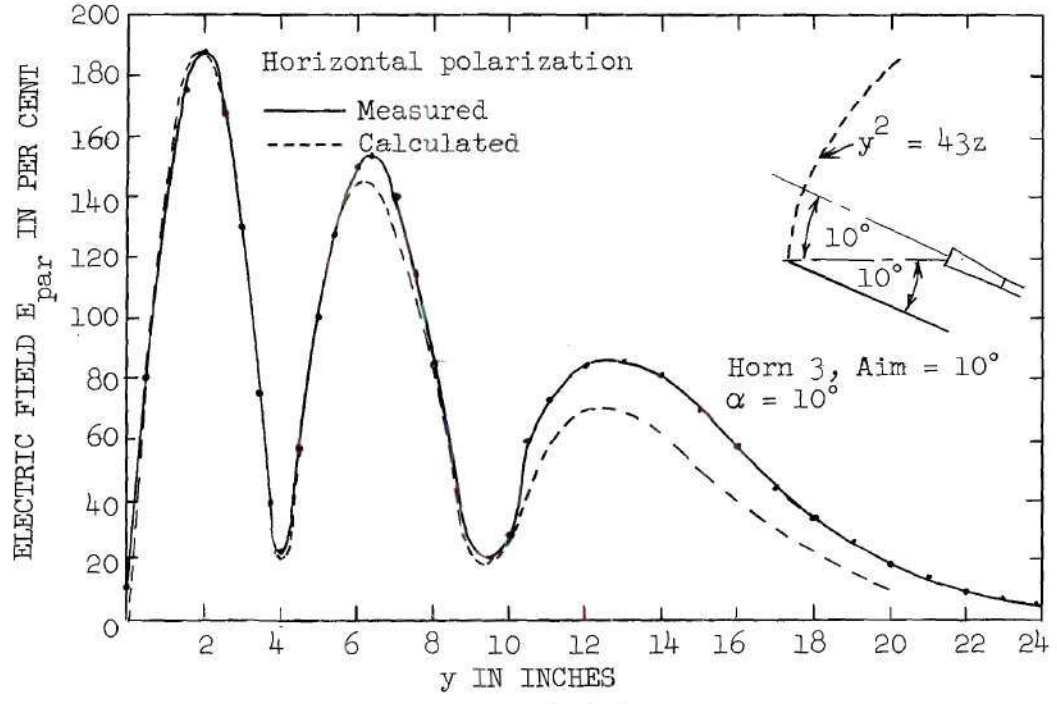

Figure 14 (a)

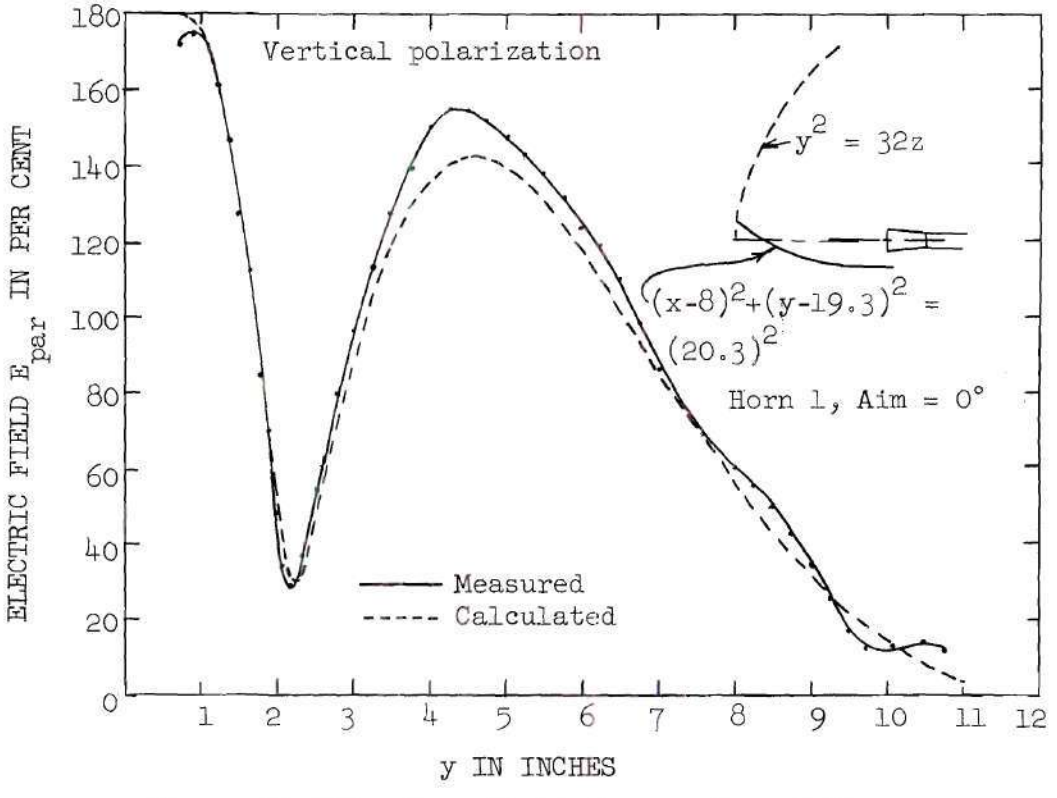

Figure 14 (b). Near Field Above a Ground Plane

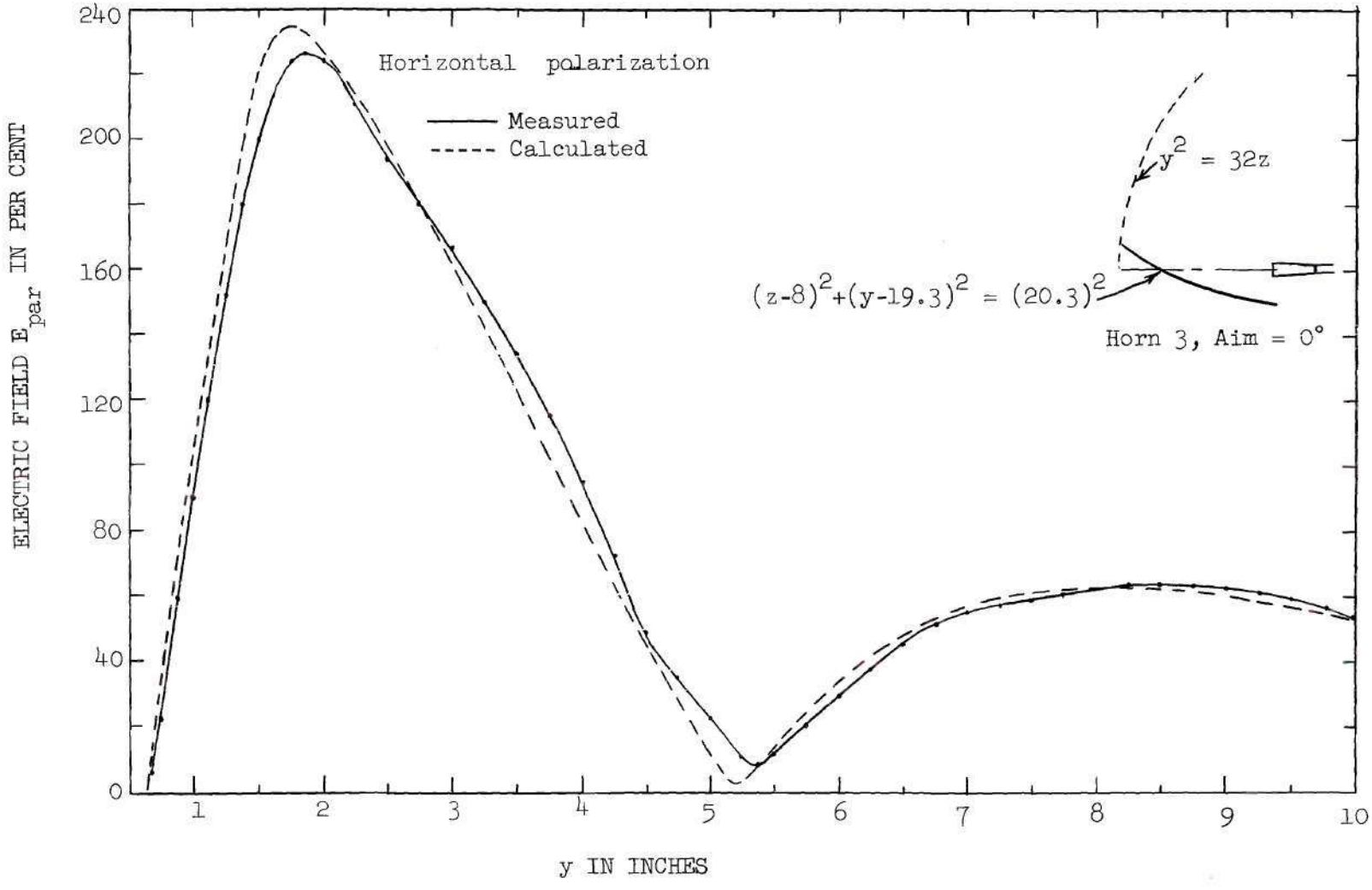

Figure 15. Near Field Above a Ground Plane

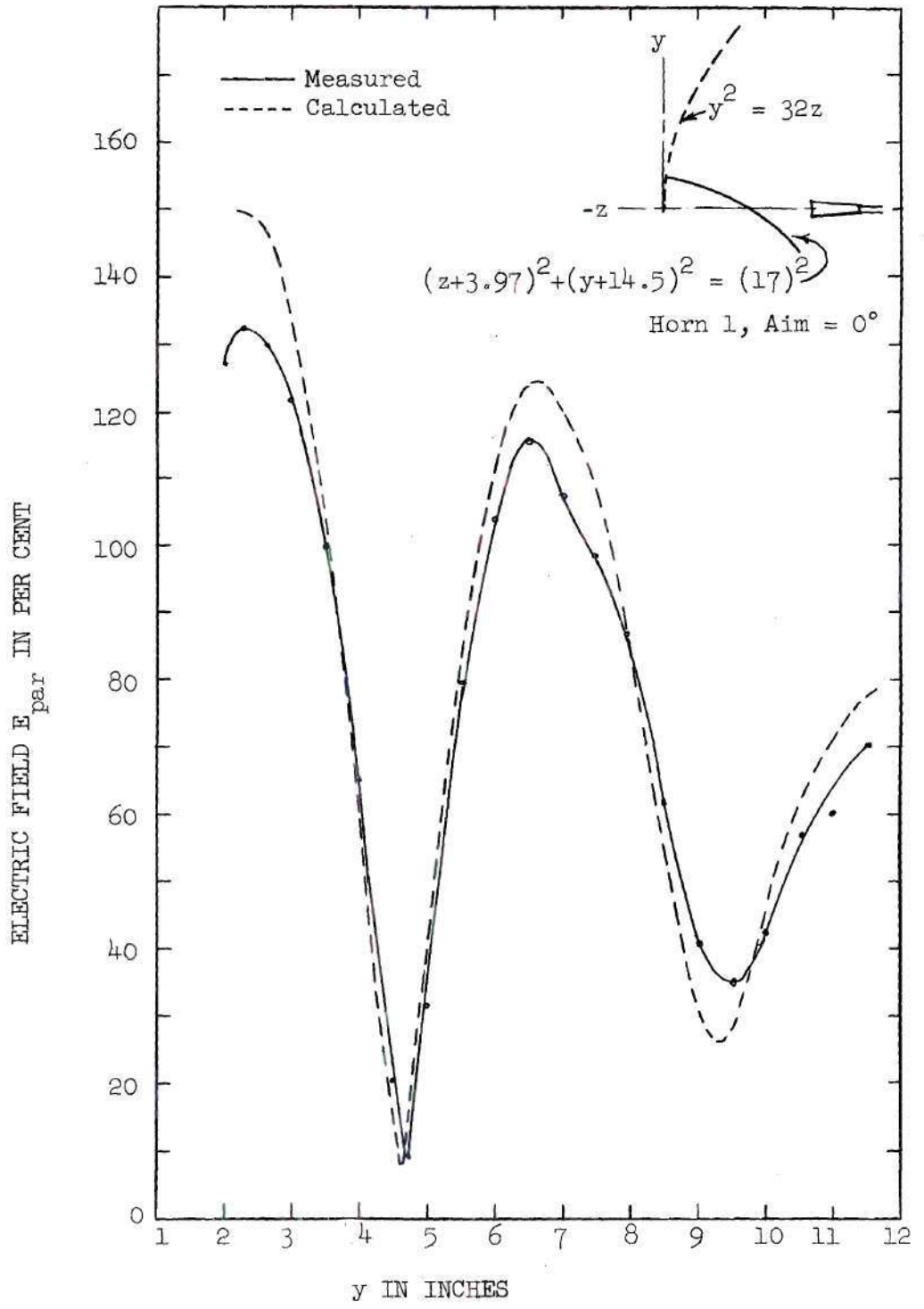

Figure 16. Near Field Above a Ground Plane (Vertical Polarization)

The theoretical values of the field intensity parallel to the dipole can be calculated in a reasonable time by programming a digital computer to find $\dot{E}_{par}$ in terms of y and then repeating the problem at intervals close enough to obtain sufficient data to plot a curve of field intensity vs. y. To be consistent with the measured results, the calculated fields are normalized by using the field at y = 0 with no ground plane as the reference or 100 per cent value. The calculated fields as shown in Figures 11, 12, and 13 were calculated using Equation (12), which holds only for the field above a flat ground plane. The measured radiation patterns of the horns, see Figure 29, were used to obtain the functions of $G(\psi)$ and $G(\phi)$.

The fields above the curved ground planes as shown in Figures 14(b) and 16 cannot be calculated by using Equation (12), but Equation (11) can be easily modified to give the field above the curved ground plane. The second term in Equation (11) is changed by multiplying it by $\cos(\xi - \psi)$ to get the component of this field parallel to the dipole. Thus the calculated fields $\dot{E}_{par}$ in Figures 14(b) and 16 were obtained from

$$\dot{E}_{par} = \eta K_1 \sqrt{P_t\, G(0)} \left\{ \left[\frac{G(\psi)}{\rho} \right]^{\frac{1}{2}} \epsilon^{-j\beta\rho} + \left[\left| \frac{R_1}{r_2 + R_1} \right| \frac{G(\phi)}{r_1} \right]^{\frac{1}{2}} \cos(\xi - \psi)\, \epsilon^{-j\beta(r_1 + r_2)} \right\} . \tag{13}$$

The excellent agreement between the calculated and measured fields above the ground planes excited by a vertically polarized source justifies the assumption that geometrical optics can be used to calculate the

magnitude and phase of the waves reflected from the ground planes having a large radius of curvature. The reasons for the small differences in the calculated and measured curves will be discussed in the next section.

As mentioned earlier, the magnetic field is of more interest than the electric field, but because of practical difficulties it was necessary to measure the electric field. The agreement between the calculated and measured electric fields proves the validity of this method of calculating reflections, so it follows that the magnetic field can be accurately calculated using the same procedure.

Sources of error for vertical polarization.--There are five points to be discussed which explain why the calculated and measured fields shown in the previous figures were not in exact agreement.

(1). Field calculations were made assuming the horn radiation emanates from a line source. The horn aperture is not a line, but in the quasi-radiation zone the waves are treated as emanating from some "center of feed," a somewhat nebulous and partially fictitious quantity. Figure 17 shows an enlarged cross section view of a typical feed. If a receiving antenna is rotated at some fixed distance R_p from the center of feed, the phase of the voltage induced in the antenna will be constant. Over limited angles, the radiation from the horn can be treated as coming from a center of feed inside the mouth of the horn. Obviously the fields at angles greater than ψ_{max} cannot be treated as coming from the center of feed, but fortunately the low energy levels at such large angles are often of secondary importance.

(2). For the polarization shown in Figure 9, one end of the dipole antenna touches the ground plane when the center of the dipole is

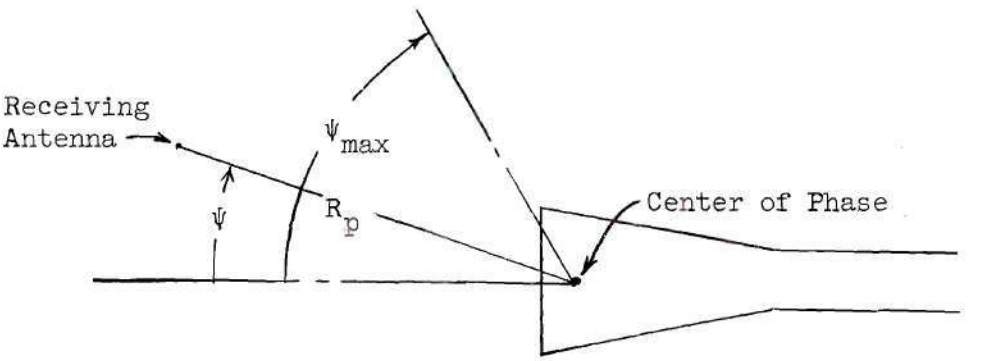

Figure 17. Cross-section View of a Line-source Type Feed

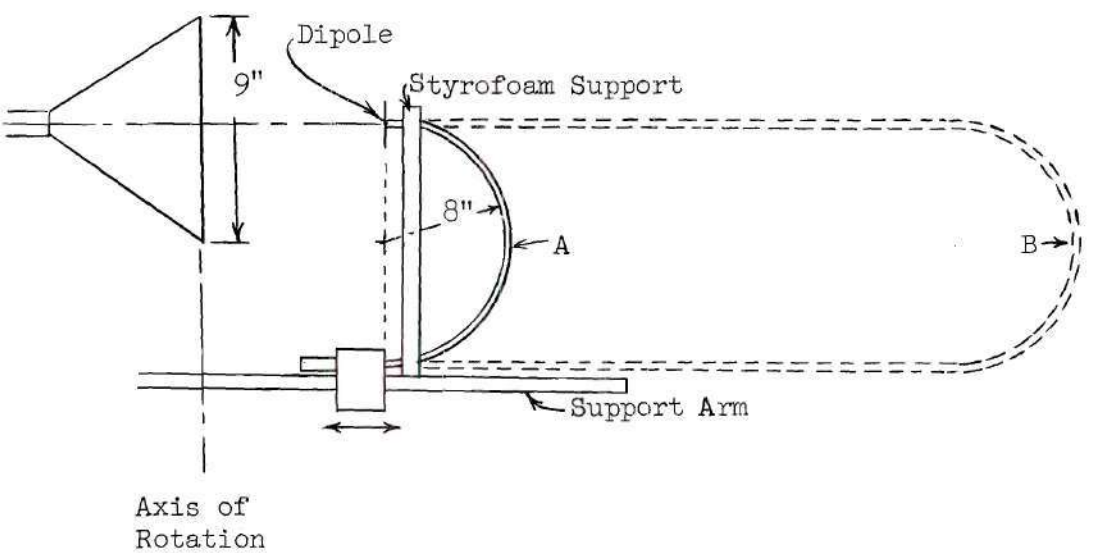

Figure 18. Near-field Apparatus for Measuring Electric Field From Source Polarized Parallel to Long Dimension of Source

0.32 inch above the ground plane. The proximity of the dipole to the ground plane accounts for the discrepancy between the calculated and measured fields at values of y just above the ground plane.

(3). The averaging error caused by the finite length, 0.63 inch, of the dipole might seem to eliminate the possibility of measuring the field intensities at the sharp minima shown in Figures 11 and 12. However, this is not true because there is a rapid phase variation with y at the minima, and the net voltage induced in the dipole is proportional to an average of the field intensity along the dipole. At a true null, for example, there is a 180 degree phase reversal of the electric field intensity, so the field intensity at one side of and close to the null is almost the negative of the field an equal distance on the other side of the null. Thus the average field over the length of the short dipole could be almost zero and the measured field would be very near the true field at the null. The agreement between the measured and calculated minima in Figures 11 through 16 shows the averaging error is not serious.

(4). The presence of the sampling dipole assembly always alters the original field to some extent and causes a perturbation error. However, the very small cable leading to the dipole is perpendicular to the E-vector and thus gives almost no reflections. The only part of the sampling dipole assembly that causes any appreciable reflection is the dipole itself. The dipole was made as small as practicable to reduce this error to a minimum.

(5). Reflections from surrounding objects always cause errors in the readings at the minima. However, by proper orientation of equipment

in a room 25 by 40 feet, it was possible to reduce reflection errors to 0.2 to 0.5db at energy levels 25db below the maximum. These figures are based on measurements made indoors and outdoors for the same ground-plane, horn settings.

Waves polarized parallel to ground plane.--The measurement problem is simplified when the electric field intensity is parallel to the surface of the ground plane. First, the dipole is also parallel to the ground plane, so measurements can be made at the surface of the ground plane. Second, the height of the dipole is constant as y varies, and the averaging error caused by the finite length of dipole is common to all readings and does not affect the curves of Figures 14(a) and 15. The averaging errors due to the dimensions of the antenna in the plane of rotation are negligible because the diameter of the dipole is only 0.0004 wavelengths.

The only complicating factor associated with this polarization is the perturbation of the field caused by the coaxial cable supporting the dipole. A vertical coaxial cable similar to the one shown in Figure 9 is not satisfactory, regardless of the diameter of the cable. A desirable coaxial-cable feed is shown by the dotted line B in Figure 18, but the mechanical problems involved do not warrant its use. The shorter cable A is far enough back of the dipole to minimize reflections from the cable and short enough to provide some mechanical support. Additional mechanical support is provided by a styrofoam rod between the coaxial cable at the dipole and the detector mount. Readings made with and without the styrofoam support showed it has no measurable effect on the field at the dipole.

It is not possible to measure the field caused by the image system alone, but the reliability of this method of field calculation is justified by the data presented in Figures 11 through 16. The positions and magnitudes of the minima in these experiments are very sensitive to the position of the center of feed of the horn. This position is not precisely known. By trial and error adjustment of the horn position, the agreement between calculated and measured values can be made even better than that shown in the figures.

CHAPTER IV

THE FAR FIELD IN TERMS OF THE REFLECTOR CURRENT DISTRIBUTION

The far field of an aperture-type antenna of maximum dimension D is not well-defined, but it is usually taken as that region greater than $2D^2/\lambda$ from the antenna. The problem of finding the far field of such an antenna is usually solved by use of one of two methods, both of which use geometrical optics to find the fields near to or on the antenna. The first method is the aperture-field method[15] which evaluates the far field by first assuming a closed surface, near to and enclosing the antenna, to be made up of a set of infinitesimal electric and magnetic current radiators, and then performing a vector-phasor summation of the effects of all the radiators on the surface. In cases where the surfaces are large compared to a wavelength, the individual radiator on the surface is often treated as a Huygens source. The aperture-field method is useful to calculate the beam from a surface which has a zero field over all parts except one side which is a flat equiphase surface. For this type of problem, the equations developed in nearly any antenna book can be used with no modification, so that no detailed treatment of this method is presented here. The second method is the current-distribution method, which treats the currents on the antenna surface as a set of infinitesimal electric current radiators and expresses the far field as a vector-phasor summation of the contributions from all the individual radiators. Because ray theory, which

is approximate at microwave frequencies, is applied twice to calculate the fields on the closed surface associated with the aperture-field method and is applied only once to calculate the currents used in the current-distribution method, the current-distribution method is the more accurate of the two methods when applied to far-field calculations of image beam-shaping antennas. For all but the equiphase apertures, where the aperture-field method is best, there is little difference between the complexity of the two methods, since both involve very complicated integrals. The purpose of this chapter is to adapt the general current-distribution equations to cylindrical reflectors fed by line sources.

The current-distribution method.--In this analysis, the current-distribution method of obtaining scattered fields is applied to a reflector which will be treated as a perfect conductor. This method sums the effects of contributions of three source distributions: (1) the surface electric currents over the reflector suface, (2) the surface electric charges on the reflector surface, and (3) the line-charge distribution around the reflector boundary. Silver[16] shows that if the current and charge distributions satisfy the equation of continuity of current, the scattered fields can be expressed in terms of the currents alone. The scattered field intensity in the far field given in terms of the incident magnetic field intensity $\bar{H}_i$ on the reflector S_o, shown in Figure 19, is[17]

$$\bar{E}_s = \frac{-j\omega\mu}{2\pi R_o} \epsilon^{-j\beta R_o} \int_{S_o} \left\{ (\bar{n}\times\bar{H}_i) - \left[(\bar{n}\times\bar{H}_i)\cdot\bar{r}_1 \right]\bar{r}_1 \right\} \epsilon^{j\beta(\bar{\rho}+\bar{i}x)\cdot\bar{r}_1} \, ds. \quad (14)$$

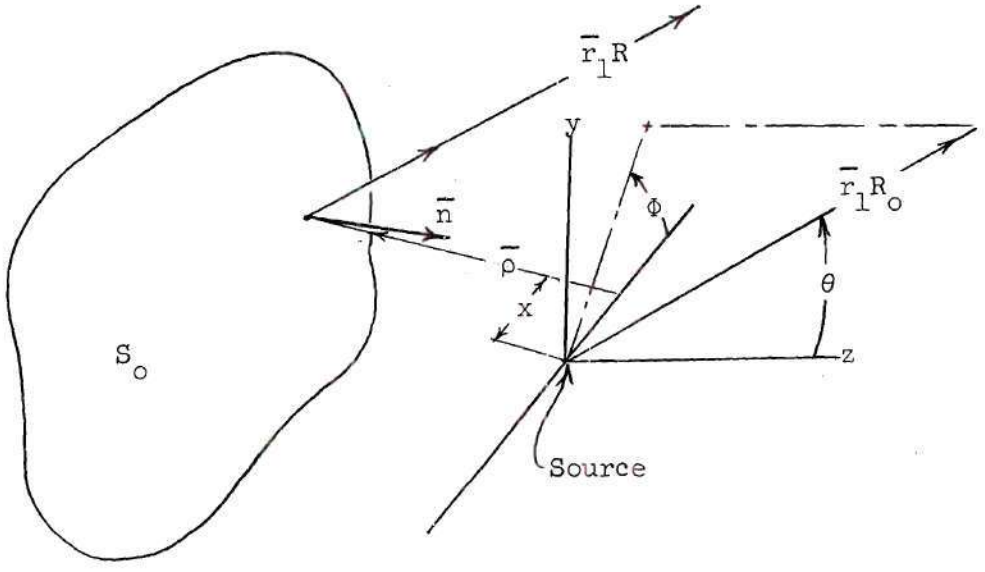

Figure 19. Reflector-feed Geometry

$\bar{E}_s$ is the scattered far-field electric field intensity, β is $2\pi/\lambda$, and $\bar{H}_i$ is the magnetic field intensity incident at the reflector surface. Equation (14) can be expressed in terms of currents by applying the well-known relationship

$$\bar{K} = 2(\bar{n} \times \bar{H}_i), \tag{15}$$

where $\bar{K}$ is the surface current density in amperes per meter.

It is well known that in the far field, the electric and magnetic fields are mutually perpendicular to each other and to the direction of propagation of energy, i.e., the two fields have no radial components involving 1/R. In the following section, relationships are developed (1) to show that the scattered far field as given by Equation (14) has only com-

ponents transverse to $\bar{r}_1$ and (2) to adapt this equation to cylindrical surfaces. The analyses for horizontal and vertical polarization differ, so they will be treated separately.

Vertical polarization.--For a wave linearly polarized in the vertical plane, the magnetic field intensity incident on the surface of the reflector in Figure 20 is

$$\bar{H}_i(\rho,\psi,x) = \bar{i}\dot{H}_i(\rho,\psi,x), \tag{16}$$

and the conduction current on the reflector is in the direction of the unit vector $\bar{\tau}$ which is tangent to the surface. It follows that

$$\bar{r}_1\left[(\bar{n}x\bar{H}_i)\cdot\bar{r}_1\right] = \bar{r}_1\left[(\bar{n}x\bar{i})\cdot\bar{r}_1\dot{H}_i\right] = \bar{r}_1(\bar{\tau}\cdot\bar{r}_1)\dot{H}_i = \bar{r}_1\dot{H}_i\cos u, \tag{17}$$

where u is the angle between $\bar{\tau}$ and $\bar{r}_1$. The vector $(\bar{n}x\bar{H})$ can also be expressed in spherical coordinates as

$$\bar{n}x\bar{H}_i = \bar{\tau}\dot{H}_i = \dot{H}_i(\bar{r}_1\cos u + \bar{\theta}_1\sin u), \tag{18}$$

where $\bar{r}_1$, $\bar{\theta}_1$, and $\bar{\Phi}_1$ are the three unit vectors used in a standard spherical coordinate system. From the information in Equations (17) and (18) it can be shown that the integrand of Equation (14) has only a $\bar{\theta}_1$ component and hence can be written

$$\dot{E}_{s\theta} = \frac{-j\omega\mu}{2\pi R_o}\epsilon^{-j\beta R_o}\int_{S_o}\dot{H}_i(\rho,\psi,x)\sin u\,\epsilon^{j\beta(\bar{\rho}+\bar{i}x)\cdot\bar{r}_1}\,ds. \tag{19}$$

Also $(\bar{\rho}+\bar{i}x)\cdot\bar{r}_1$ can be simplified by expressing $\bar{r}_1$ and $\bar{\rho}$ in terms of rectangular coordinates as

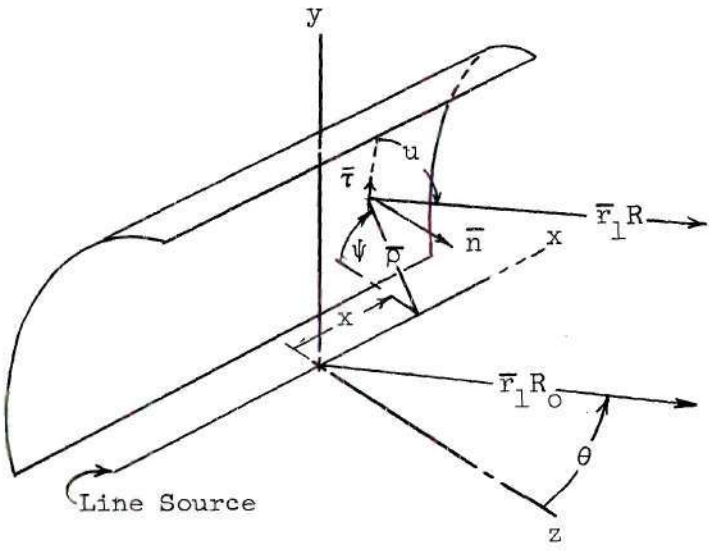

Figure 20 (a)

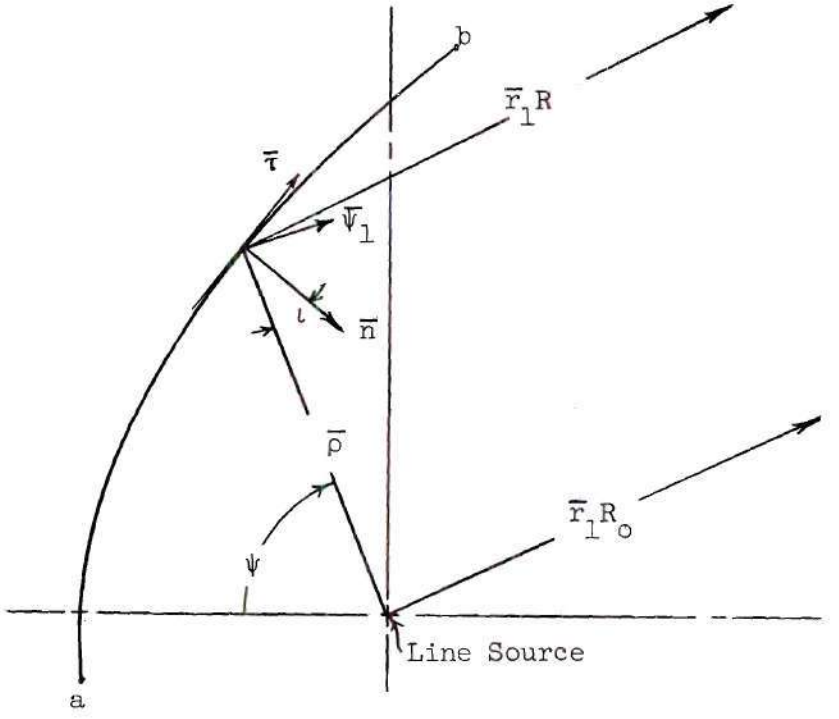

Figure 20 (b). Geometry for a Cylindrical Reflector Fed by a Line Source

$$(\bar{\rho}+\bar{i}x)\cdot\bar{r}_1 = (\bar{i}x + \bar{j}\rho \sin\psi - \bar{k}\rho\cos\psi) \cdot(\bar{i}\cos\Phi\sin\theta + \bar{j}\sin\Phi\sin\theta + \bar{k}\cos\theta) \tag{20}$$

$$= x\cos\Phi\sin\theta + \rho\sin\Phi\sin\psi\sin\theta - \rho\cos\psi\cos\theta.$$

If $\bar{r}_1$ is in the y-z plane, $\Phi = \pi/2$, and

$$(\bar{\rho}+\bar{i}x)\cdot\bar{r}_1 = -\rho\cos(\psi+\theta). \tag{21}$$

The reflector is in the quasi-radiation zone of the line feed, so the expression for the magnetic field is separable into the product of two functions as in Equation (1). However, it is convenient to express the incident magnetic field $\dot{H}_i(\rho,\psi,x)$ in terms of the product of two functions $N(x)$ and $\dot{M}(\rho,\psi)$, instead of $G(x)$, $\frac{G(\psi)}{\rho}$, and $\epsilon^{-j\beta\rho}$, so let

$$\dot{H}_i(\rho,\psi,x) = N(x)\,\dot{M}(\rho,\psi). \tag{22}$$

The units for $N(x)$ and $\dot{M}(\psi,\rho)$ are not important because these terms are used only to calculate radiation patterns where units are unimportant. By using Equations (21) and (22), the scattered field can be written as

$$\dot{E}_{s\theta} = \frac{-j\omega\mu}{2\pi R_o}\,\epsilon^{-j\beta R_o}\int_{-\frac{\ell}{2}}^{\frac{\ell}{2}} N(x)\,dx \int_{\text{path a-b}} \dot{M}(\rho,\psi)\sin u\;\epsilon^{-j\beta\rho\cos(\psi+\theta)}\,d\ell. \tag{23}$$

This equation gives the magnitude and phase of the scattered field in terms of the reference distance R_o measured from the center of the line

feed. In many cases the numerical evaluation of the integrals is simplified by putting the origin at some other point. By referring to Figure 20(b), it is evident that

$$R_o + \rho \cos(\theta + \psi) = R, \tag{24}$$

when $\bar{r}_1$ is the y-z plane. After substitution of this relationship into Equation (23), the scattered field equation becomes

$$\dot{E}_{s\theta} = \frac{\dot{C}}{R_o} \int_{\text{path a-b}} \dot{M}(\rho,\psi) \sin u \, \epsilon^{-j\beta R} \, d\ell, \tag{25}$$

where

$$\dot{C} = \frac{-j\omega\mu}{2\pi} \int_{-\frac{\ell}{2}}^{\frac{\ell}{2}} N(x) \, dx. \tag{26}$$

An examination of the integrand of Equation (25) shows that it has the same form as the radiation field of an infinitesimal electric dipole carrying a current proportional to $\dot{M}(\rho,\psi)$. The function $\dot{M}(\rho,\psi)$ does not have the units of current, but it is directly proportional to current on the reflector surface. To show this, consider a reflector with no ground plane fed by a single line source as shown in Figure 20. An inspection of the magnetic field intensity incident on the surface of the reflector, given in Equation (1), shows that

$$\dot{M}(\rho,\psi) = \left[\frac{G(\psi)}{\rho}\right]^{\frac{1}{2}} \epsilon^{-j\beta\rho}, \tag{27}$$

if

$$N(x) = K_1\left[P_i G(x)\right]^{\frac{1}{2}}. \tag{28}$$

Since the magnetic field is proportional to $\left[\frac{G(\psi)}{\rho}\right]^{\frac{1}{2}}$ and the surface current density equals the tangential component of $\bar{H}$ incident on the surface, the total $\bar{H}$ for this polarization, certainly $\dot{M}(\rho,\psi)$ is proportional to the current on the surface for this case. This condition and the common form of the far field of an electric dipole and the integrand of Equation (25) warrant calling $\dot{M}(\rho,\psi)$ a "current". So even though this function is not a true current, it behaves as one and will be written as

$$\dot{M}(\rho,\psi) = I(y)\epsilon^{j\phi(y)}. \tag{29}$$

When the ground plane is added to the reflector, the expression for $\dot{M}(\rho,\psi)$ is more complicated than that given by Equation (27), but it can still be calculated using the formulas given in Chapter II. Thus the form of the far-field integral for $\dot{E}_{s\theta}$ is written as

$$\dot{E}_{s\theta} = \frac{\dot{C}}{R_o} \int_{\text{path a-b}} \left[I(y)\epsilon^{j\phi(y)} \right] \sin u \; \epsilon^{-j\beta R} \, d\ell. \tag{30}$$

Theoretically, each part of the integrand in Equation (30) can be expressed in terms of y, z, and θ, and if the reflector-surface cross section is $y = f(z)$, the integrand can be expressed in terms of a single variable y and the parameter θ. This is demonstrated in the following pages by considering the reflector to be a cylindrical parabola. The

following relationships given by Equation (31) apply to the parabola shown in Figure 21.

$$\left.\begin{aligned} &\tan\delta = \frac{dy}{dz}, \qquad \sin\delta = \frac{dy}{d\ell}, \qquad \cos\delta = \frac{dz}{d\ell}, \\ &d\ell = \left[1 + \left(\frac{dz}{dy}\right)^2\right]^{\frac{1}{2}} dy, \qquad \tan\nu = \frac{y}{z}, \qquad \sin\nu = \frac{y}{d}, \\ &\cos\nu = \frac{y^2}{4Fd}, \qquad R_v - R = d\cos(\nu - \theta), \qquad u = \delta - \theta, \\ &d\ell\sin(\delta - \theta) = dy\left(\cos\theta - \frac{y}{2F}\sin\theta\right), \\ &d\cos(\nu - \theta) = \frac{y}{4F}(y\cos\theta + 4F\sin\theta). \end{aligned}\right\} \tag{31}$$

When the relationships in Equation (31) are used to express the far-field integral in terms of y and θ, the form of the equation is

$$\dot{E}_{s\theta} = \frac{\dot{C}}{R_o}\epsilon^{-j\beta R_v}\int_{y_a}^{y_b} I(y)\left[\cos\theta - \frac{y}{2F}\sin\theta\right] \times \epsilon^{j\left[\frac{\beta y}{4F}(y\cos\theta + 4F\sin\theta) + \Phi(y)\right]}dy. \tag{32}$$

Equation (32) can be used to find the far field due to currents on the parabola caused by a line feed at the focal line or in any position parallel to the focal line, so long as the reflector is in the quasi-radiation zone of the feed.

Equation (32) is called the "final" form of the far-field integral for vertically polarized waves because this is the equation that

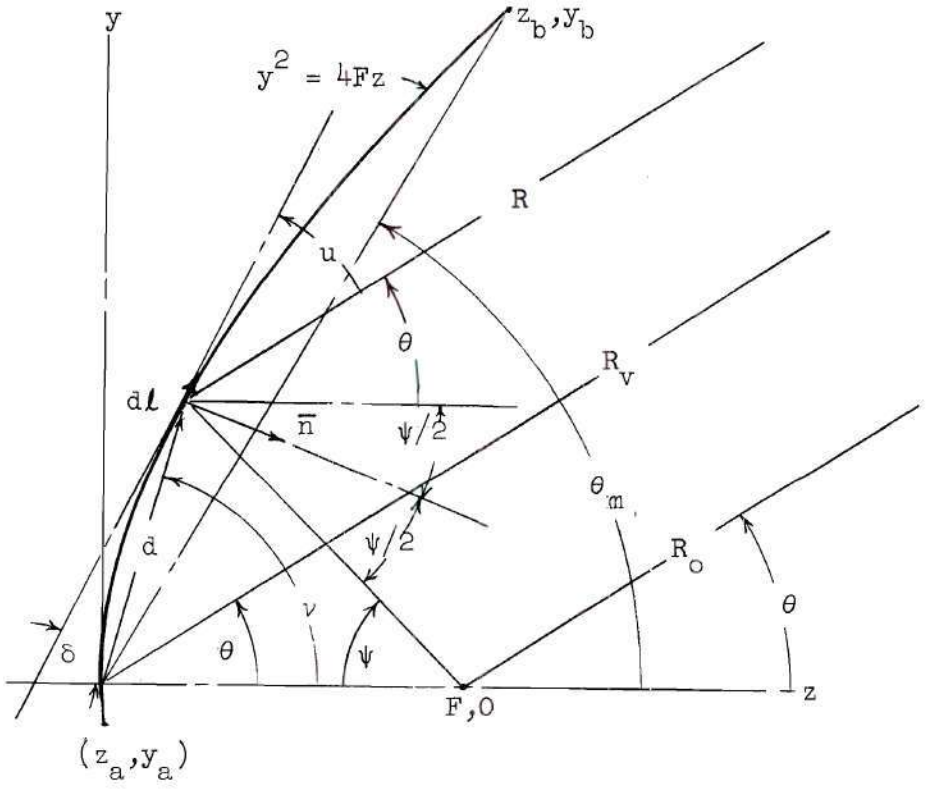

Figure 21. Parabolic-cylinder and Line-feed Geometry

will be used to calculate the shape of the main and image beams of the vertically polarized antenna discussed in Chapter VI. The current distribution due to direct radiation from the horn into the parabola is used to calculate the main beam, and a separate current distribution caused by energy reflected from the ground plane into the parabola is used to calculate the image beam. The reasons for not finding the sum of the main and image beams in one operation are discussed in Chapter VI. The integral, Equation (32), will be evaluated when a preliminary

problem is first worked to find the values of $I(y)$ and $\phi(y)$ at equally spaced intervals of y and then the integral is approximated by a finite summation of phasor terms. The far field will then be evaluated at selected values of θ to find the shape of the beam.

In the following paragraph, the "final" form of the far-field equation as given by Equation (32) will be simplified for the special case where the feed is at the focal line. Several approximations will be made to show the connection between the current-distribution and aperture-field methods of representing the far field of an antenna.

When a line feed is placed along the focal line of a cylindrical parabola with no ground plane, the "current" on the surface is given by

$$I(y)\epsilon^{j\phi(y)} = \left[\frac{G(\psi)}{\rho}\right]^{\frac{1}{2}} \epsilon^{-j\beta\rho}, \tag{33}$$

and

$$\rho = F + z = F + \frac{y^2}{4F}. \tag{34}$$

From the phase function $\phi(y)$ expressed in terms of F and y, the exponent of ϵ is Equation (32) is

$$j\beta\left[\frac{y^2}{4F}(\cos\theta - 1) + y\sin\theta - F\right].$$

For very small angles, this quantity can be approximated by $j\beta(y\sin\theta - F)$, since $(\cos\theta - 1) \approx 0$. This approximation is useful in calculating beam shapes for antennas very large compared to a wavelength, because for large antennas most of the radiation is restricted to a narrow region close to the axis of the parabola. Also for small

angles, $(\cos\theta - \frac{y}{2F}\sin\theta) \approx 1$, because $\sin\theta$ is very small and for most antennas y is less than 2F. From these approximations Equation (32) is written

$$\dot{E}_{s\theta} = \frac{\dot{C}}{R_o} \epsilon^{-j\beta(R_v+F)} \int_{y_a}^{y_b} \left[\frac{G(\psi)}{\rho}\right]^{\frac{1}{2}} \epsilon^{j\beta y \sin\theta}\, dy, \tag{35}$$

which is one form of the far field as given by the aperture-field method when applied to an equiphase surface. The magnitude of the integrand in Equation (35) is $\left[G(\psi)/\rho\right]^{\frac{1}{2}}$, and this term is directly proportional to the field intensity at the surface of the reflector. Because of the collimating properties of the parabola, $\left[G(\psi)/\rho\right]^{\frac{1}{2}}$ is also proportional to the field intensity on the equiphase aperture represented by the mouth of the parabolic reflector. For this reason, $\left[G(\psi)/\rho\right]^{\frac{1}{2}}$ is the aperture illumination function F(y) for the parabolic cylinder fed by the line source.

Horizontal polarization.--When the source is horizontally polarized,

$$\bar{\bar{H}}_i(\rho,\psi,x) = \bar{\psi}_1 \dot{H}_i(\rho,\psi,x), \tag{36}$$

where $\bar{\psi}_1$ is the unit vector normal to $\bar{\rho}$ as shown in Figure 20(b). It follows that

$$\bar{r}_1\left[(\bar{n}x\bar{\bar{H}}_i)\cdot\bar{r}_1\right] = \bar{\bar{r}}_1\left[(-\bar{i}\dot{H}_i \cos\iota)\cdot\bar{r}_1\right] \tag{37}$$

$$= -\bar{\bar{r}}_1 \dot{H}_i \cos\iota \sin\theta \cos\Phi,$$

and

$$\bar{n}x\bar{H}_i = -\bar{i}H_i \cos \iota \tag{38}$$

$$= -H_i \cos \iota \left[\bar{r}_1 \sin \theta \cos \Phi - \bar{\theta}_1 \cos \theta \cos \Phi - \bar{\Phi}_1 \sin \Phi\right] ;$$

where ι is the angle of incidence of the wave from the feed as it strikes the cylindrical surface shown in Figure 20.

Next, the results of Equations (37) and (38) can be used to show that the far field as given by Equation (14) has no radial component for this polarization. In the y-z plane, where $\Phi = \pi/2$, the electric field is in the $\bar{\Phi}_1$ direction and is given by

$$\dot{E}_{s\Phi} = \frac{-j\omega\mu}{2\pi R_o} \epsilon^{-j\beta R_o} \int_{S_o} H_i(\rho,\Psi,x) \cos \iota \, \epsilon^{j\beta(\bar{\rho}+\bar{i}x)\cdot\bar{r}_1} \, ds. \tag{39}$$

Equation (39) is the horizontal-polarization equivalent of Equation (19) and it is reduced to

$$\dot{E}_{s\Phi} = \frac{\dot{C}}{R_o} \int_{\text{path a-b}} \dot{M}(\rho,\psi) \cos \iota \epsilon^{-j\beta R} \, d\ell \tag{40}$$

in exactly the same manner as Equation (19) was reduced to Equation (25). The $\dot{C}$ above is still given by Equation (26). The only difference in Equations (25) and (40) is that the sin u in Equation 25 is replaced by cos ι in Equation (40). The angle u is the angle between the tangent to the reflector in Figure 20 and the vector $\bar{r}_1$, whereas ι is the supplement of the angle between the normal to the reflector and the vector

$\bar{\rho}$. The vector $\bar{\rho}$ gives the reverse of the direction of propagation of energy from the feed. Note that ι is not a function of θ but u is. Since ι is not a function of θ, the cos ι term will be included as a factor in determining I(y) for this polarization. Thus, when the source is horizontally polarized,

$$\dot{M}(\rho,\psi) \cos \iota = I(y)\epsilon^{j\phi(y)} = \left[\frac{G(\psi)}{\rho}\right]^{\frac{1}{2}} \cos \iota \, \epsilon^{j\phi(y)}. \tag{41}$$

Now Equations (27) and (41) are both consistent with the well-known relationship that the surface current on a conductor is directly proportional to the component of magnetic field intensity parallel to the conducting surface. For horizontal polarization, the surface currents are flowing perpendicular to the y-z plane, and individually the current elements, considered as infinitesimal radiators, are non-directional in this plane. When the relationship given in Equation (41) is substituted into Equation (40), the far-field equation is written

$$\dot{E}_{s\Phi} = \frac{\dot{C}}{R_o} \int_{\text{path a-b}} I(y)\epsilon^{j\phi(y)} \, \epsilon^{-j\beta R} \, d\ell. \tag{42}$$

The term $\phi(y)$, as given by Equation (41) is equal to $-\beta\rho$, but this is a special case of the current caused by a single line source in Figure 20. For more complicated feeds, $\phi(y)$ must be found by other methods (see Chapter II), but regardless of the complexity of the terms, Equation (42) gives the far field due to "currents" $I(y)\epsilon^{j\phi(y)}$ excited by a horizontally polarized source.

When the cross section of the reflector is parabolic, Equations (31) and (41) are used to express all variables in terms of y and the "final" form of the far-field integral is

$$\dot{E}_{s\Phi} = \frac{\dot{C}}{R_o} \epsilon^{-j\beta R_v} \int_{y_a}^{y_b} I(y) \left[1+\left(\frac{y}{2F}\right)^2\right]^{\frac{1}{2}} \epsilon^{j\left[\frac{\beta y}{4F}(y\cos\theta + 4F\sin\theta + \Phi(y)\right]} dy. \quad (43)$$

This equation will be used to calculate the main and image beams of the horizontally polarized antenna discussed in Chapter VI. Although Equation (43) can be used only to calculate the fields of parabolic reflectors, the line feed does not have to be at the focal line but it must be parallel to the focal line.

As in the case of the vertically polarized antenna, the far-field integral Equation (43) can be simplified for the special case when the feed is at the focal line. From Figure 21 it can be seen that when the feed is at the focal, the angle of incidence ι is $\psi/2$. From the basic equation of a parabola,

$$\cos\frac{\psi}{2} = \sqrt{\frac{F}{\rho}}, \quad (44)$$

and

$$\rho = F + z = F\left[1 + \left(\frac{y}{2F}\right)^2\right]. \quad (45)$$

When Equations (41), (44), and (45) are used, Equation (43) can be written

$$\dot{E}_{s\Phi} = \frac{\dot{C}}{R_o} \epsilon^{-j\beta R_v} \int_{y_a}^{y_b} \left[\frac{G(\psi)}{\rho}\right]^{\frac{1}{2}} \epsilon^{j\beta\left[\frac{y^2}{4F}(\cos\theta - 1) + y \sin\theta - F\right]} dy. \qquad (46)$$

If the dimensions of the reflector are large compared to a wavelength, the beam is narrow, so Equation (46) is written

$$\dot{E}_{s\Phi} = \frac{\dot{C}}{R_o} \epsilon^{-j\beta(R_v+F)} \int_{y_a}^{y_b} \left[\frac{G(\psi)}{\rho}\right]^{\frac{1}{2}} \epsilon^{j\beta\, y \sin\theta}\, dy, \qquad (47)$$

which is the same as the far-field integral used in finding radiation patterns using the aperture-field method. The far fields from horizontally and vertically polarized antennas differ for wide-angle beams, but Equations (35) and (47) show that the differences in the beam shapes decrease as the dimensions of the antenna increase.

CHAPTER V

GENERAL CHARACTERISTICS OF MAIN AND IMAGE BEAMS OF PARABOLIC ANTENNAS

It will be shown in Chapter VI that the calculated and measured radiation patterns of image beam-shaping antennas are in good agreement except at very low power levels. However, obtaining a certain radiation pattern by assuming reflector shapes and calculating the corresponding patterns until the desired result is obtained is a long and costly procedure. The digital computer time alone required to calculate one pattern is from three to six hours, depending on the beam shape and the angular spacing between calculated points. The time required to calculate the shape of one pattern necessitates some short-cut method to give the general shape of the beams without having to evaluate the far-field integrals. The parabolic reflector has been found experimentally to be well-suited to image beam-shaping problems. Because of the nature of the diffraction fields from parabolic antennas and because of additional practical restrictions on the feed and parabola, the radiation patterns encountered in image beam-shaping applications have certain predictable features which can be used to plot "universal" design curves. These curves are used to find approximate beamwidths, beam magnitudes and positions, and phase relationships between the fields of the main and image beams. The main beam, by definition, is the beam caused by the currents on the parabola which were caused by direct radiation from the feed. This current is called the main-beam current. The beamwidth and

other features of this beam can be predicted from a knowledge of the reflector dimensions in wavelengths and the main-beam current distribution on the reflector. The image beam, by definition, is the beam caused by the currents on the parabola resulting from reflections from the ground plane. The image beam caused by a ground plane of arbitrary shape cannot be predicted accurately, but the features of the image beam caused by a flat ground plane and also by specific curved ground planes can be predicted using the design curves presented in this chapter. The flat ground plane gives at best a shaped beam with a limited angular coverage. The curved ground plane is used to give a wide-angle shaped beam. The use of the design curves obviates many preliminary far-field integrations, but in general these curves cannot be expected to give results accurate enough to eliminate all integrations. The design curves also show the effects of variation of all parameters of the antenna.

As stated earlier, the main and image beams combine with the direct ground-plane beam and the direct-horn beam to give the total far field at any elevation angle. In the angular region near the peak of the main beam, the direct ground-plane and direct-horn beams are always very small and can be neglected in determining the total field near the peak of the beam. The most critical angular region in the pattern is that region between the main- and image-beam peaks where the two field intensities are of comparable magnitude. Improper phase relationships here can result in a distinct null between the peaks of the two beams.

For any one combination of a flat ground plane and parabolic reflector, the design curves can be used to predict the magnitude of the main- and image-beam field intensities and the phase relationships

between them. To obtain complete information on both beams, it is necessary to examine the following pertinent points:

(1). The magnitude and phase of the field intensity in the main beam, using the peak of the beam as a reference;

(2). The magnitude and phase of the image beam, caused by a flat ground plane, relative to the field at the peak of the image beam;

(3). The magnitude and phase of the field intensity at the peak of the image beam relative to the peak of the main beam;

(4). The angular position of the peak of the image beam in terms of the position of the flat ground plane;

(5). Changes in the shape of the image beam as the flat ground plane is made convex.

These pertinent points are examined in detail in the following sections.

The magnitude and phase of the main beam.--The main beam of the parabolic reflector is calculated by using either Equation (32) or (43), depending on the polarization. Approximate main-beam values for either polarization can be calculated by using Equation (35). The form of Equation (35) is the same as that of the aperture-field method if $\left[G(\psi)/\rho\right]^{\frac{1}{2}}$ is replaced by $F(y)$, which is called the illumination function of the aperture. Before presenting the design curves for the main beams, it is necessary to discuss briefly the effects of changing the illumination function $F(y)$. This discussion is based on the use of Equation (35), which is approximate but reliable for apertures large compared to a wavelength.

It is usually convenient in far-field calculations to normalize the field intensity, so Equation (35) is written as

$$\dot{U}_m = U_m \epsilon^{j\Omega_m} = K_3 \int_{y_a}^{y_b} F(y) \epsilon^{j\beta y \sin\theta} dy \tag{48}$$

$$= K_3 \left[\int_{y_a}^{y_b} F(y) \cos(\beta y \sin\theta) dy + j \int_{y_a}^{y_b} F(y) \sin(\beta y \sin\theta) dy \right],$$

where

$$K_3 = \frac{1}{\int_{y_a}^{y_b} F(y) dy}. \tag{49}$$

U_m is the magnitude of the normalized field intensity of the main beam for either polarization and always has a maximum value of one at $\theta = 0$. Ω_m is the time phase angle of the field intensity with respect to the phase at $\theta = 0$. One feature of the main beam which is evident from Equation (48) is that U_m is an even function of θ, and Ω_m is an odd function. In general, each different illumination function produces a different radiation pattern. To illustrate the differences in the main beams caused by different illumination functions, three specific examples have been worked out in detail using Equation (48). The results of these calculations are shown in Figure 22. The three examples A, B, and C have sinusoidal type illumination functions with different degrees of asymmetry over an aperture 11 wavelengths high, λ being one inch. The origin is placed at the bottom of the aperture. The main purpose of these curves is to illustrate the difference between the symmetrical illumination

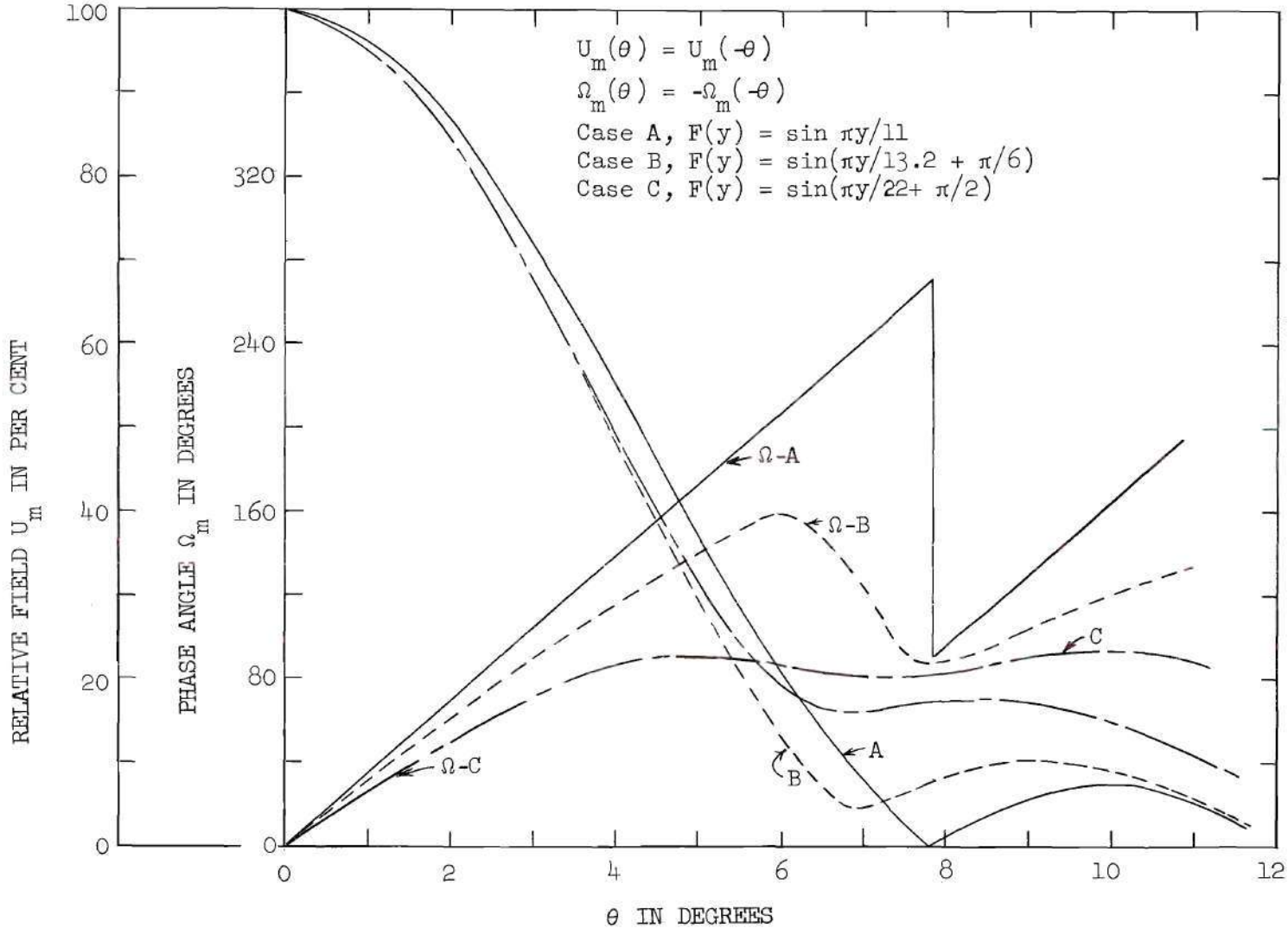

Figure 22. Typical Characteristics of Main Beams

of case A and the asymmetrical illuminations of cases B and C. The symmetrically illuminated aperture is similar to that found in most conventional parabolic antennas, and the asymmetrically illuminated aperture shown here is representative of problems encountered in image beam-shaping applications. The most noticeable difference between the curves of cases A and C is in the minor lobe structure. This difference can be explained by reference to Equation (48) when it is applied to a symmetrically illuminated aperture. If y_c is the center of the aperture as shown in Figure 23, the substitution of $y' = y - y_c$ into Equation (48) gives

$$\dot{U}_m = K_3\left[\int_{-D/2}^{0} F(y' + y_c)\, \epsilon^{j\beta(y' + y_c)\sin\theta}\, dy' + \int_{0}^{D/2} F(y' + y_c)\, \epsilon^{j\beta(y' + y_c)\sin\theta}\, dy'\right]. \tag{50}$$

When the substitution $y'' = - y'$ is made in the first integral, Equation (50) becomes

$$\dot{U}_m = K_3\, \epsilon^{j\beta y_c \sin\theta}\left[\int_{0}^{D/2} F(y_c - y'')\, \epsilon^{-j\beta y''\sin\theta}\, dy'' + \int_{0}^{D/2} F(y_c + y')\, \epsilon^{j\beta y'\sin\theta}\, dy'\right]. \tag{51}$$

If the illumination function is even about the center of the aperture,

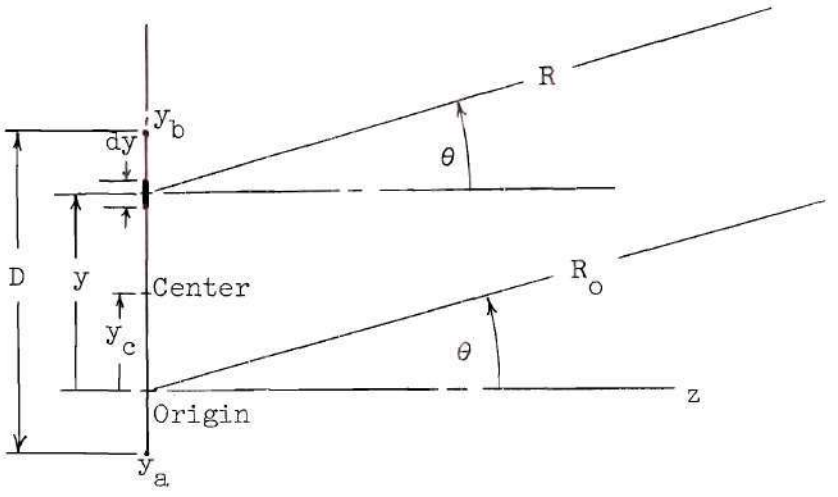

Figure 23. Geometry of Two-dimensional Diffraction Problem

$$\dot{U}_m = 2K_3 \epsilon^{j\beta y_c \sin\theta} \int_0^{D/2} F(y_c + y') \cos(\beta y' \sin\theta)\, dy'. \qquad (52)$$

Equation (52) verifies the well-known fact that the magnitude of the far field is not dependent on the position of the origin, but the phase is. If the origin is placed at the center of the aperture, $y_c = 0$, $\dot{U}_m$ becomes a real number, and obviously a pattern null occurs where the integral is zero. The total pattern consists of a single principal lobe and a series of minor or side lobes separated by well-defined nulls. Unless the illumination is symmetrical, the resultant field is a complex number regardless of the position of the origin. The real and imaginary parts are represented by different functions and very rarely are both terms zero at the same angle θ. Since the total field is the square root of the sum of the squares of the real and imaginary parts, true nulls are

unusual for apertures with asymmetrical illumination. As shown in Figure 22, the sharpness of the minima between the lobes decreases as the illumination is made more asymmetrical. While the different illumination functions give different beam shapes, the values of U_m and Ω_m for any one aperture illumination, plotted as a function of β D/2 sin θ, are independent of D and λ so long as $D \gg \lambda$.[18] This plot of U_m or Ω_m vs. β D/2 sin θ can be loosely called a "universal" design curve for this illumination. Practical limitations on antennas in certain categories often restrict the aperture illumination sufficiently to allow universal design curves to be used effectively. For example, the antenna used to give a "pencil beam" has an illumination F(y) almost symmetrical about the center of its aperture because the symmetrical feed-horn pattern must be directive enough to prevent excessive spillover energy at the edges of the reflector. To facilitate the design of this type antenna, semi-empirical formulas and curves have been developed to give the half-power beamwidths and side-lobe levels in terms of λ/D and the taper of the illumination at the edges of the aperture.

All image beam-shaping antennas of the cylindrical type also have certain common features which restrict the illumination functions. For example, the main-beam current distribution is necessarily asymmetrical because the horn must be aimed below the reflector center so that energy is directed into the ground plane to give an image beam. The exact aim of the feed is determined by the desired amplitude of the image beam relative to the main beam. The resulting main-beam current on the bottom of the parabola is much greater than that at the top because spillover restrictions still limit the energy level at the top. Experiments by the

author show that the horn for most beam-shaping applications will be aimed at a point not more than $y_o = D_v/5$ above the vertex and not below the vertex. D_v is the vertical height of the parabolic reflector above the vertex, as shown in Figure 26.

Universal design curves for illuminations typical of main beams of image beam-shaping antennas are shown in Figures 24 and 25. The data for these curves were calculated using Equation (48) with the origin at the vertex of the reflector. The curves give essentially the same beams as those obtained using Equations (32) and (43). Consistent with Equations (35) and (47), the aperture illumination was calculated using

$$F(y) = \left[\frac{G(\psi)}{\rho}\right]^{\frac{1}{2}}, \tag{53}$$

where $G(\psi)$ is the gain function of the practical line feed, see Figure 29 for typical primary patterns. The unit of the abscissa in Figures 24 and 25 is the half-power beamwidth which differs from the units of $\beta\, D/2 \sin\theta$ by a constant, since $\sin\theta \approx \theta$ for the narrow beams. The parameter in these figures is the normalized illumination function $f(y_m)$, which is given by

$$f(y_m) = \frac{F(y_m)}{F(y_o)} \times 100 = \left[\frac{G(\psi_m)}{\rho_m} \div \frac{G(\psi_o)}{\rho_o}\right]^{\frac{1}{2}} \times 100, \tag{54}$$

where ψ_o is the aim of the horn as shown in Figure 26. Figure 24 shows the effect of changing the level of $f(y_m)$ when the maximum illumination is at the bottom of the reflector. The aperture illumination used in calculating these data is based on monotonically decreasing gain functions

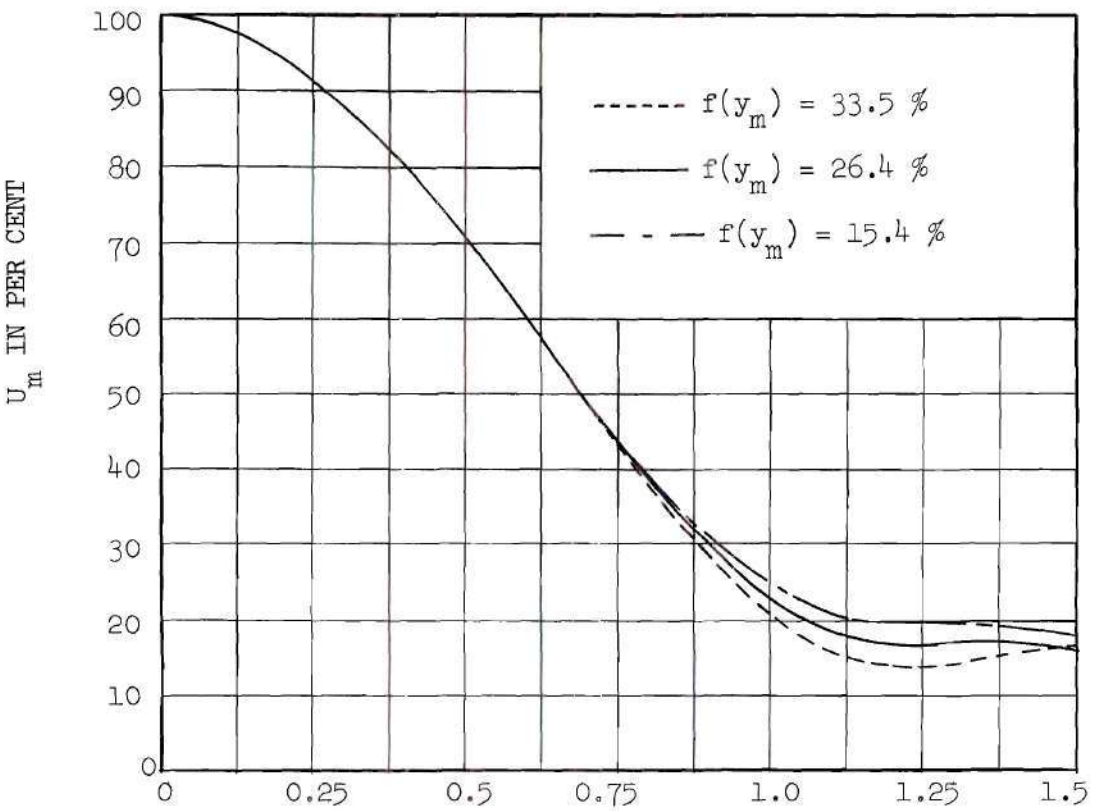

Figure 24(a)

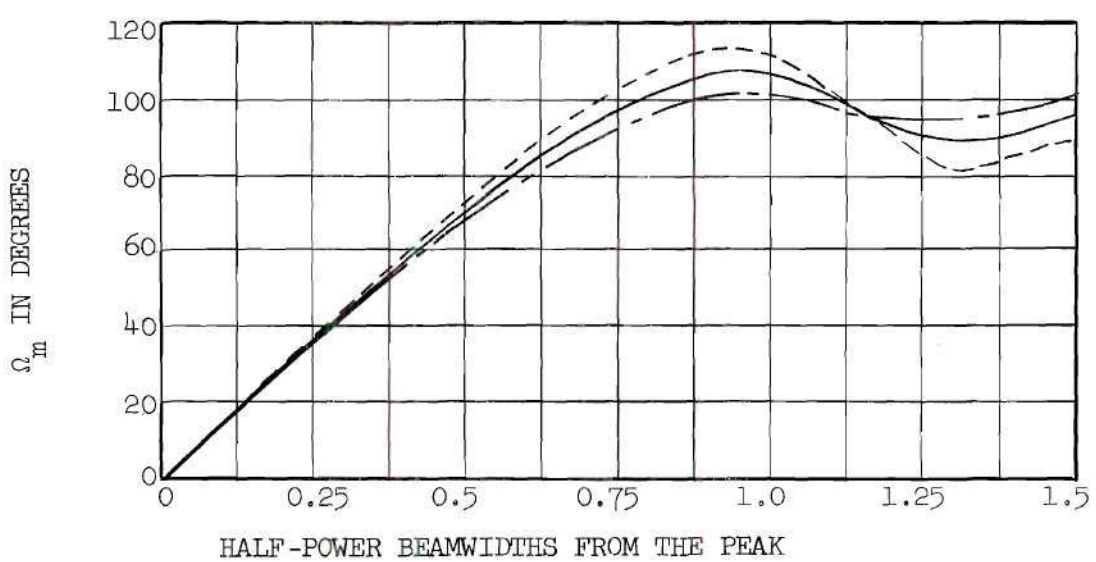

Figure 24 (b). Main Beam Design Curves for $y_o = 0$

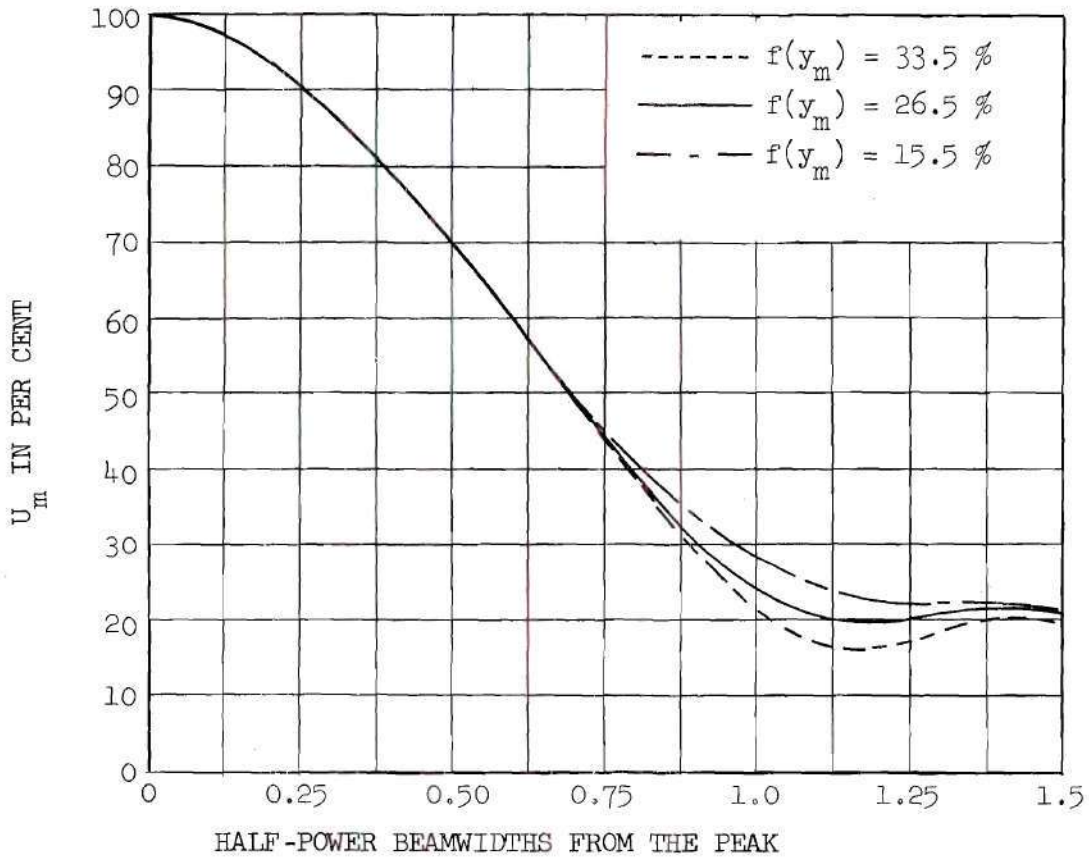

Figure 25 (a)

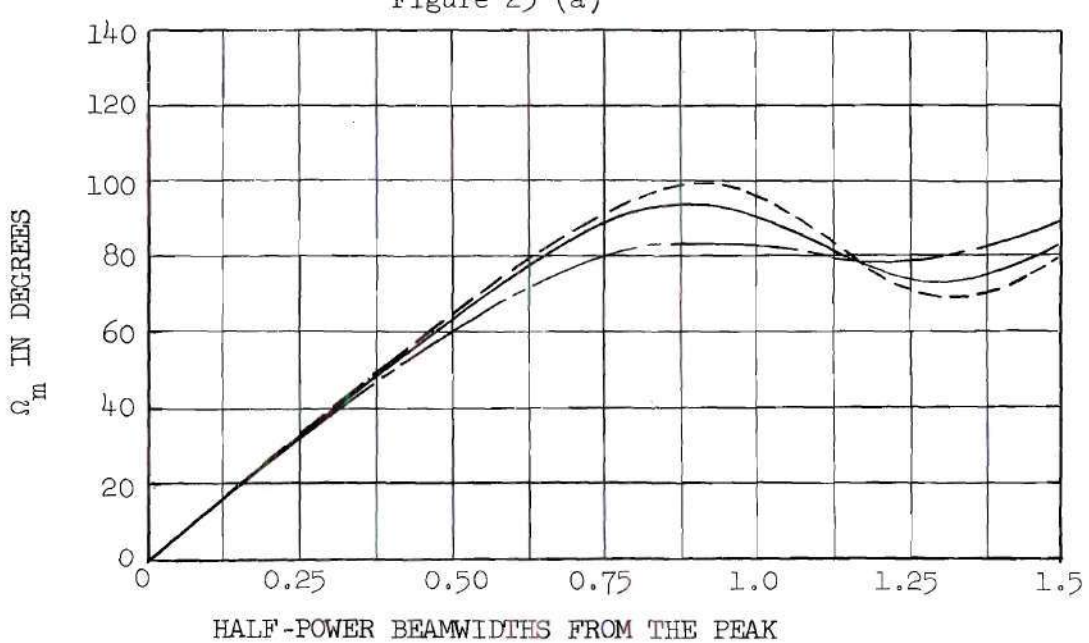

Figure 25 (b). Main Beam Design Curves for $y_o = D_v/5$

for the horns as shown in Figure 29, so that the value of $f(y_m)$ tells more than just the illumination at the top of the aperture. Figure 25 is the same as Figure 24, except the maximum illumination occurs at a point $D_v/5$ above the bottom of the aperture. It has been found experimentally that, to limit the spillover energy to an acceptable value, the gain of the feed in the ψ_m direction should be about 10 db below the maximum gain of the feed. For reflectors used in image beam-shaping applications, the value of $G(\psi_m) = -10$ db gives a value of $f(y_m)$ in the neighborhood of 25 per cent, the actual value depending on the ratio of the focal length to the height of the reflector. In some cases it may be necessary to make $G(\psi_m)$ as large as - 8 db and in others it may be as low as - 12 to - 14 db, but the - 10 db figure is usually a good starting point.

The radiation from the section of the parabola blocked by the feed requires special treatment. In calculations of the far field by the aperture-field method, the portion of the aperture blocked by the horn is assumed to have F(y) equal to zero.[19] In the current-distribution method, the section of the parabola masked by the horn feed is a function of the angle θ. Since both methods involve approximations, main-beam calculations were made in which only the section of the parabola above the vertex was considered as being active and the blocking action of the horn was neglected. In the final antenna, this blocking action is usually unimportant because the flat ground plane of Figure 26 will usually be changed to a curved ground plane similar to the one shown in Figure 4 where the ground plane extends above the level of the top of the horn.

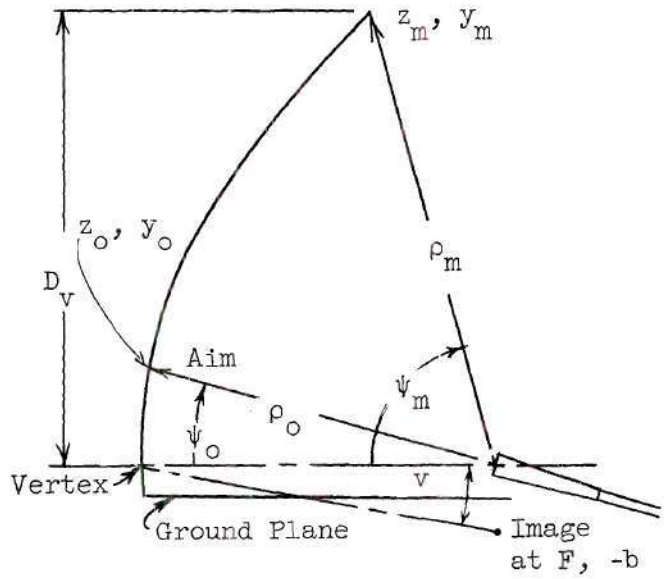

Figure 26. Reflector-horn Geometry

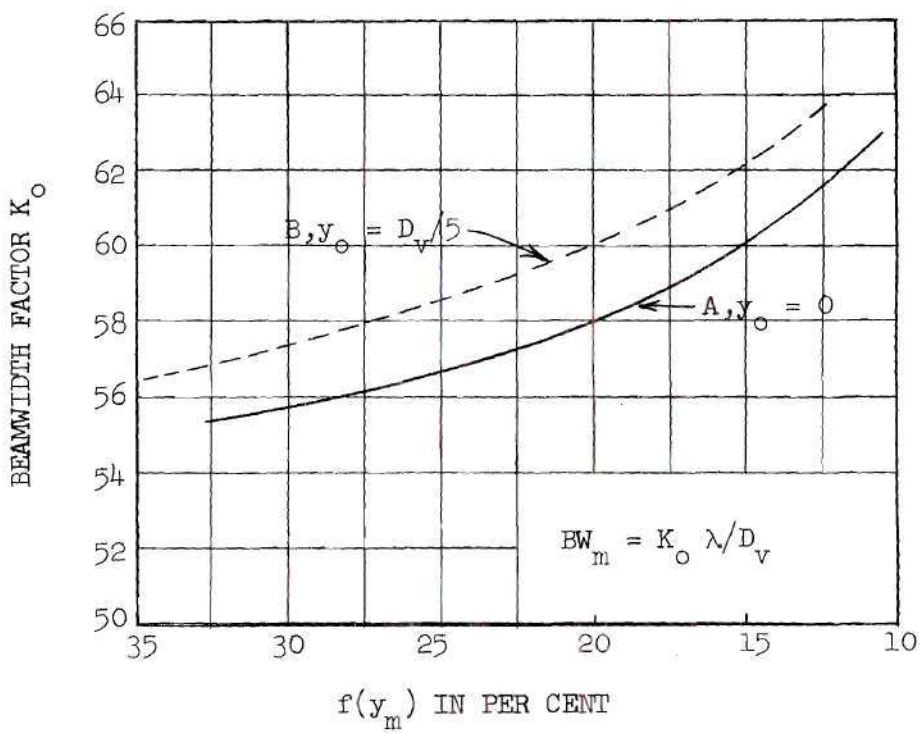

Figure 27. Beamwidth Factor vs. Illumination at the Top of the Aperture

The universal-design phase curves are based on the origin being at the bottom of the aperture, the vertex of the parabola; therefore, in cases where y_a is above the origin, a corrective phase term ($\beta y_a \sin \theta$) must be added to the values obtained from the curves. The magnitude of the main beam is not affected by changing the position of the origin.

Before any numerical values can be assigned to the field intensity in the main beam, the half-power beamwidth BW_m must be known. For any flat equiphase aperture, the beamwidth is given by the well-known relationship

$$BW_m = K_o \frac{\lambda}{D_v}, \tag{55}$$

where K_o is the beamwidth factor determined by the illumination function $F(y)$, and D_v is the height of the parabola above the vertex. For antennas with uniform illumination, K_o is about 51 and for some low side-lobe-level antennas it may be as high as 100. The design curves in Figure 27 show the theoretical constant K_o as a function of the normalized illumination at the upper edge of the reflector. Curve A is based on the horn being aimed at the vertex of the parabola and giving a maximum $F(y)$ at the bottom of the aperture. Curve B is used when the horn is aimed at a point $D_v/5$ above the vertex. Values of K_o for intermediate horn aims can be obtained by interpolation between curves A and B.

The magnitude and phase of the image beam.--The shape of the image beam is a function of the shape and location of the ground plane, the aim and directivity of the feed, the size of the parabolic reflector, and the frequency. It is not practical to provide design curves or data to

predict the image beam caused by a ground plane of arbitrary shape, but design curves for flat ground planes are practical. A wide variety of problems can be treated by a consideration of the flat ground plane as a building block and then a modification of the shape of the ground plane to give increased angular shaped-beam coverage. Thus the flat ground plane, which is most important, is seldom used in practice, except as an intermediate step in the design of the final curved ground plane.

The image beam caused by a flat ground plane is similar to the secondary pattern of a parabola fed by an off-axis source. This type of antenna has the property that as the line source is displaced below the axis of the parabolic reflector, the resulting secondary beam will be displaced on the upper side of the axis by an angle proportional to the feed displacement. As the angular displacement increases, both the beamwidth and side-lobe level increase, slowly at first and then more rapidly as the angle increases. The widening of the image beam in the vertical plane is advantageous because the wider beam gives greater vertical-plane coverage.

As was the case with the main-beam current distribution, the current distribution which causes the image beam, called the image-beam current, is also restricted by practical limitations. Because the feed-horn pattern is symmetrical, the current on the parabola resulting from reflections from a flat ground plane is a maximum at the bottom of the reflector, except in isolated cases where the horn is aimed well below the vertex of the parabola. In order to get a shaped beam with a large angular coverage, the position of the ground plane should be adjusted so that the peak of the image beam is as far from the main beam as possible

without creating a dip or null in the overall pattern in the region between the main and image beams. The shapes of the main and image beams limit the peak of the image beam to an angular position less than two main-beam beamwidths from the axis of the parabola. The physical size of the feed prevents the ground plane from being closer than half the height of the feed from the axis. As a result of these restrictions, the peak of the image beam will usually be between one and two beamwidths from the peak of the main beam.

Another restriction on the antenna is the ratio of the focal length F to the height D_v of the reflector. This ratio is important because it dictates the directivity of the line feed. From the standpoint of the accuracy of the calculated ground-plane reflections, the vertical dimension of the feed should be as small as possible to approximate a true line source. Since the feed must be directive enough to limit spillover at the top of the reflector, a larger vertical dimension for the feed is needed. Also from the discussion on the center of feed in Chapter III, it is obvious that the feed cannot properly illuminate the reflector if the required 10 db beamwidth is as much as 180 degrees. The net results of the above restrictions and the results of actual pattern measurements show the F/D_v ratio should be between 0.5 and 0.8.

The restrictions on the antenna employing a single flat ground plane parallel to the axis of the parabola are summarized below.

(1). The primary feed is aimed at a point between the vertex and $D_v/5$ above the vertex of the parabola.

(2). The gain of the feed in the ψ_m direction is nominally 10 db below the maximum gain.

(3). The F/D_v ratio of the parabola is between 0.5 and 0.8.

As previously stated, the integrals involved in the current-distribution method of finding the far fields are difficult to evaluate, even for such simple problems as a parabola fed by a line source at the focal line. When the horn is moved off-axis, the integrals are so complex that the only practical way to find the far field is by the use of a digital computer. Figure 28 shows three typical image beams calculated on an IBM 650 computer using Equation (32). The current distribution results from illumination by horn number 1, see Figure 29, aimed at the vertex of a parabola having a F/D_v ratio of 0.77. The focal length of the parabola is 8.0 inches and the flat ground plane is parallel to the axis and below it by distances of 0.75, 1.0, and 1.25 inches respectively for beams A, B, and C. The curves were not normalized, so that changes in amplitude with ground-plane position could be studied. It can be seen from Figure 28 that the three beams have similar shapes but that the asymmetry of the beams increases slightly as the beam displacement angle increases. The information contained in Figure 28 and additional data on twenty typical image beams were used to plot the design image beam shown in Figure 30. Only one curve each is shown for U_i and Ω_i because the image-beam current distribution and the resulting secondary image beams will all be similar if the antenna is subject to the restrictions listed on page 74. The accuracy of the design image beam is not as good as that of the design curves for the main beams, but it is sufficiently accurate for preliminary design work.

In the treatment of the main beam, the portion of the parabola below the vertex was neglected because of the blocking action of the

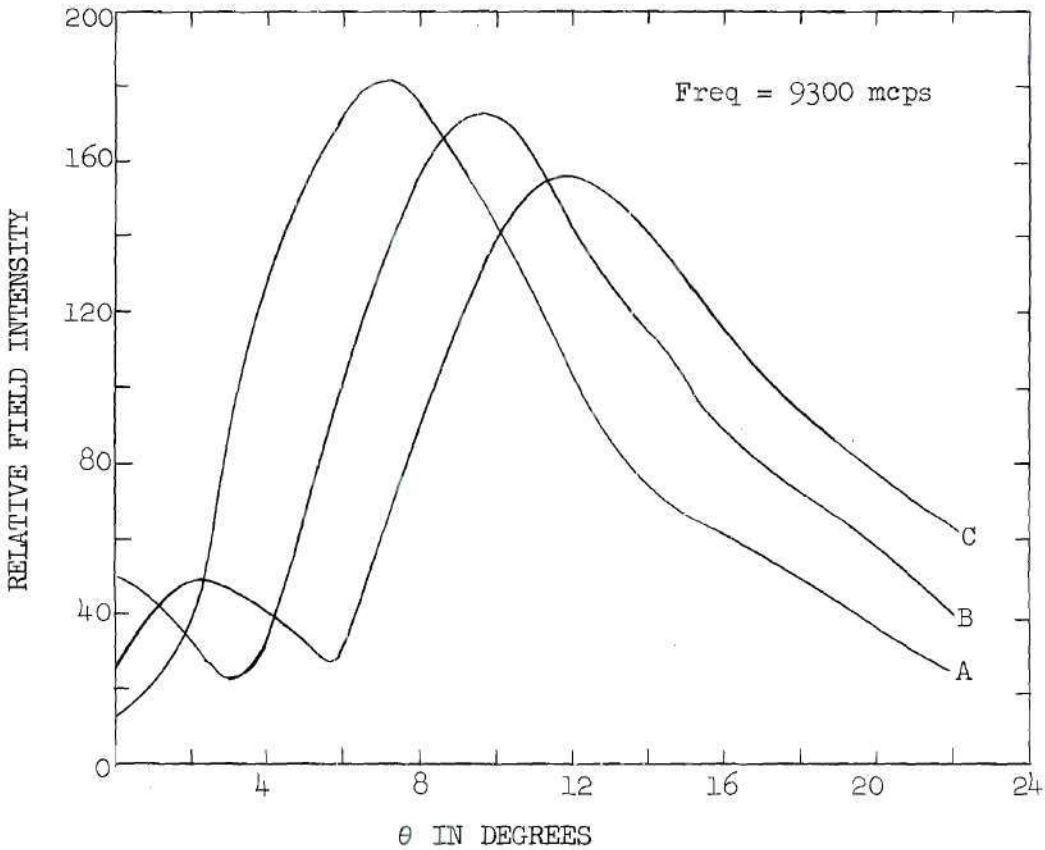

Figure 28. Typical Calculated Image Beams

feed. The treatment of the image beam is different because its peak is above the axis of the parabola. From the blocking standpoint, the horn has little effect on the image beam above its peak, but it does have some effect on the beam between the peak and the axis of the parabola. However, calculations in the study were made under the assumption that the entire parabola is active in determining the image-beam shape. This assumption is justified if it is noted how the image beam would be calculated by the aperture-field method. Consider the aperture to be used, as a plane parallel to the y-axis and passing through the focal line in Figure 26. Note that the ray from the image that hits the bottom of the

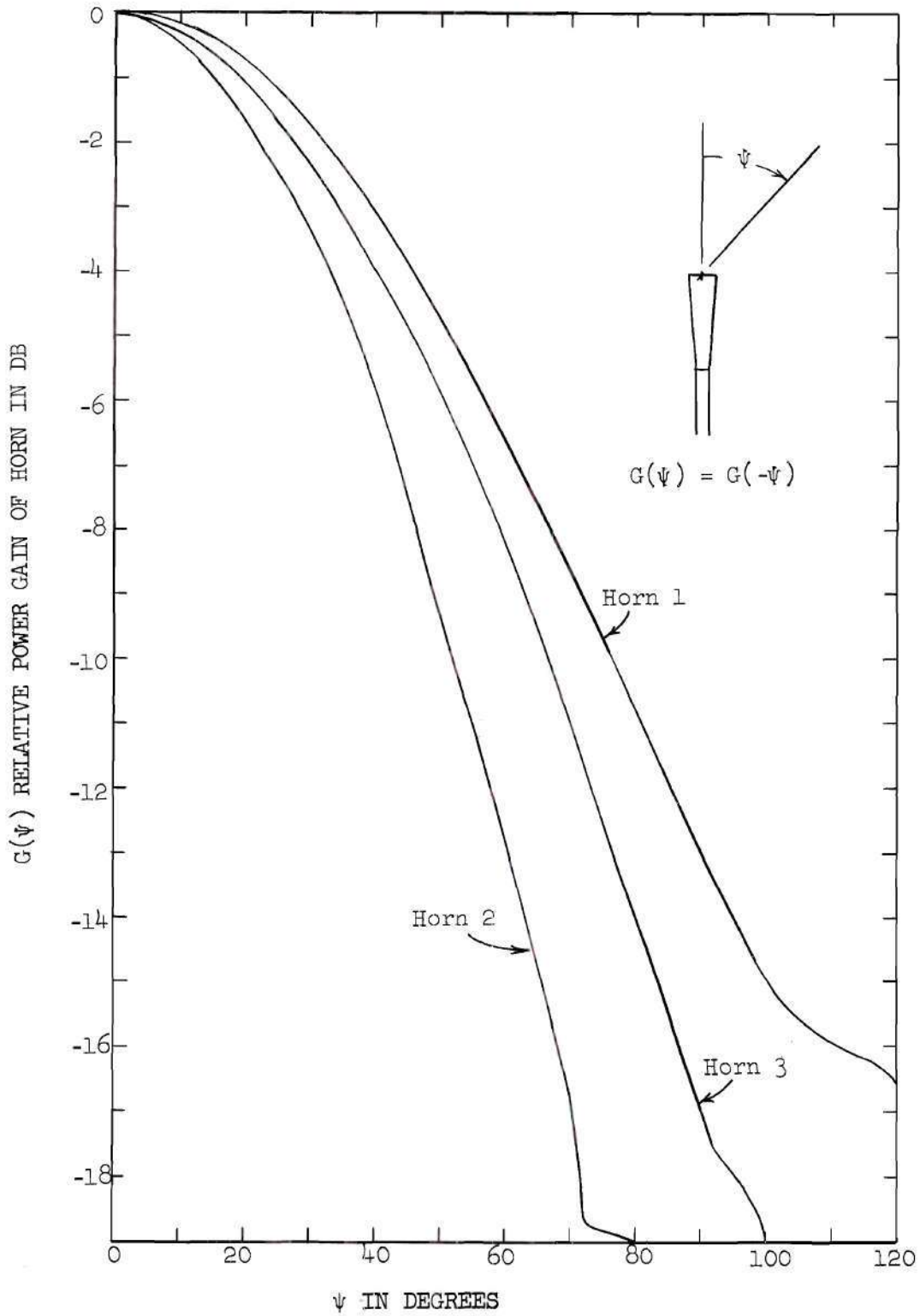

Figure 29. Typical Primary Radiation Patterns Used in Finding Design Curves

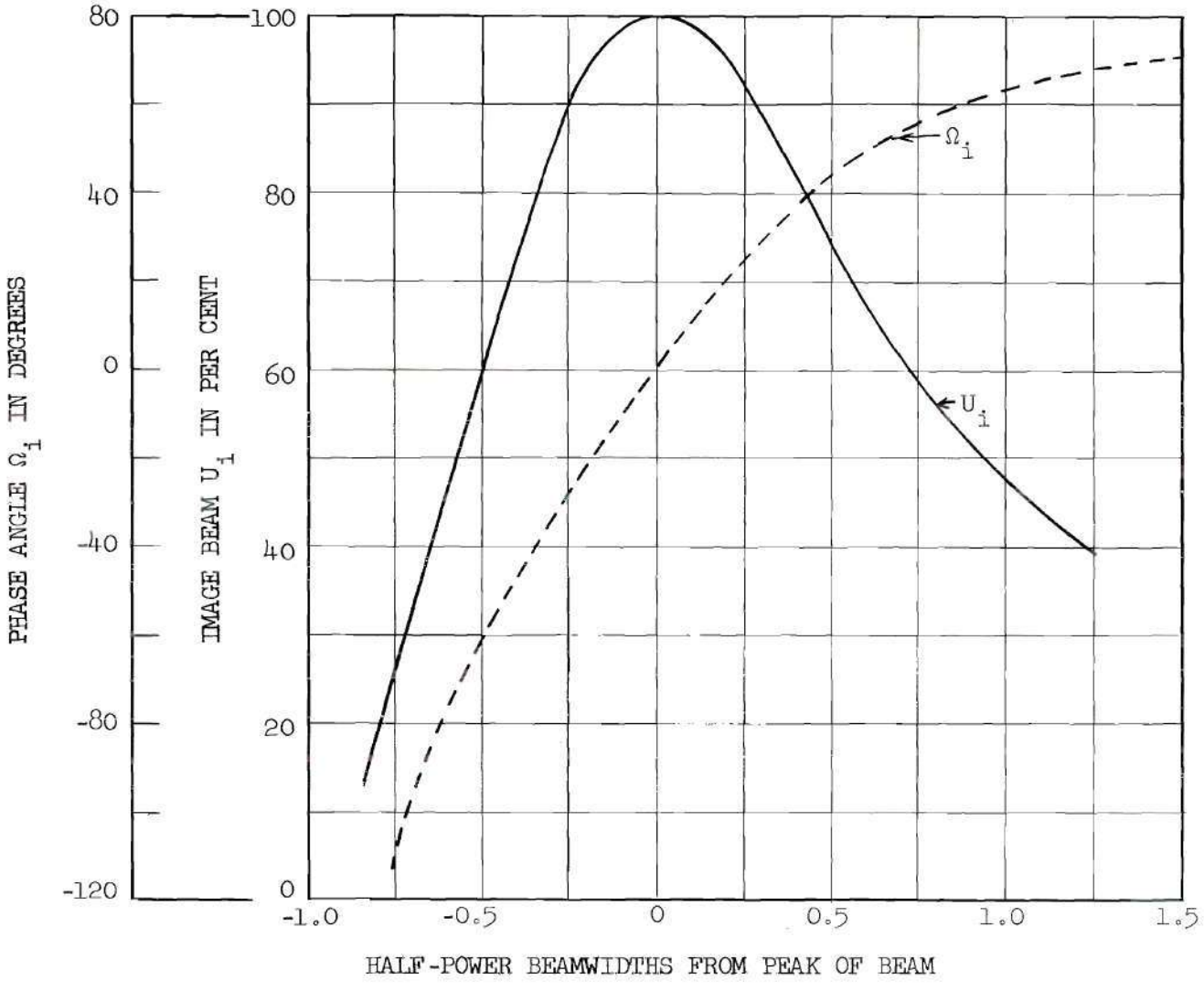

Figure 30. Universal Image-beam Design Curves

parabola is reflected so that it intersects the plane through the focal point at a point above the focal line. All other rays from the image that are reflected from the parabola also go through the aperture at points above the focal line. Since there is a one-to-one correspondence between points on the reflector and points on the aperture, the aperture illumination function is determined by all parts of the parabola and therefore calculations by the aperture-field method would in effect be made using the entire parabola. Since the aperture-field and current-distribution methods of calculating far fields give comparable results when properly applied, the blocking action by the horn is not considered when the current-distribution method is used in these calculations.

Before the actual image-beam field intensity can be found using Figure 30, the half-power beamwidth must be known. The half-power beamwidth of the image beam cannot be conveniently expressed as $K_o \lambda/D$ because the beam shape, as well as position, depends upon the position of the image, which determines the phase of the current distribution on the parabola. This beamwidth is dependent on so many factors that a family of curves must be used to represent it. The curves in Figures 31 and 32 which were plotted from data calculated from Equations (32) and (43), show how rapidly the image-beam beamwidth increases as the image is moved away from the axis of the reflector. The shape of these curves can be explained by use of Figure 26. It is evident in this figure that the rays emanating from the image deviate from parallelism after reflection from the parabola because only rays from a horn at the focal line will be collimated by the parabola. Geometrical optics applied to rays from the image shows that the ray incident at the vertex is reflected

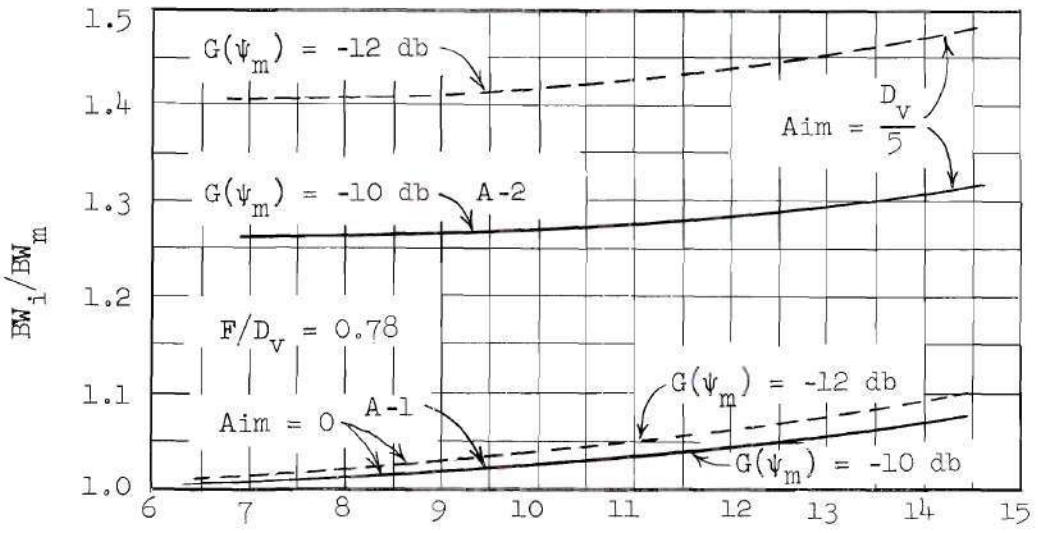

Figure 31 (a)

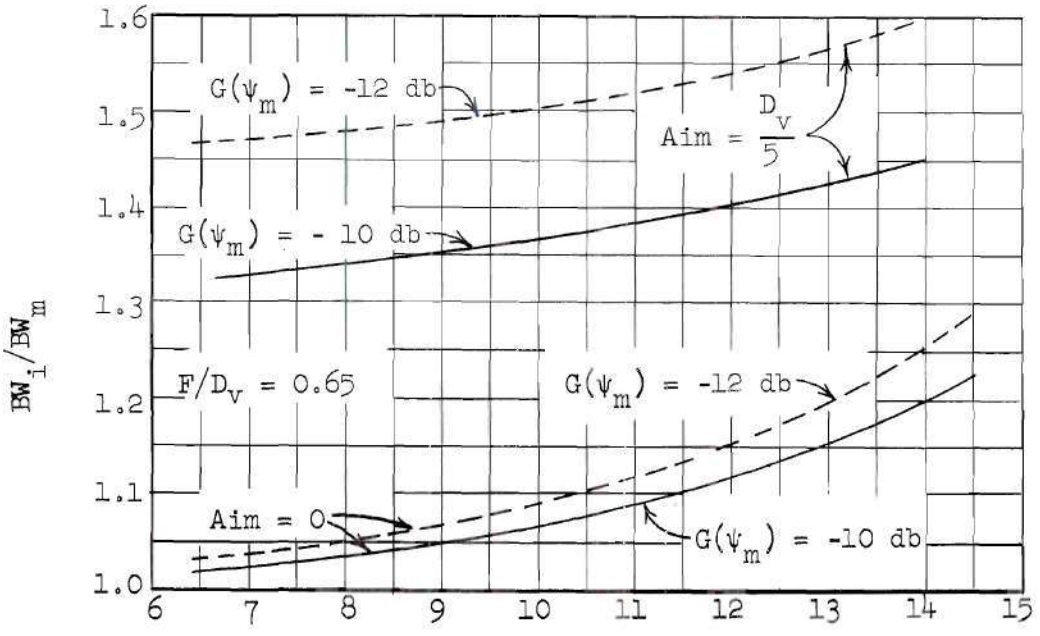

Figure 31 (b). Image-beam Main-beam Beamwidth Ratio as a Function of Image Displacement

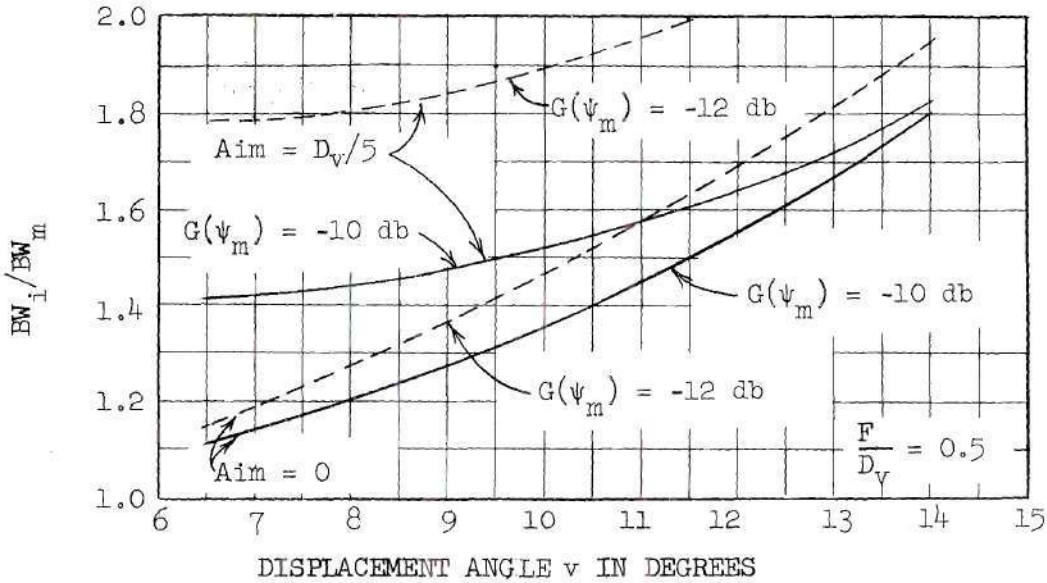

Figure 32. Image-beam Main-beam Beamwidth Ratio as a Function of Image Displacement

above the axis at an angle equal to the angular displacement of the image below the axis. The ray hitting any part of the parabola between y = 0 and y = 2F will be reflected above the axis by an angle which decreases from arctan b/F for y = 0 to an angle 0 at y = 2F. Since the reflected rays are not parallel, the position of the peak of the image beam and its shape will depend on which section of the parabola carries the largest image-beam-producing currents. For any one frequency and position of the image, the phase of the currents on the parabola are fixed, but beamwidth and position of the image beam depend on the magnitude of the currents, which in turn is dependent on the aim and directivity of the primary feed. These factors account for the differences in the curves A-1 and A-2 in Figure 31(a) which differ only in the horn and horn aim. The data for A-1 were calculated using the current

distribution resulting from a horn aimed at the vertex and having $G(\psi_m)$ = 10 db below the peak horn gain, while the data for A-2 were based on a horn aimed $D_v/5$ above the vertex and also having $G(\psi_m)$ = - 10 db. For both conditions, the restrictions on image beam-shaping antennas give an image-beam current distribution having a maximum at the bottom of the reflector, but the current for A-2 falls off much more rapidly with increasing y than the current in A-1 because the directivity of the horn horn for A-2 is greater than that used in A-1. For condition A-2, a large section of the parabola carries an image current so small that it has little effect on the half-power beamwidth. The "active" section of the reflector determines the beamwidth so that the beamwidth for A-2 is larger than the beamwidth in the corresponding condition in A-1.

These design curves also show that the ratio of image-beam beamwidth to main-beam beamwidth increases as F/D_v decreases because the beamwidth of the main beam decreases more rapidly than the beamwidth of the image beam.

Phase of image beam at the peak.--When the far field is treated as the summation of the fields from a finite number of small radiating current elements, the phasors representing the contributions from the individual radiators may be placed end-to-end as shown in Figure 33 to give the total contribution. This plot is typical of an off-axis-fed parabola such as those discussed throughout this thesis. For perfect focusing by the parabola, the phasor contributions from the current elements at some elevation angle would be in phase and form a straight line. For the image beam there is no elevation angle where all the phasors are in time phase, so the image beam is said to be defocused. Obviously if, at

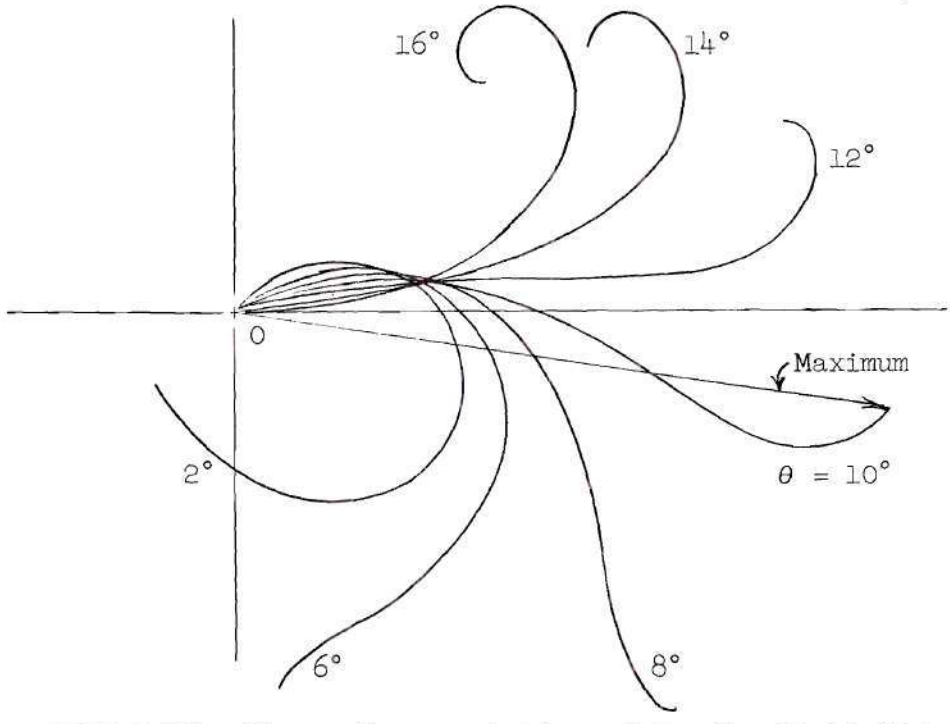

Figure 33. Phasor Representation of the Far Field for a Typical Image Beam

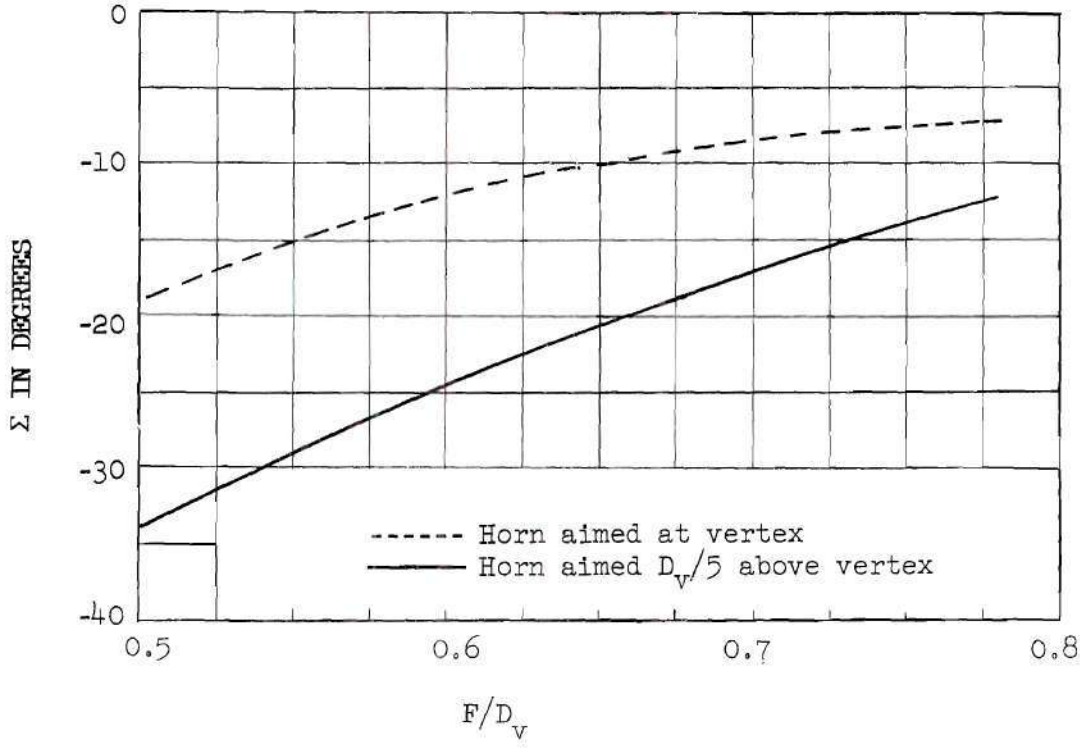

Figure 34. Dependence of Phase Angle Σ on F/D_V

the peak of the beam, all the phasor quantities were in time phase, the phase of the far field at this elevation angle would be the same as the current element at the origin. This phase, of course, does not consider the $\epsilon^{-j\beta R_V}$ factor in Equation (43) because it is a common multiplier of each far-field term and has no effect on the relative phase. Figure 33 shows that, for the particular image beam shown, the contributions from various elements are not in time phase at $\theta = 10$ degrees, which is the maximum of this image beam. The net phase of the far field at the maximum is - 9 degrees when the image current at the vertex is used as the zero reference. The symbol for this phase angle between the far-field maximum field intensity and the current at the vertex is Σ. The term Σ is a function of F/D_V, the horn aim, the primary radiation pattern, and the position of the image; but calculations on thirty image beams show that the horn aim and the F/D_V ratio are the most important factors. Here again the common features of the image beam, subject to the previously mentioned restrictions, make the use of design curves practical for predicting the phase of the field at the peak of the image beam. The curves in Figure 34 show average values of Σ for two different horn aims. These curves are not extremely sensitive to changes in $G(\psi_m)$, but best results are obtained when $G(\psi_m)$ is close to the recommended 10 db value.

Peak magnitude of the image beam.--The magnitude of the image beam depends on the percentage of the horn energy intercepted by the ground plane and on the position of the image horn. The ratio of the peak magnitude of the image beam to the peak magnitude of the main beam is proportional to the square root of the ratio of the power intercepted by the ground plane divided by the power in the parabola. The problem

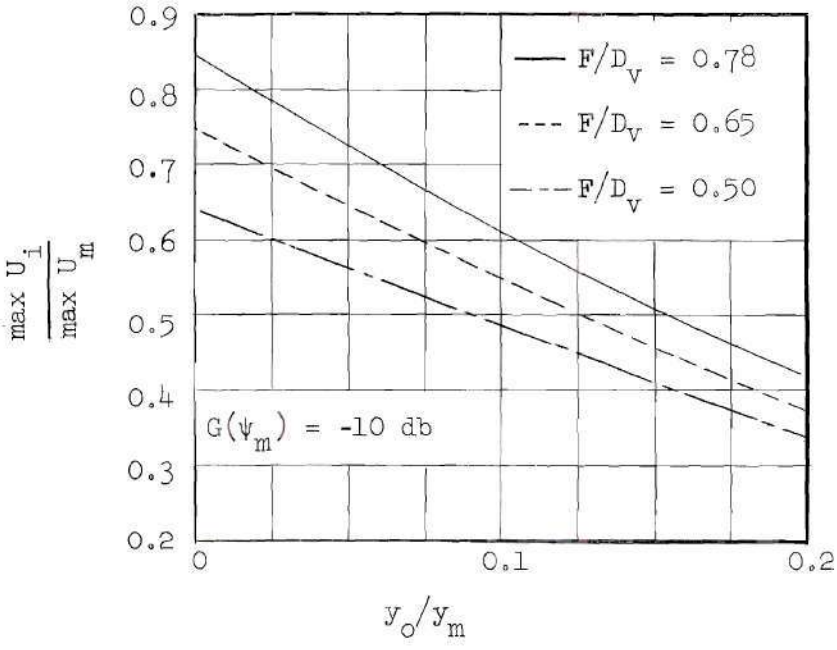

Figure 35 (a)

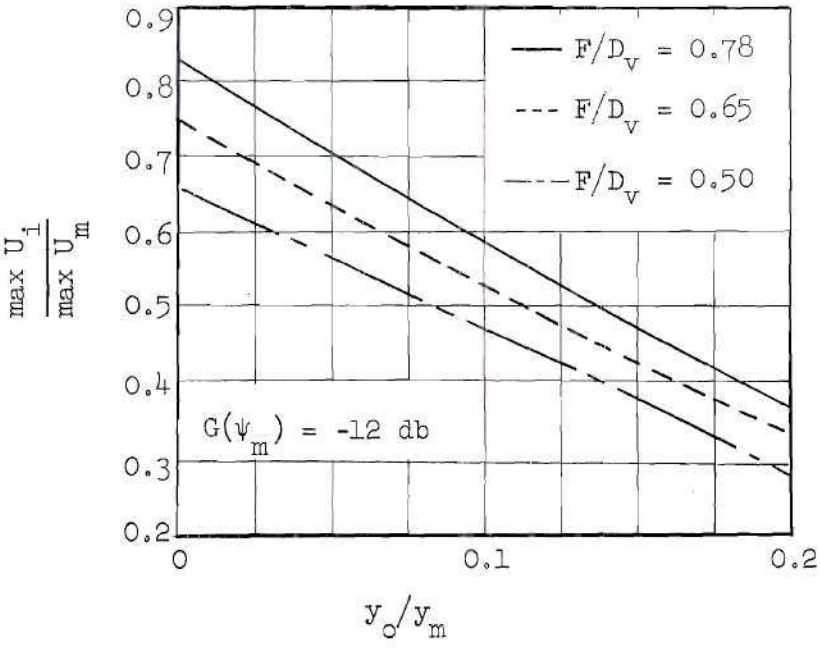

Figure 35 (b). Change in Relative Magnitude of Image Beam with Horn Aim and F/D_v

of predicting the ratio of beam magnitudes is complicated because the image beam is not as well focused as the main beam. The defocusing of the image beam is difficult to predict accurately without the use of graphs since the defocusing is affected by the F/D_v ratio, the position of the image, and the aim and radiation pattern of the primary feed. The data presented in Figure 35 show how fast the magnitude of the image beam changes as the horn aim is changed. These figures show the effects of defocusing and changes in energy division between the ground plane and the parabola. The data of Figure 35 were calculated using an image horn displaced 14 degrees below the axis of the parabola having an 8 inch focal length. This setting gives an image beam between one and two main-beam beamwidths from the axis. For any one ground-plane-reflector combination the defocusing effects are secondary to power division effects. In image-beam-shaping antennas the image-horn position is restricted, so Figure 35 can be used for all images encountered in beam-shaping antennas using the design procedure suggested in this study.

The position of the image beam.--The beam deviation factor of a reflector is defined as the ratio of the angular displacement of the image-beam peak above the axis to the angular position of image horn below the axis. Silver and Pao[19] investigated the beam deviation factor for paraboloids of revolution and found that it changes from 0.75 to 0.98 as the F/L ratio is changed from 0.25 to 0.9. The term F is the focal length of the parabola and L is the diameter of the circular aperture. This information is based on the aperture of the reflector subtending an angle approximately equal to the 10 db beamwidth of the horn feed. It should be obvious that the beam deviation factor of a cylindrical parabola,

similar to that shown in Figure 26, will be different from that of the paraboloid because the reflected rays from a parabola fed off-axis are not parallel and the resulting secondary-beam position will depend on which portion of the parabola is most heavily illuminated. The reflector illumination caused by the flat ground plane will be maximum at the bottom of the reflector for all cases where the horn is aimed above the vertex of the parabola. The curves in Figure 36 show the variation of the beam deviation factor as a function of the F/D_v ratio of the reflector. The solid curves are used with reflectors energized by horns aimed at the vertex and the dashed curves are used when the horn is aimed $D_v/5$ above the vertex. The horn patterns used to obtain the information in Figure 36 were of the same general shape as the measured radiation patterns shown in Figure 29. These curves show that, for any one horn aim and constant $G(\psi_m)$, the beam deviation factor increases as the F/D_v ratio increases. This is expected because, as F/D_v increases, the curvature of the parabola decreases or the parabola looks more like a flat plane. The beam deviation factor for a flat plane is unity, since the angle of reflection is equal to the angle of incidence. As the horn is aimed above the vertex, with $G(\psi_m)$ remaining constant, the ratio of the image-beam current at the top of the reflector to that at the bottom of the reflector decreases and the beam deviation factor increases. The beam deviation factor for horn aims between the vertex and $D_v/5$ above the vertex can be found by interpolation. For any one setting of the horn aim, the position of the peak of the image beam depends on the position of the image horn, but the beam deviation factor can be treated as a constant, as long as the peak of the image beam is between $\frac{1}{2}$ and 2

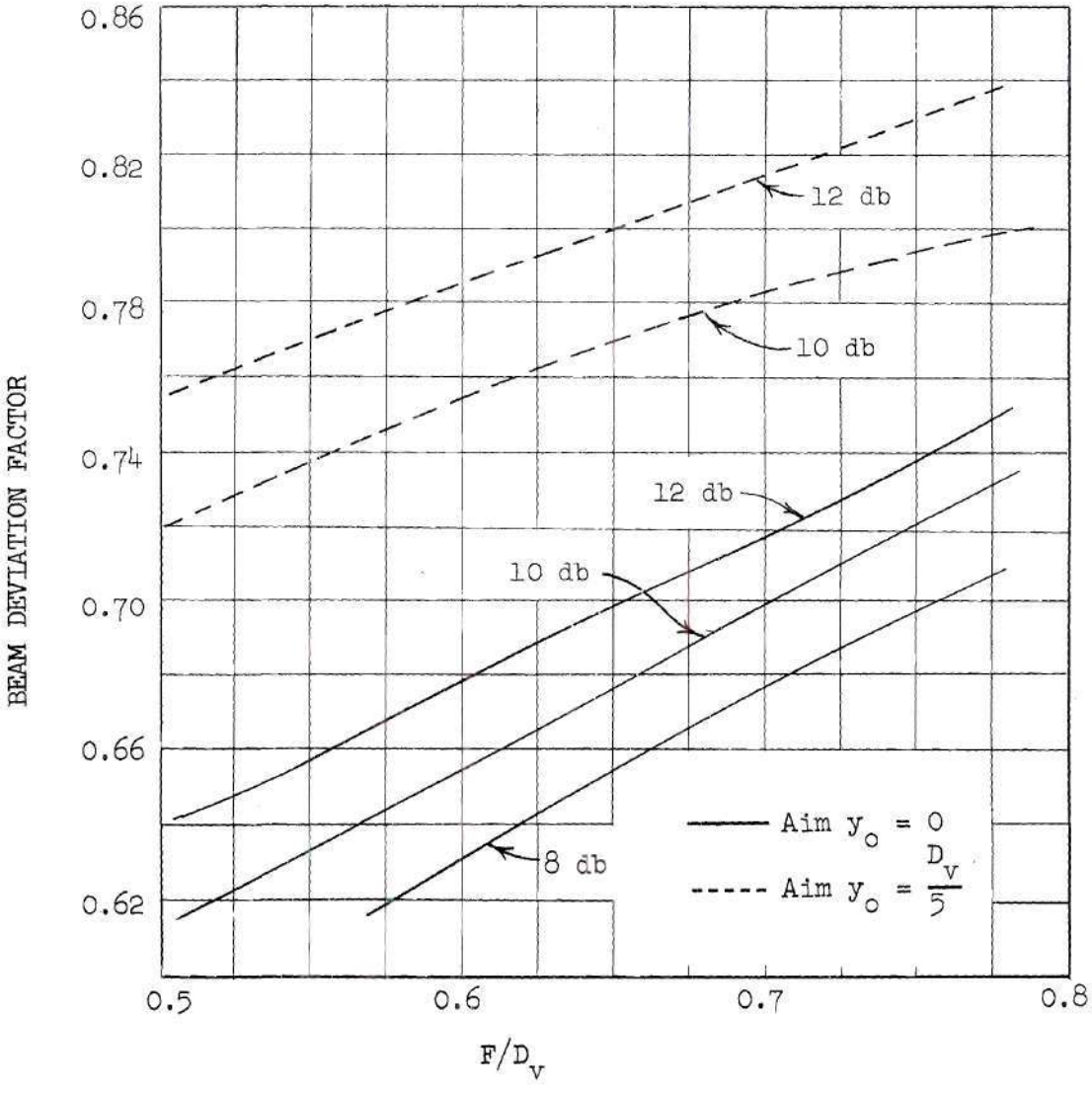

Figure 36. Beam Deviation Factor as a Function of Reflector Shape and Horn Aim

half-power main beamwidths from the axis of the parabola.

Image beams from curved ground planes.--The vertical radiation pattern of an antenna formed by a parabolic reflector, a line feed, and a flat ground plane can at best provide a shaped beam over a limited angular region. If wider vertical coverage is necessary, the phase of the reflector currents that cause the image beam must be altered to scatter the energy over a wider vertical angle. Several possible ground-plane shapes which widen the image beam are shown in Figure 37. These ground planes all have the common feature that they establish multiple images feeding the reflector. The ground plane in Figure 37(a) which is made of two flat planes, causes two or more images depending on the angle α. The broken ground plane of Figure 37(b) creates two images but does not provide a radiation pattern as smooth as the curved ground plane shown in Figure 37(c). This curved plane creates a continuous image and has proved very satisfactory in beam-shaping problems.

Calculations, with Equations (32) and (43), for circular ground planes similar to Figure 37(c) show that the magnitude and phase of the image beam between the main- and image-beam peaks are relatively insensitive to changes in ground-plane curvature. Consider for example the antenna in Figure 38, which shows a horizontal flat ground plane and a circular ground plane tangent at $Z = F$ and $y = -b/2$. The cross section of the ground plane is a circle with its center at $Z = F$ and $y = R_c - b/2$, where R_c is the radius of the circle. Curves A in Figures 39 and 40 show the magnitude and phase of the image beam for the antenna where R_c is infinite (the ground plane is flat), $b = 2.0, F = 8.0$, and $y_m = 10.5$ inches. For this particular example the horn is aimed at the vertex, the

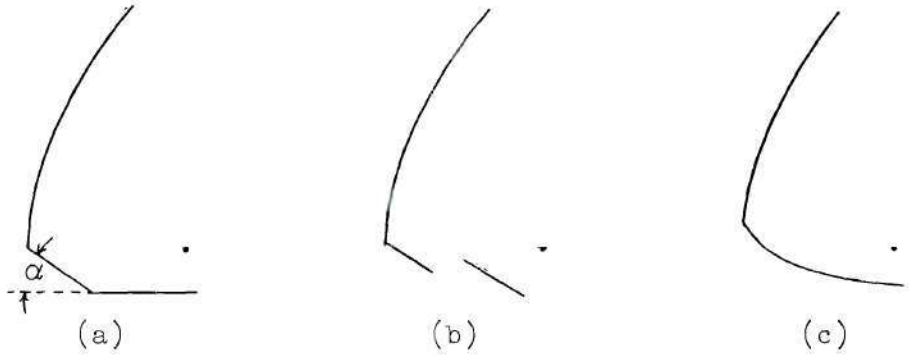

Figure 37. Ground Planes That Give Multiple Images

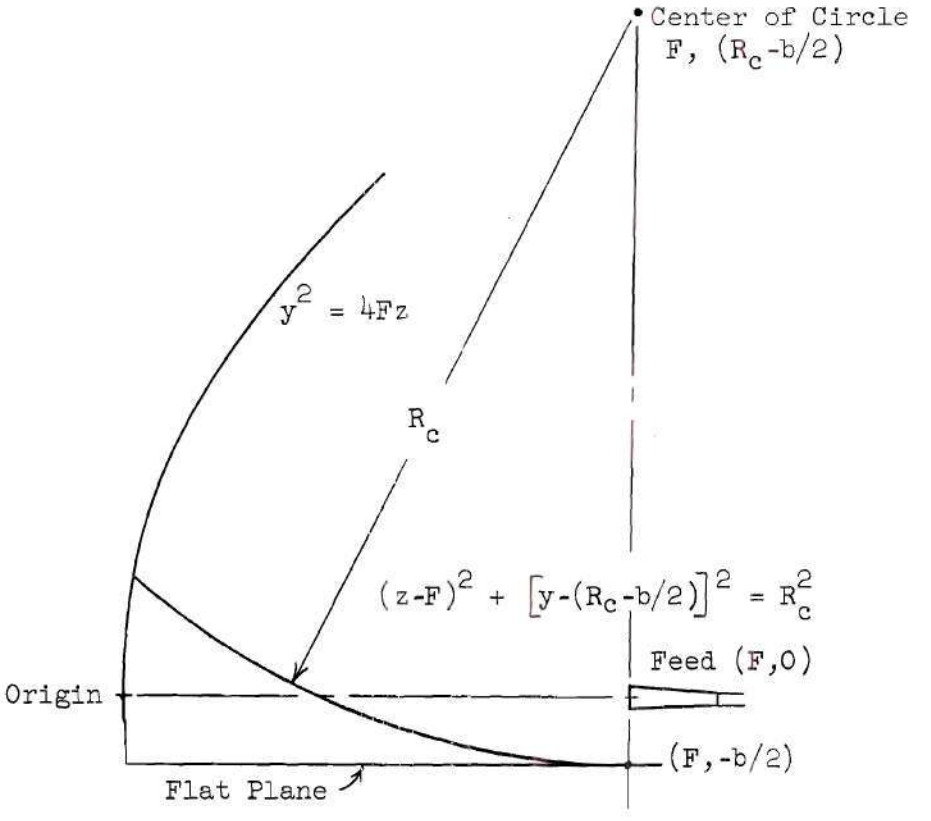

Figure 38. Cross Section of Reflector Used in Image Beam-shaping Antennas

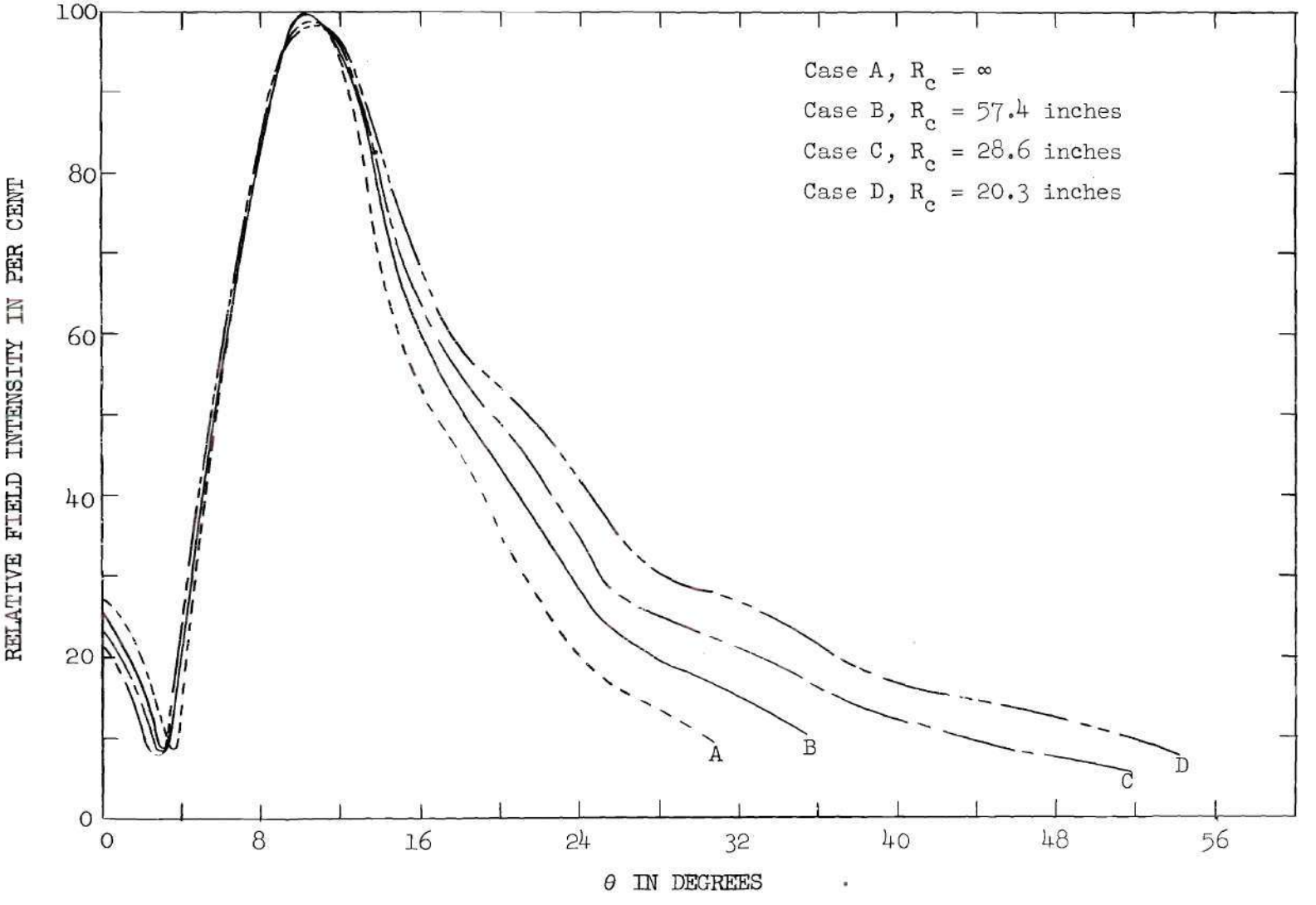

Figure 39. Typical Image Beams from Circular Ground Planes

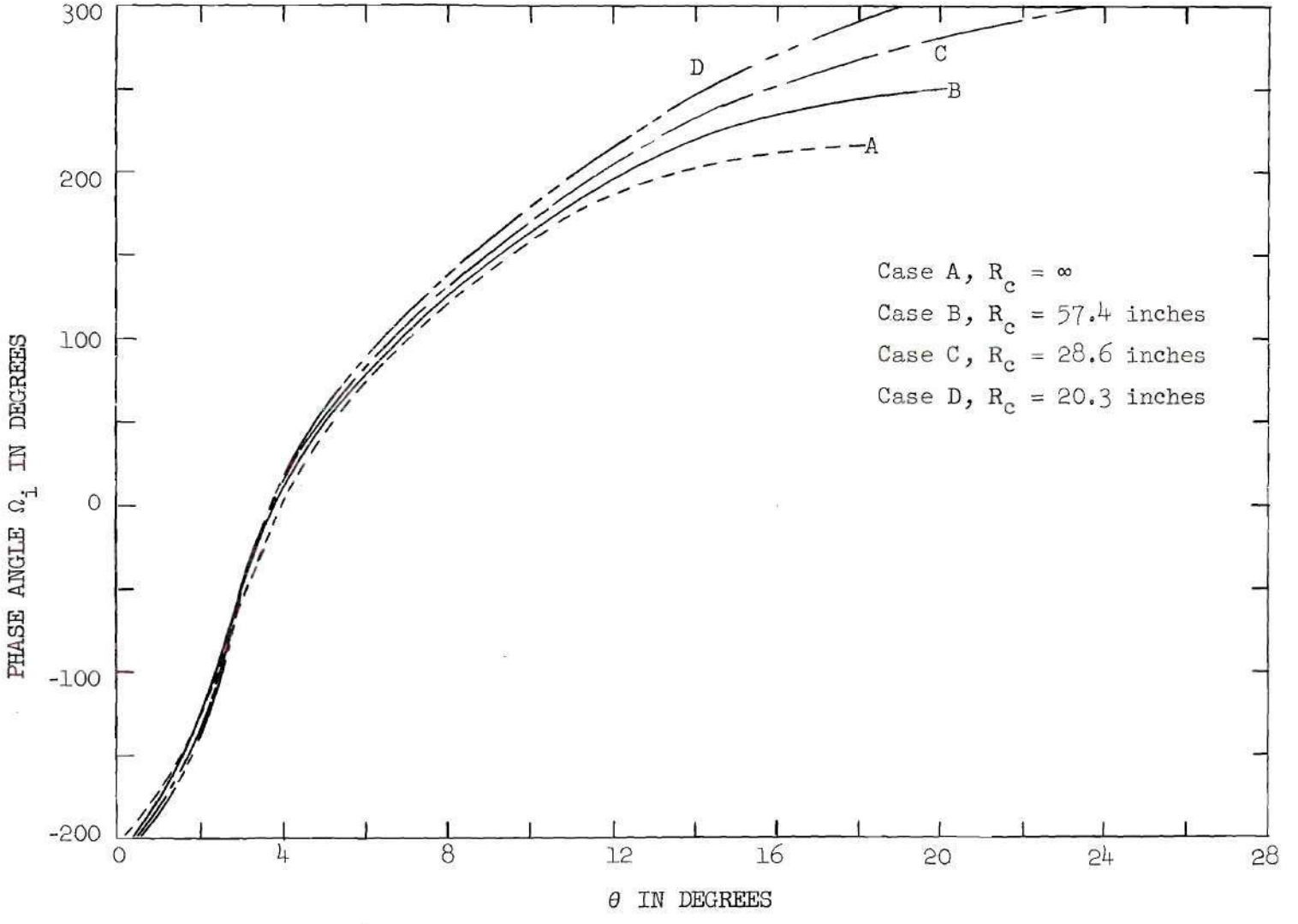

Figure 40. Typical Phase Relationships of Image Beams of Circular Ground Planes

gain of the horn $G(\psi_m)$ is about 10 db below the peak horn gain, and the frequency is 9300 mcps. The curves for B, C, and D show the image beams caused by circular ground planes with radii of 57.4, 28.6, and 20.3 inches respectively, all other factors being constant. These curves show that the image beam in the critical region between the main- and image-beam peaks changes very little with changes in ground-plane curvature. This same behavior was observed for other antennas having different F/D_v ratios and different horn aims. The curves in Figures 39 and 40 are not intended for use as design curves, but they can be useful in a qualitative preliminary design.

As the radius of the ground plane decreases, the magnitude of the direct ground-plane beam increases and in some instances it can cause undesirable effects. For example, calculations in Chapter VI show that the sum of the direct ground-plane and direct-horn beams, for the antenna of Figure 38 with R_c = 20.3 inches, is as large as the image beam at the larger elevation angles. Improper phase relationships of the beams can give a very irregular pattern. Thus the minimum ground-plane radius is determined by the allowable direct ground-plane radiation.

Since changing the ground-plane curvature does not change the image beam in the region between the main and image-beam peaks, only changes in the main beam have to be considered in estimating the shape of the total field in the region between the main and image beams. Although the circular gound plane discussed is very useful, it is only one of a myriad of possible ground-plane shapes.

CHAPTER VI

DESIGN PROCEDURES AND COMPARISONS OF CALCULATED AND MEASURED RADIATION PATTERNS

The purpose of this chapter is to show the agreement between the calculated and measured radiation patterns of antennas employing image beam-shaping principles and to demonstrate the usefulness of the design curves presented in Chapter V. In order to show the usefulness and applicability of image beam-shaping principles as presented in this study, three examples are treated. In the first example, calculated data and measured radiation patterns are presented to show that images can be used to obtain a radiation pattern that closely approximates a $\csc^2\Theta$ pattern over a wide angular region. The design procedure in this example is that suggested in Chapter V, namely to use the design curves to obtain a radiation pattern that approximates a shaped beam over a small angular region and then to increase the angular coverage by changing the shape of the ground plane. The feed of the first example is vertically polarized, whereas the feed of the second example is horizontally polarized. These examples show that the beam shape obtained by using a horizontally polarized source is radically different from that obtained using the vertically polarized source. The third example shows through measured patterns that partial ground planes can also be used to create asymmetrical radiation patterns suitable for some radar applications.

Example 1.--In the following example it is assumed that a vertically polarized shaped beam is needed at 9300 mcps to provide vertical-plane coverage from an elevation angle Θ of ten degrees to as large an angle as possible, ninety degrees being the maximum value. It is desirable but not physically possible to make the antenna gain zero outside the specified angular region. Even if the upper elevation angle had been specified, there is no single antenna that must be used to obtain a radiation pattern that approximates the specified pattern. There are, however, factors discussed in the following paragraph which help in the determination of the first parabolic reflector used in solving this problem.

To achieve a sharp cut-off below $\Theta = 10$ degrees, the height of the reflector should be large, but from the standpoint of wide-angle beam shaping, the height should be small. Since the image beam must be wide to give the large angular coverage, the feed must be aimed near the vertex to provide sufficient energy into the ground plane. The choice of the F/D_V ratio is due in part to the maximum angle of the $\csc^2\Theta$ coverage. It can be seen from an examination of Figure 21 that the main and image beams will be zero above an angle $\theta = \theta_m$ from the axis of the reflector because of the blocking action of the top of the reflector, so from this standpoint the F/D_V ratio should be as large as possible. However, if F/D_V is too large, the direct radiation from the ground plane and horn will cause trouble at the larger elevation angles. As a result of the factors mentioned above, a reflector was selected that had a focal length of 8 inches and a height

D_v of 10.5 inches. The reflector was fed by a vertically polarized feed, horn number one in Figure 29, aimed at the vertex of the parabola. The position of the flat ground plane will be selected after the main-beam properties have been ascertained.

The first step in the solution of the problem is to determine the characteristics of the main beam. With the dimensions of the reflector given above and from Figures 26, 29, and 38, it can be seen that $\psi_m = 66.5$ degrees and $G(\psi_m) = -8$ db. The illumination at the top of the reflector is a little above the nominal 10 db value, but a wide-angle primary beam is desirable to give a high incident energy into the ground plane. The normalized illumination function $f(y_m)$ is a factor in determining the beamwidth and is calculated using Equation (54).

$$f(y_m) = 100 \left[\frac{15.87}{11.42}\right]^{\frac{1}{2}} + \left[\frac{100}{8}\right]^{\frac{1}{2}} = 33.3 \text{ per cent.} \qquad (56)$$

This illumination level gives, using curve A in Figure 27, a beamwidth factor K_o of 55.4 which is used in Equation (55) to give

$$BW_m = 55.4 \left[\frac{1.27}{10.5}\right] = 6.71 \text{ degrees.} \qquad (57)$$

Since the curves of Figure 24 are plotted for a horn aimed at the vertex, no interpolation is necessary and the values of the field intensity in the main beam can be taken directly from the design curve since the beamwidth is known. The values of the field intensity of the main beam are given in Table 1.

Table 1. Values of Main Beam, Example 1, Taken from Design Curves and Calculated Using Equation (32)

θ	Design Curves $\mathring{U}_m$	Equation 32 $\hat{U}_m$
0	100 /0	100 /0
1	97 /20	--
2	87 /39	87.6 /40.2
3	75 /59	--
4	59.5 /77	60.1 /76.2
5	45.5 /91	--
6	30 /100	31 /98.6
7	20 /92.5	--
8	17 /75	17.3 /85
9	19 /70	--
10	20 /78	18.4 /82.1

The next step in the solution of the problem is to select the position of the ground plane. The first choice of this position is really a guess based on previous experience by the designer. However, certain facts about the image beam can be determined from the design curves independent of the position of the ground plane. For example, the F/D_v ratio of the reflector is 0.76, so the beam deviation factor is found from Figure 36 to be about 0.7. Also it is evident from Figure 31(a) that the beamwidth of the image beam will be less than 1.1 times greater than the main beam. Further, it can be seen from Figure 35 that the peak magnitude of the image beam will be about 88 percent of the peak magnitude of the main beam. With these facts in mind, rough calculations show that, from a magnitude standpoint only, an image beam having a peak near θ = 10 degrees will provide a field large enough to give an overall radiation pattern that is smooth in the region between the peaks of the main and image beams. The phase relationships are very important, but they cannot be determined until the position of the image has been established. The initial ground plane is then placed at y = -1.0 inch, which gives an image at z = 8.0, y = 2.0 inches and an image-displacement angle v of arc tan 2/8 = 14.04 degrees. This image position creates an image beam with a peak at 0.7 x 14.04 = 9.83 degrees, which is close to the 10 degrees mentioned above. The ratio of the image-beam to main-beam beamwidth is found from Figure 31(a) to be 1.05. Since the beamwidth of the main beam is 6.71 degrees, the beamwidth of the image beam is 7.06 degrees. The phase of the field intensity of the image beam at its peak can be seem from Figure 34 to lag the image-

beam current at the vertex by about 7.5 degrees. The phase of the image-beam field intensity at the peak is ζ and is given by

$$\zeta = -\beta\left[\sqrt{F^2 + b^2} - F\right] + \Sigma \qquad (58)$$

$$= -\frac{360}{1.27}\left[\sqrt{8^2 + 2^2} - 8\right] \quad -7.5 = -77 \text{ degrees},$$

where the negative sign indicates a phase lag. The first term in Equation (58) accounts for the phase lag of the image-beam current due to the difference in distances from the focal line to the vertex and the image to the vertex. The main-beam current at the vertex is used as the reference in all these calculations.

With the information just found on the image beam, Figure 30 is used to find the field intensity of the image beam at the various elevation angles. These values of the image beam taken from Figure 30 are given in Table 2. Also included in Table 2 are the values of the image beam calculated using Equation (32). In evaluating Equation (32), the integral was represented by a finite series of 92 terms, each representing the field from a section of the parabola $\Delta y = 0.125$ inch in height. Calculations based on a larger element spacing of 0.25 inch were accurate in finding the fields near the peak of the beam but inaccurate at values below about 20 per cent of the peak.

A comparison of the field intensities in Tables 1 and 2 as calculated using the design curves and also using Equation (32) shows the accuracy of the design curves. The last step in finding the radiation pattern of the parabola and the flat ground plane is the simple addition

Table 2. Values of the Image Beam, Example 1, Taken from the Design Curves and Calculated Equation (32)

θ	Design Curves $\dot{U}_i$	Equation (32) $\dot{U}_i$
0.00	Not available from	25.4 $\angle$-125.6
2.00	design curves	17.1 $\angle$-26.2
4.00	17.6 $\angle$-197	15.7 $\angle$-212
5.00	30.8 $\angle$-169	--
6.00	48.4 $\angle$-144	51.0 $\angle$-151
7.00	64.2 $\angle$-125	--
8.00	78.3 $\angle$-109	80.5 $\angle$-115
9.00	86.2 $\angle$-96	--
9.83	88.0 $\angle$-77	--
10.00	87.5 $\angle$-76	89.5 $\angle$-82
11.00	85.2 $\angle$-58	--
12.00	77.4 $\angle$-46.5	78.0 $\angle$-50
14.00	59.0 $\angle$-28.5	59.0 $\angle$-33
16.00	46.0 $\angle$-16.5	45.0 $\angle$-26

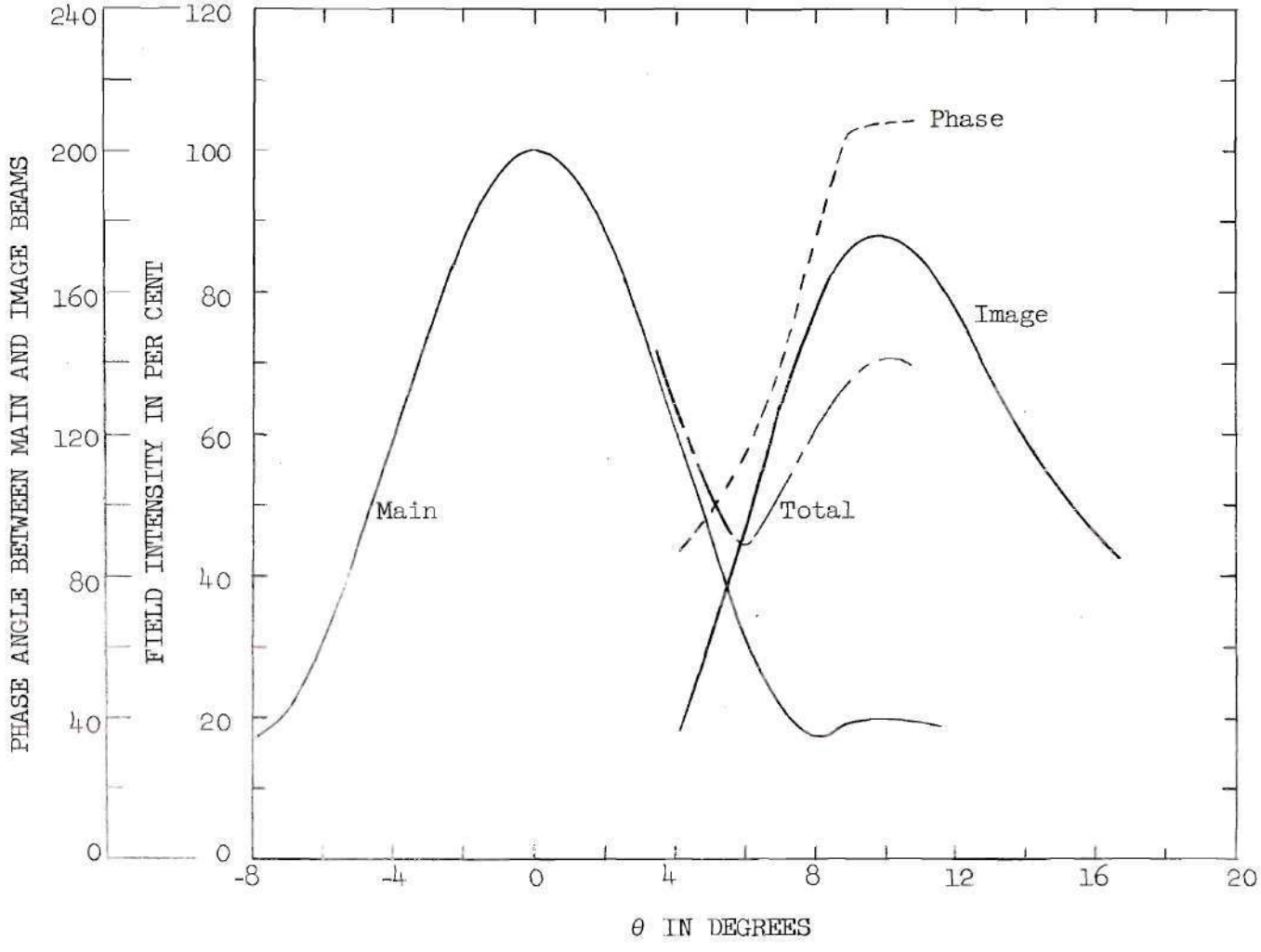

Figure 41. Fields Calculated Using Design Curves

of the main and image beams. Note that data obtained from the design curves does not give the total beam, except in the region between the two beams. However, this is the most important part of the pattern because this is the region where improper phase relationships can cause a null in the pattern. Even though the total beam cannot be calculated at all angles, the information obtained from the design curves and plotted in Figure 41 gives a good indication of the shape of the overall radiation pattern.

The calculated and measured radiation patterns for this antenna with the flat ground plane are shown in Figure 42. The first feature to note about this figure is that the abscissa is plotted in terms of the elevation angle Θ and the peak radiation is 10 degrees above the horizon. In the previous discussion, the radiation pattern of each antenna has been given in terms of θ as measured from the axis of the parabola instead of the angle Θ which, as is shown in Figure 1, is the angle measured from the horizontal. In cases where the peak radiation is to be along the surface of the earth, the two angles θ and Θ are the same. However, the desired radiation pattern for the antenna in example 1 is to be cosecant-squared, starting at an elevation angle of 10 degrees so that the axis of the reflector will be tilted up in order that the maximum radiation will be 10 degrees above the horizon. Thus for this case $\Theta = \theta + 10$ degrees. The second feature to note about Figure 42 is the excellent agreement between the calculated and measured patterns, particularly between the main- and image-beam peaks. Also shown at discrete points in Figure 42 are the values of the total field

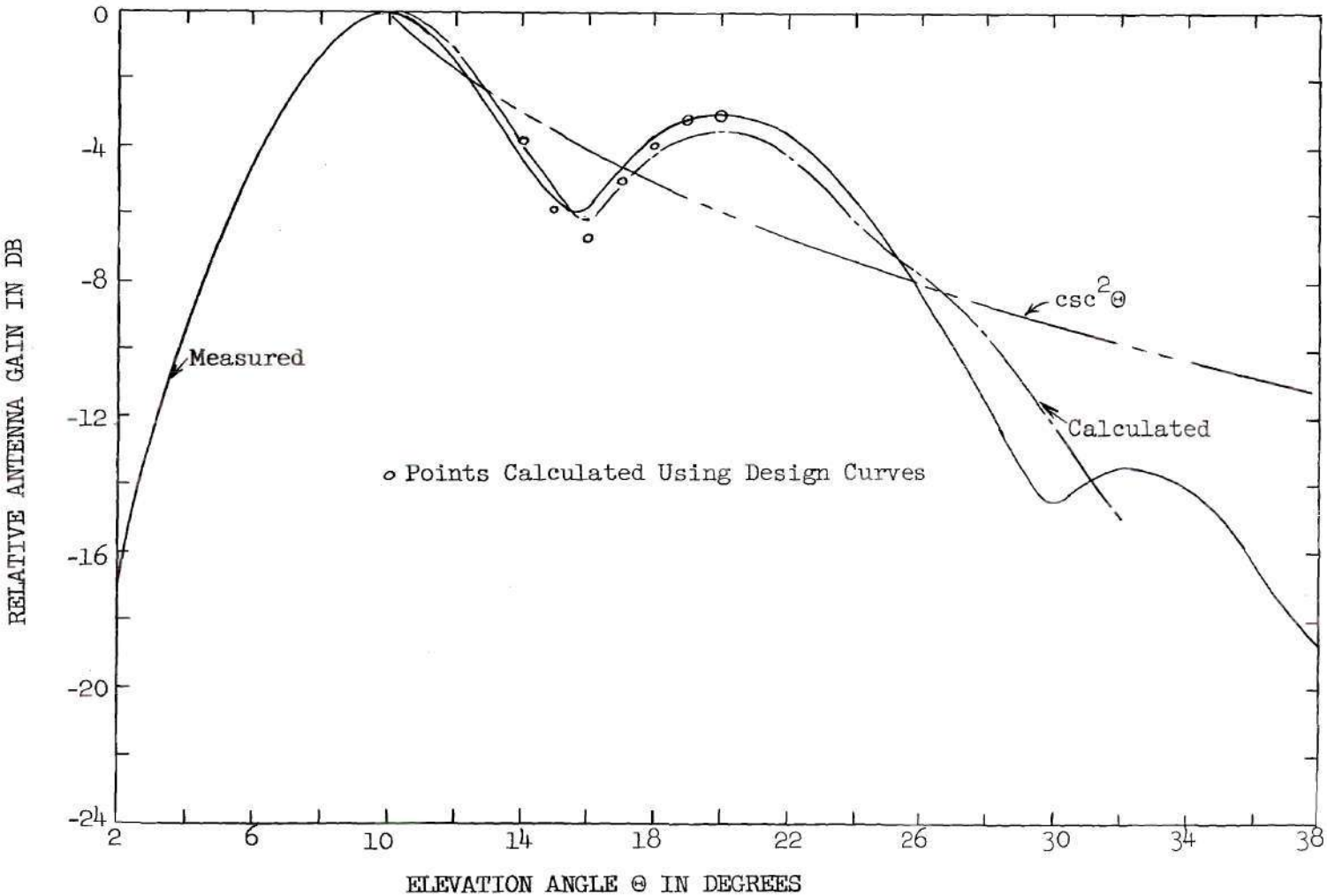

Figure 42. Calculated and Measured Radiation Pattern of Cylindrical and Flat Ground Plane

as taken from the design curves. The design-curve data were made to agree with the measured value at $\Theta = 20$ degrees because the design-curve value of the total field is not known at $\Theta = 10 (\theta = 0)$. A third important feature of the curves in Figure 42 is the shape of the measured pattern as compared with the $\csc^2\Theta$ pattern. It is evident that the field at $\Theta = 16$ degrees should be increased if possible to make it conform with the desired beam. The first thought is to move the image beam closer to the main beam to "fill in" this minimum. However, an analysis using the design curves shows that moving the image beam closer to the axis by moving the ground plane, changes the phase relationships and actually gives a more pronounced dip between the two beams. This predicted behavior has been verified experimentally. Moving the image beam further from the axis makes the main- and image-beam intensities more nearly in phase than before at the point where the fields are the same magnitude, but makes the fields at the crossover point smaller. Moving the image beam further from the axis gives no net improvement in the beam shape.

Fortunately, when the ground plane is made convex to give more energy at the higher elevation angles, the minimum between the beams is made less pronounced because of changes in the main beam. Making the ground plane circular, as shown in Figure 38, has the obvious effect of increasing the width of the main beam because the main-beam aperture is reduced. Perhaps not so obvious is the change in the phase relationships in the main beam caused by cutting off the bottom of the parabola. Since the origin, after the change, is no longer at the bottom of the

aperture, the design curves of Figure 24(b) must have a corrective term $\beta y_a \sin\theta$ added. The term y_a is the distance from the axis to the intersection of the ground plane and the parabola. The size of this corrective term can be shown by a consideration of the case where $y_a = 0.65$ inch and the frequency is 9300 mcps. The change of 0.65 inch causes the phase of the main beam at $\theta = 6$ degrees ($\Theta = 16$) to be 120 degrees leading compared with 100 degrees for the flat ground plane. If the image beam at $\theta = 6$ degrees is not affected by the change in the ground-plane shape, then the phase difference between the main and image beams will be changed from 115 to 95 degrees. Decreasing the radius of curvature of the ground plane tends to increase slightly the image beam below the peak as shown in Figure 39, so this also tends to make the dip in the over-all pattern less pronounced. To summarize, making the ground plane concave will reduce the sharpness and depth of the minimum between the main and image beams, make the image beam extend over a wider angular range, and decreases the magnitude of the main beam relative to the image beam.

The first circular ground plane tested had a radius of curvature of 20.3 inches and was tangent to the flat ground plane at z = 8.0, y = -1.0 inch. The measured radiation pattern of this antenna is shown by the solid curve in Figure 43. The dashed pattern in this figure was calculated using only the main and image beams, i.e., the beam due only to currents on the parabola. The calculated beam was evaluated by using a finite series of terms to represent the integral in Equation (32). In the evaluation of the series, the distance betweeen current

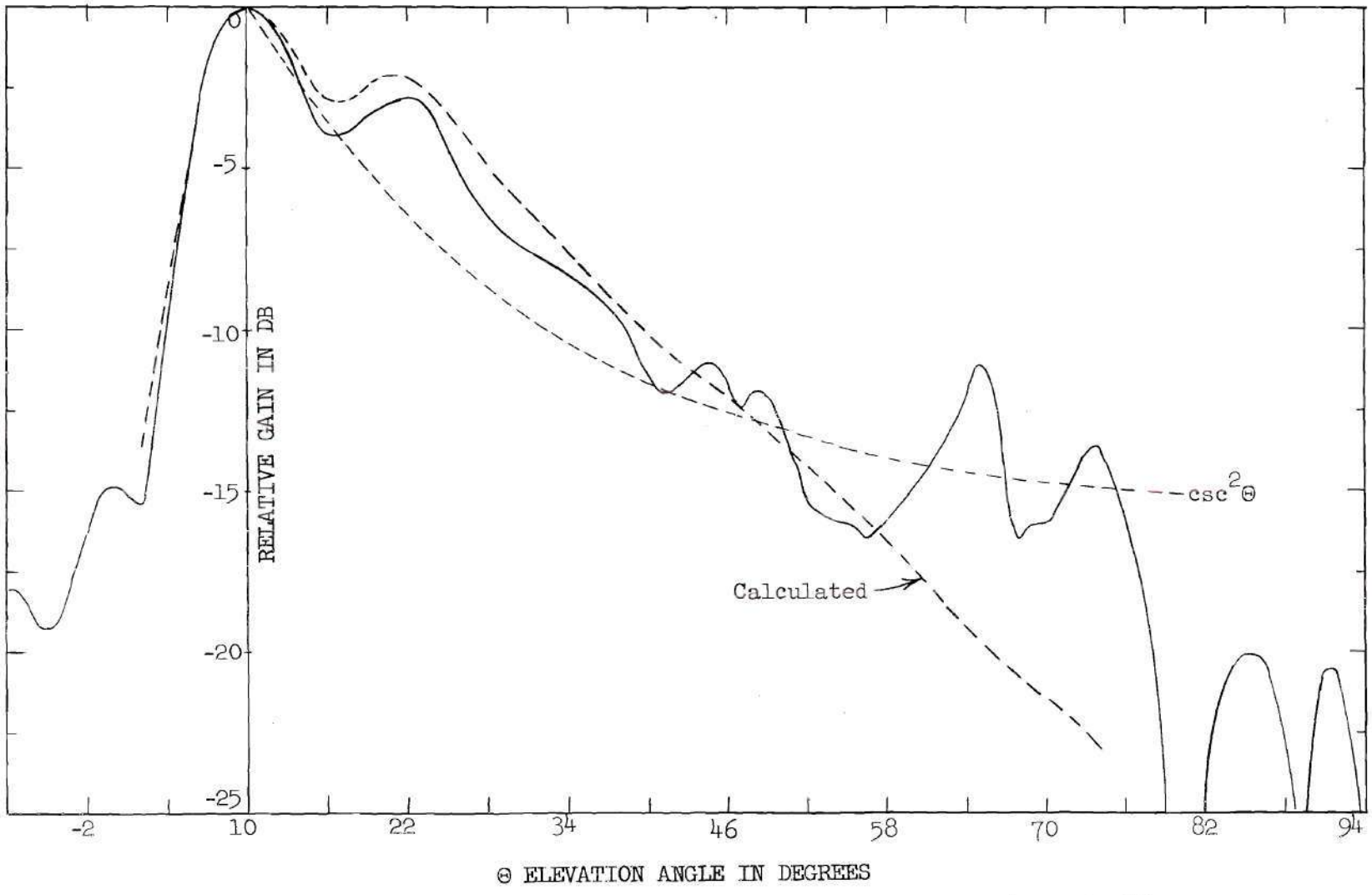

Figure 43. Radiation Pattern of Image Beam-shaping Antenna (Example 1)

elements was 0.125 inch. Breaking the calculated pattern up into components shows which portion of the total pattern is due to direct radiation from the horn and ground plane and which portion is due to currents on the parabola.

Before continuing the discussion of Figure 43, it is necessary to note the shape of the radiation pattern of the horn and ground plane because this feature accounts for the irregularities in the pattern in Figure 43 at the larger elevation angles. When the parabolic section of the reflector is removed, the radiation pattern is the sum of the direct ground-plane and direct-horn beams. This beam in the region above the ground plane consists of many well-defined minor lobes as shown in Figure 44. The shape of this radiation pattern, called the direct pattern, is not as important in this problem at elevation angles greater than $\Theta = 80$ degrees as the shape of the pattern at angles $\Theta < 80$ degrees, because the direct radiation in the former range is partially or completely blocked by the parabola. It is the direct radiation at $\Theta < 80$ degrees, which is essentially unchanged by the presence of the parabola, that can cause irregularities in the final pattern. The minor lobe structure of this pattern, Figure 44, is typical of the radiation from two separate sources, the horn and the ground plane in this case. The fields due to the two sources will be alternately in and out of time phase as the elevation angle changes, and the result is a series of minor lobes more or less evenly spaced and separated by well-defined minima. The minor lobes are not all the same size because each of the two sources is directive to some extent.

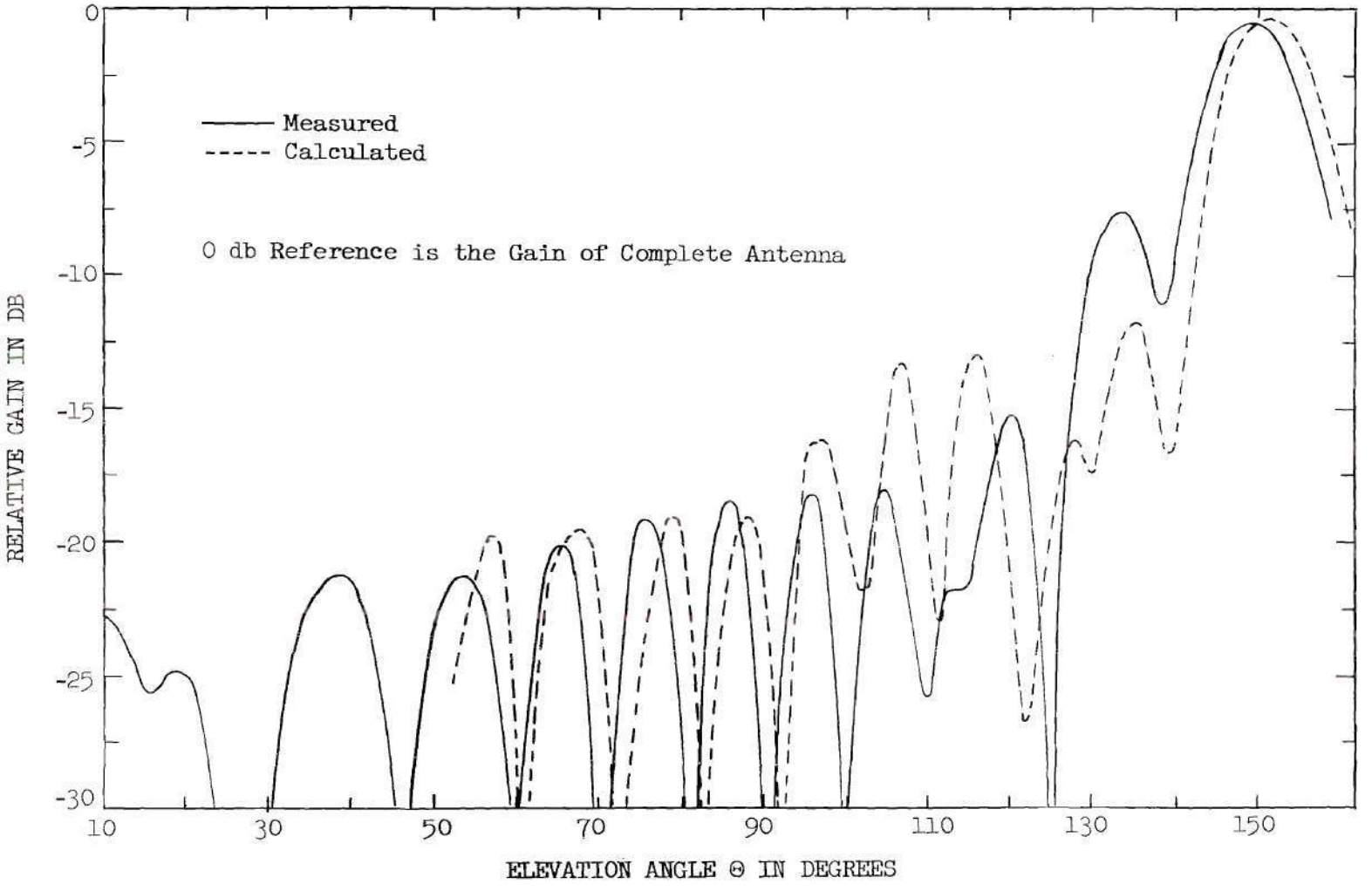

Figure 44. Radiation Pattern of Horn and Circular Ground Plane of Example 1

The calculated direct beam is also shown in Figure 44. Before the direct ground-plane beam and direct-horn beam can be combined to get the calculated direct beam, the gain of the feed relative to the gain of the ground plane must be found by a procedure similar to that given in Appendix II. Most of the calculated minor lobes have the same magnitudes as the corresponding measured lobes but the positions of the calculated lobes are in error. The difference in the positions of the lobes can be easily explained in terms of the phase of the direct radiation from the feed. The magnitude of the direct-horn beam was obtained from the measured primary pattern, but phase angles were based on energy coming from some center of phase inside the mouth of the horn. This obvious error in calculating the phase of the direct-horn radiation, using the center of feed, at large values of ψ is the main reason for the disagreement between the measured and calculated patterns in Figure 44. However, the differences in the positions of the calculated and measured minor lobes can be tolerated because the main purpose of the calculations is to show the magnitudes of the lobes. If the minor lobes of the direct beam are comparable in size to the image beam, then the total pattern will be irregular. However, some control of these irregularities is obtained by changing the horn position slightly. Small movements of the horn along the axis of the reflector have a large effect on the beam shape at the larger elevation angles and a small effect near the peak of the beam. If the irregularities cannot be properly controlled, the ground-plane shape must be altered even at the expense of decreased angular coverage of the shaped beam.

Returning to the discussion of Figure 43, it can be seen that the irregularities in the total pattern are caused by the direct beam combining with the image beam. Actually in the radiation pattern shown in Figure 43, this is not too serious for $\Theta < 80$ degrees because there are no serious dips in the pattern below 80 degrees. In this particular example, the direct beam has been used to advantage to extend the shaped-beam coverage by a small amount. It should not be inferred, however, that the direct radiation will always be beneficial.

In this example the author was fortunate in having the first curved ground plane provide a satisfactory shaped beam. If the radius of curvature of the ground plane had been much smaller than that used, the direct beam would have been too large for use and of course a larger radius of curvature would not have provided the wide angle $\csc^2\Theta$ pattern desired. This problem certainly contains a minimum number of calculations. The number of attempts necessary to get a desired beam depends of course on the experience of the designer and on how close the final pattern must come to the specified patterns.

Example 2.--In the previous example it was shown that the flat ground plane used with a cylindrical parabola and a vertically polarized feed gives a radiation pattern with a dip between the main and image beams. Making the ground plane concave gave a smoother pattern but there was still a slight dip between the peaks of the main and image beams. In some applications it is desirable to have the image beam merge with the main beam so that the antenna gain function $G(\theta)$ decreases monotonically with increasing θ. It will be shown in this example that this can be

accomplished easily with horizontally polarized waves. This example further demonstrates the value of the design curves of Chapter V. No particular beam shape is set as a goal, but the beam will be of the shaped-beam variety.

The antenna used in this second example consists of horn number 3, see Figure 29, aimed 11.0 degrees above the vertex of a cylindrical parabola having a focal length F of 7.0 inches and a height D_v of 13.5 inches. The flat ground plane is parallel with the axis of the parabola and 0.525 inch below it, i.e., b in Figure 38 is 1.05 inches. The F/D_v ratio for this reflector is 0.516 and the frequency is 9300 mcps. The horn is aimed $D_v/10$ above the vertex, which gives a primary-feed gain $G(\psi_m)$ of 12 db below the peak gain. Using Equation (54), $f(y_m)$ is found to be 17.3 per cent which when used with Figure 27 gives a beamwidth factor K_o of 60. Using $K_o = 60$ in Equation (55) gives a beamwidth of 5.65 degrees for the main beam. Since the displacement angle v of the image horn is 8.5 degrees, arctan 1.05/7, the beamwidth of the image beam is found by interpolation between Figures 31(b) and 32 to be about 8.4 degrees. The phase of the field at the peak of the image beam is

$$\zeta = -\frac{360}{1.27}\left[\sqrt{7^2 + (1.05)^2} - 7\right] + 180 - 27 = 128.8 \text{ degrees}, \qquad (59)$$

where the 180 degrees accounts for the phase shift at the ground plane and the 27 degrees is Σ as found from Figure 34. It can be seen from Figure 35(b) that the peak of the image beam is about 49 per cent of the peak magnitude of the main beam. Since the beam deviation factor is 0.695, see Figure 36, the peak of the image beam will be at the value $\theta = 8.5 \times 0.695 = 5.9$ degrees.

The information obtained on the main and image beams has been used in conjunction with Figures 24, 25, and 30 to obtain the predicted beam as given in Table 3. Also shown in Table 3 are the main and image beams calculated using Equation (43). The agreement between the field taken from the design curves and the field calculated using Equation (43) is poorer than in the first example because in the use of the design curves interpolation was necessary in Example 2 but not in Example 1. In this second example the peaks of the two beams are close enough together so that the total field can be predicted at the peak of both beams as well as in the region between the beams. The design data in Table 3 show that the phase difference between the main and image beams is less than 28 degrees in the region between θ = 0 and 5 degrees. It is evident from the data in Table 3 that the main and image beams merge into a single asymmetrical beam with the peak shifted slightly above the axis of the parabola.

When the flat ground plane is changed to one having a radius of curvature of 20.3 inches, the ground plane and parabola intersect at y_a = 0.75 inch. The phase corrective term $\beta y_a \sin\theta$ amounts to about 11 degrees for the main beam at θ = 3 degrees, so at this angle the time phase angle between the main and image beams is 7 degrees as opposed to 18 degrees for the flat ground-plane case. The measured radiation pattern for this antenna, Figure 45, verifies the prediction that the main and image beams merge into a single asymmetrical beam. Figure 45 also shows the agreement between the measured pattern and that

Table 3. Values of the Main and Image Beams, Example 2, Taken from Design Curves and Calculated Using Equation (43)

θ	Design Curves $\dot{U}_m$	Design Curves $\dot{U}_i$	Design Curves Total	Equation (43) $\dot{U}_m$	Equation (43) $\dot{U}_i$
0	100/0	15.5/30	114.0	100/0	12.7/58.6
1	95.3/23	23.5/55	116.0	--	--
2	82.0/46.5	32/72	114.5	85/45.7	36/74.8
3	68.0/68	39/86	96.5	--	--
4	48.0/83	45/104	92.5	51/82.3	58/110.3
5	32.0/90	48/118	79.0	--	59/128
6	23.5/90	49/130	69.4	25.8/90	59/142.5
7	21.0/87	48/143	57.7	--	57/158
8	21.0/90	40/155	51.5	23/80	52/170

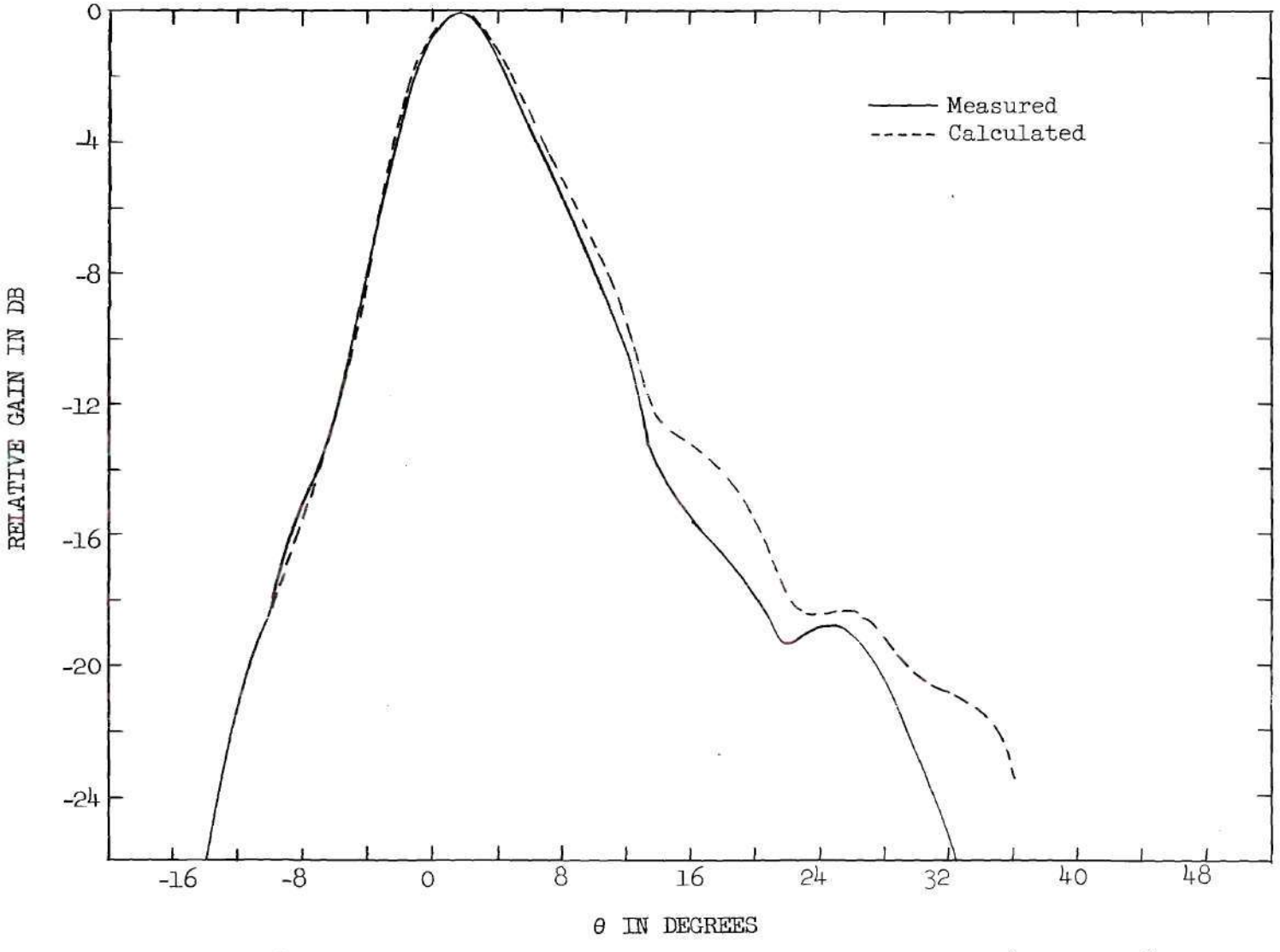

Figure 45. Radiation Pattern of Image Beam-shaping Antenna (Example 2)

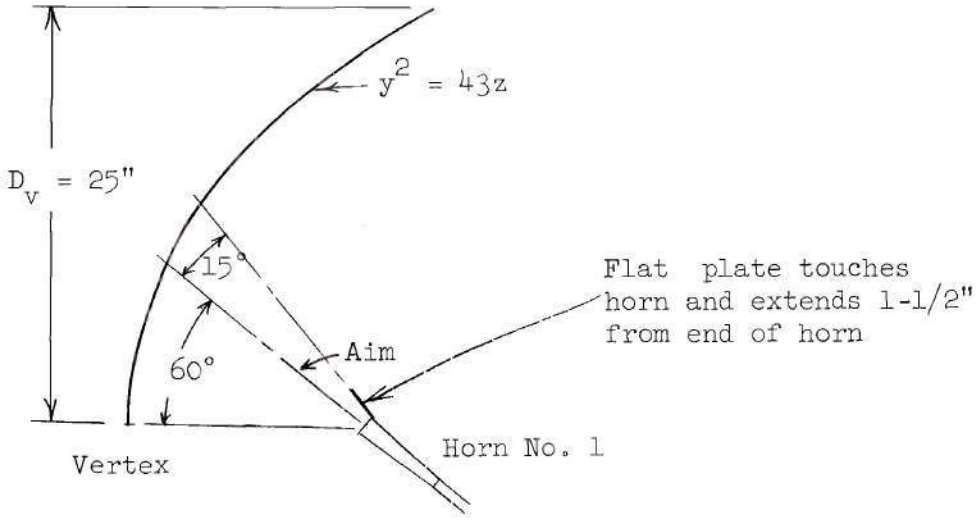

Figure 46. Geometry of Antenna Using a Partial Ground Plane

calculated using Equation (43). The direct radiation from the horn and ground plane was not used in the calculated pattern because most of the energy is concentrated near the axis where the direct radiation is very small.

This example shows that because of the 180 degree phase shift of the wave reflected from the ground plane, the image beam can be moved very close to the main beam without causing a dip in the pattern similar to that encountered in the problem of the antenna with the vertically polarized source. However, it can be seen that moving the image beam closer to the axis is undesirable if a wide-angle shaped beam is needed. If the ground plane is moved away from the feed in order to produce a wider image beam, a sharp null will appear between the main and image beams when the peak of the image beam is at $\theta = 9$ degrees.

Example 3.--The antenna described in this third example is a by-product

of the work done on the antennas employing ground planes that extend from the horn to the parabola. The antenna of Example 3 uses a partial ground plane above the horn as shown in Figure 46. Since the ground plane does not extend from the horn to the parabola, the design procedure used in Examples 1 and 2 is of no value for this antenna. The radiation pattern of this antenna, Figure 47, has an asymmetrical beam caused by the small ground plane above the horn. This pattern, Figure 47, is a type well suited to harbor-control radar installations where there is a need for a narrow beam to search the surface of the harbor, and also a need for extra energy radiated below the peak of the beam to show small objects on the surface such as bouys or floating objects hazardous to shipping.

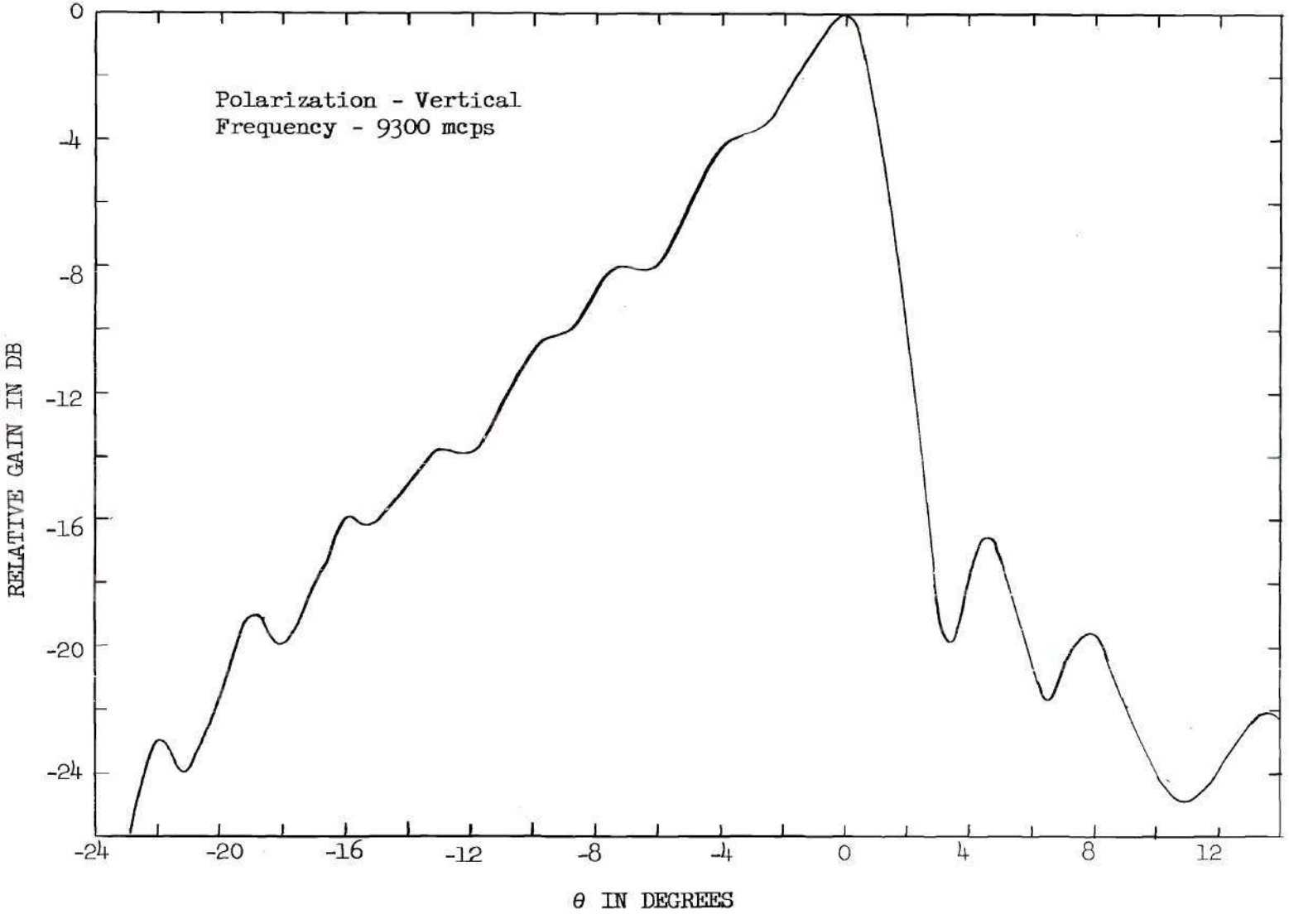

Figure 47. Radiation Pattern of Antenna with Partial Ground Plane (Example 3)

ground plane than with multiple horns, the simplicity and good impedance match of the feed used in the image method makes it by far the more desirable. The chief disadvantage of the image beam-shaping antenna described in this study is that of the relatively high gain required of the line source, an undesirable feature of any cylindrical-reflector antenna.

The agreement between the calculated and measured fields along the parabolic curves above the ground planes as shown in Chapter II proves that geometrical optics can be used to find the magnitude and phase of the waves reflected from ground planes as small as six wavelengths wide. Limitations on the radius of curvature of the ground plane are given in Chapter II.

The agreement between the measured radiation patterns in Examples 1 and 2 in Chapter VI and the patterns calculated using the current distribution integrals of Chapter IV demonstrates the applicability of these integrals to image-beam shaping problems. The data in Examples 1 and 2 show that narrow-beam patterns can be calculated from the main and image beams only but that wide-angle patterns must be calculated from the direct ground-plane and direct-horn beams in addition to the main and image beams. The inaccuracy of the calculated patterns at the larger elevation angles is due to a lack of knowledge of the phase of the direct-horn radiation at large values of ψ.

The design procedure presented in this study is to use the parabolic reflector and flat ground plane as the basic antenna. The approximate desired beam shape of the radiation pattern of the basic antenna

is obtained by use of the design curves, and then the ground plane is made convex to increase the angular coverage of the shaped beam. The data given in Examples 1 and 2 show that the design curves can be used to obtain information on the beam shape of the basic antenna without the necessity of evaluating the complicated far-field integral. The evaluation of the far-field integral is necessary only after approximate beam shapes have been obtained using the design curves.

Recommendations.--As a result of this study, two points have been brought out which warrant further investigation.

(1). A complete analysis of the partial ground plane as described in Example 3 is desirable.

(2). A continuation of this study would be to investigate improvements in the shaped beam which might result from modifications of the parabolic section of the reflector.

CHAPTER VII

CONCLUSIONS AND RECOMMENDATIONS

Conclusions.--The experimental radiation patterns presented in this study demonstrate conclusively that the image method of beam shaping can be used to obtain a cosecant-squared radiation pattern over a wide angular region. Although either polarization can be used, the phase relationships in the horizontally polarized antenna make it better suited for use on narrow-beam cosecant-squared applications. The wide-angle shaped beam represents the addition of four individual beams which can be made to give a pattern with no deep minima over a narrow frequency range. In narrow beam applications the total pattern is approximately the sum of only the main and image beams, so the frequency sensitivity is better than that of the wide-angle beam.

Because of the double-reflection process which takes place at the reflector surface, the parabolic section is "used" twice and is therefore smaller than the single-reflection-surface antenna, designed by Chu's method to give a beam of commensurate shape. Although the image-beam antenna is smaller than the corresponding shaped reflector of Chu, the radiation pattern in general is not as good an approximation of the cosecant-squared pattern as the shaped reflector.

The image beam-shaping method represents a significant improvement over the multiple-feed method. While the control of the field intensity at any one elevation angle is more difficult with the

$\dot{E}_r$ the phasor electric field reflected from the surface of a reflector.

$\dot{E}_{par}$ the phasor component of the electric field parallel to the pick-up dipole, see Figure 10.

$\dot{E}_{s\theta}$ the $\bar{\theta}_1$ component of the vector electric field scattered from a conducting surface.

$\dot{E}_{s\Phi}$ the $\bar{\Phi}_1$ component of the vector electric field scattered from a conducting surface.

$\left[E(\Theta)\right]_a$ the far field of a beam caused by antenna a.

F the focal length of a parabola.

$F(y)$ the aperture illumination function which is directly proportional to the field intensity on an equiphase aperture.

$f(y)$ the normalized aperture illumination function.

$G(x)$ the relative gain of the primary feed in the x-direction.

$G(\psi)$ the relative gain of the primary feed in the ψ-direction.

$\left[G_{max}(\Theta)\right]_a$ the maximum gain of antenna a.

h the height of a radar target above the earth.

$\bar{H}$ the vector magnetic field intensity, a function of time and space.

$\dot{H}$ the phasor magnetic field intensity, a function of time and space but not a vector.

$\dot{H}_d$ the phasor magnetic field intensity on the parabolic curve in Figure 7 or 8 due to direct radiation from the horn feed.

APPENDIX I

GLOSSARY OF NOTATIONS AND DEFINITIONS

English Letters

b	the y-coordinate of the position of the image horn as shown in Figure 7.
BW_i	the half-power beamwidth of the image beam.
BW_m	the half-power beamwidth of the main beam.
d	the distance from the vertex of the parabola to any point on the parabola as shown in Figure 21.
D	a dimension of the aperture of an antenna.
D_v	the vertical height of the parabolic antenna as measured from the vertex to the top, see Figure 26.
$\bar{E}$	the vector electric field intensity, a function of time and space.
$\dot{E}$	the phasor electric field intensity, a function of time and space but not a vector.
$\dot{E}_d$	the phasor electric field intensity on the parabolic curve in Figure 7 or 8 due to direct radiation from the horn feed.
$\dot{E}_d'$	the phasor electric field intensity on the parabolic curve in Figure 7 or 8 due to energy reflected from the ground plane.
$\dot{E}_i$	the phasor electric field incident onto the surface of a reflector.

APPENDICES

$\dot{H}_d$ the phasor magnetic field intensity on the parabolic curve in Figure 7 or 8 due to energy reflected from the ground plane.

$\dot{H}_i$ the phasor magnetic field intensity incident on the surface of a reflector.

$\bar{i}$ the unit vector along the x-axis in a rectangular coordinate system

$I(y)$ a function called the current distribution on the surface of a reflector. It is proportional to the tangential component of the magnetic field intensity at the surface of the reflector.

$\bar{j}$ the unit vector along the y-axis in a rectangular coordinate system.

$\bar{k}$ the unit vector along the z-axis in a rectangular coordinate system.

K_o the beamwidth factor, see Figure 27, used in main-beam calculations.

K_1 a constant of proportionality, see Equation (1).

K_2 a constant of proportionality, see Appendix II.

K_3 a constant used in finding the normalized far field, see Equation (49).

$\bar{K}$ the surface electric current density on the surface of a conductor.

ℓ the length of the line source, see Figure 5.

L the diameter of the mouth of a paraboloidal reflector.

$\dot{M}(\rho,\psi)$ a function proportional to the total magnetic field intensity incident on the surface of a conductor.

$N(x)$ a function directly proportional to the gain $G(x)$ of the horn feed.

$\bar{n}$ the unit vector normal to a surface.

P_i the time-average power incident onto a small surface element $(d\ell)(1)$ as shown in Figure 8.

P_r the time-average power reflected from a small surface element $(d\ell)(1)$ as shown in Figure 8.

P_t the time-average power transmitted by an antenna.

r the distance from the image horn, Figure 7, to a point on the parabola above the ground plane.

r_o the distance from a radar antenna to a target.

r_1 the distance from the horn feed to a point on the ground plane as shown in Figure 8.

r_2 the distance from the ground plane to a point on the parabola as seen in Figure 8.

$\bar{r}_1$ the unit radial vector used in the standard spherical coordinate system.

R the distance from a current element on the reflector to some point in the far field, see Figure 21.

R_o the distance from the feed horn to some point in the far field, see Figure 21.

R_1 the distance from the ground plane in Figure 8 as defined by Equation (7).

R_c the radius of curvature of the circular ground plane.

R_p the radial distance from the center of feed, Figure 17, to a point in the near field.

R_v the distance from the vertex of a parabola to some point in the far field, see Figure 21.

S_o the surface of an arbitrary reflector.

u the angle between the vector $\bar{r}_1$, and the tangent to the reflector, see Figure 20.

$\dot{U}_m$ the normalized far-field intensity of the main beam.

$\dot{U}_i$ the normalized far-field intensity of the image beam.

v the displacement angle of the image from the axis of the parabola.

x, y, z normal coordinates for the right-handed Cartesian coordinate system, the z-axis is always the axis of the parabola.

y', y" special values of y as shown in Figure 23.

y_o the y-coordinate on the parabolic reflector showing the aim of the horn, see Figure 26.

y_m the y-coordinate of the top of the reflector, see Figure 26.

Greek Symbols

α the tilt angle of a flat ground plane measured from the axis of the parabola.

β the propagation constant of a wave in free space.

γ the complement of the angle of incidence for the wave from the horn into the ground plane, see Figures 7 and 8.

δ the angle between the axis of the parabola and the tangent to the parabola as shown in Figure 21.

Δ the angle between the axis of the parabola and the tangent to the ground plane as shown in Figure 21.

ζ the time phase angle between the far-field main beam at $\theta = 0$ and the far-field image beam at the peak of the image beam, see Equation (56).

η the intrinsic impedance of free space.

θ the angle measured from the axis of the parabola.

θ_o the angular position of the peak of the image beam.

θ_m the angle between the axis of the parabola and a line drawn between the vertex and the top of the parabola, see Figure 21.

$\bar{\theta}_1$ the standard unit vector used with a right-handed spherical coordinate system.

Θ the elevation angle measured from the horizontal, see Figure 1.

ι the angle of incidence of the wave hitting the reflector surface, see Figure 20.

λ the free-space wavelength.

μ the permeability of the medium, air in this case.

ν the angle between the axis of the parabola and a line from the vertex to a point on the reflector, see Figure 21.

ξ the angle between the axis of the parabola and the reflected ray from the ground plane, see Figure 8.

ρ the distance from the feed horn to the reflector surface.

ρ_m the distance from the feed horn to the top of the reflector.

$\bar{\rho}_l$ the unit vector normal to the long dimension of the line feed.

$\bar{\tau}$ a unit vector tangential to the surface of the reflector as shown in Figure 20(b).

Φ the angle between the axis of the reflector and the ray into the ground plane, see Figures 7 and 8.

$\Phi(y)$ the phase angle of the current on the surface of the reflector. The main-beam current at the origin is used as the reference.

$\bar{\Phi}_l$ the standard unit vector associated with a right-handed spherical coordinate system.

Ψ the angle between the axis of the reflector and the ray from the horn into the reflector, see Figures 7 and 8.

Ψ_o the angle between the axis of the reflector and the direction of maximum radiation from the line feed, see Figure 26.

Ψ_m the angle between the axis of the reflector and the ray from the horn to the top of the reflector, see Figure 26.

Ψ_{max} an angle from between the aim of the horn and a line from the center of feed to the lip of the horn, see Figure 17.

$\bar{\psi}_1$ the unit vector normal to the vector $\bar{\rho}$ see Figure 20.

ω 2π times the frequency.

Ω_m the phase of the main-beam field intensity relative to the intensity of the main beam at $\theta = 0$.

Ω_i the phase of the image-beam field intensity relative to the intensity of the image beam at its peak.

APPENDIX II

FINDING THE GAIN OF THE FEED RELATIVE TO THE GAIN OF THE GROUND PLANE

When the radiation from the currents on the parabolic reflector or ground plane is evaluated by use of Equation (25) or (40), the part of the reflector under consideration is broken up into sections about 1/8 inch wide. When the main, image, and direct ground-plane beams are calculated, the reflector currents which are found using Equation (27) or (41) are used in Equation (25) or (40) when the integral is expressed as a finite series of phasor terms. The main, image, and direct ground-plane beams are evaluated using a digital computer and added directly without evaluating the constant, such as that given in Equation (26). The same constant is a multiplier for each beam and therefore is not important in determining the shape of the sum of the three beams. However, before the direct beam from the horn is added to other beams, the gain of the beam due to the reflector currents must be known relative to the gain of the feed.

The relative gain of two antennas having the same beam shapes in the azimuth plane can be found by an integration of the vertical-plane radiation patterns. The azimuth-plane patterns affect the gains, but since they are the same for the two antennas, azimuth patterns do not affect the peak gain of one antenna relative to the other. When the normalized vertical-plane radiation pattern of an antenna having a constant beamshape in the azimuth plane is known, the maximum gain G_{max} (θ)

is given by[20]

$$G_{max}(\theta) = \frac{E^2_{max}(\theta)}{K_2 \int_0^{2\pi} E^2(\theta)\, d\theta},$$

where K_2 is a constant determined by the shape of the beam in the azimuth plane. The gain of an antenna a compared to gain of an antenna b is

$$\frac{\left[G_{max}(\theta)\right]_a}{\left[G_{max}(\theta)\right]_b} = \frac{\left[E^2_{max}(\theta)\right]_a}{\int_0^{2\pi} \left[E^2(\theta)\right]_a d\theta} \times \frac{\int_0^{2\pi} \left[E^2(\theta)\right]_b d\theta}{\left[E^2_{max}(\theta)\right]_b}$$

if the beam shapes in the azimuth plane are the same. The term $\left[G_{max}(\theta)\right]_a$ is the maximum gain of antenna a, and $\left[E(\theta)\right]_a$ is the normalized field of antenna a. Since the radiation patterns are normalized,

$$\left[E_{max}(\theta)\right]_a = \left[E_{max}(\theta)\right]_b,$$

and

$$\frac{\left[G_{max}(\theta)\right]_a}{\left[G_{max}(\theta)\right]_b} = \frac{\int_0^{2\pi} \left[E^2(\theta)\right]_b d\theta}{\int_0^{2\pi} \left[E^2(\theta)\right]_a d\theta}. \qquad (60)$$

The currents on the parabolic section of the reflector do not constitute a complete antenna, but the radiation by the main-beam and

image-beam currents causes a beam which will be referred to as the radiation pattern of antenna a. The line source is called antenna b. Thus if the radiation pattern of horn 1, see Figure 29, is used to get $\left[E(\theta)\right]_b$ and the calculated pattern in Figure 43 is used to get $\left[E(\theta)\right]_a$, Equation (60) can be used to find the gain of the feed relative to the gain of antenna a. The peak gain of the overall image-beam antenna is almost the same as the gain of antenna a because the field caused by the direct ground-plane and direct-horn beams are small compared to the maximum field of antenna a.

The maximum field of the feed relative to the maximum field due to parabolic reflector currents is found from the gain ratio given by Equation (60). The peak field intensity caused by the ground-plane currents uses the same reference as the field caused by currents on the parabola, so the fields of the horn feed and the ground plane are added to give the calculated pattern in Figure 44.

BIBLIOGRAPHY

1. S. Silver, Microwave Antenna Theory and Design, McGraw-Hill Book Company, Inc., New York, 1949, pp. 465-471.

2. Ibid, p. 471.

3. S. A. Schelkunoff, Electromagnetic Waves, D. Van Nostrand Company, Inc., New York, 1948, p. 355.

4. Silver, op. cit., p. 497.

5. Ibid, p. 481.

6. P. T. Hutchison, "The Image Method of Beam Shaping," Transactions of the IRE Professional Group on Antennas and Propagation, Vol. AP-4, October, 1956, p. 604.

7. Silver, op. cit., p. 171.

8. Ibid, p. 149.

9. Ibid, p. 151.

10. Ibid, p. 152.

11. Ibid, p. 132.

12. J. D. Kraus, Antennas, McGraw-Hill Book Company, Inc., New York, 1950, p. 79.

13. D. D. King, Measurement of Centimeter Waves, D. Van Nostrand Co., Inc., New York, 1952, p. 272.

14. Silver, op. cit., p. 564.

15. Silver, op. cit., p. 158.

16. Ibid, p. 144.

17. Ibid, p. 149.

18. E. C. Jordan, Electromagnetic Waves and Radiating Systems, Prentice Hall, New York, 1950, p. 570, also Kraus, op. cit., p. 350.

19. Silver, op. cit., p. 488.

20. Kraus, op. cit., p. 24.

VITA

Paul Trice Hutchison was born in Tupelo, Mississippi, on November 2, 1922. He is the son of Paul and Many Bonner Hutchison. In 1947 he was married to Mildred Mason Hunter of Watertown, Massachusetts.

He attended public schools in Tupelo, Mississippi, and was graduated in 1940. He received the degree of Bachelor of Science in Electrical Engineering from Mississippi State College in 1944. After serving in the U. S. Navy for two years, he received the Master of Science degree in Electrical Engineering from California Institute of Technology in 1947.

From 1947 to 1954 he taught as an Assistant Professor and Associate Professor of Electrical Engineering at Mississippi State College and worked at Raytheon Manufacturing Company as a Microwave Engineer.

Since 1954 he has served as an Assistant Professor of Electrical Engineering at the Georgia Institute of Technology.

APPENDICES